

Development of a Concentration-Enhanced Mobility Shift Assay Platform for Aptamer-Based Biomarker Detection and Kinase Profiling

by

Lih Feng Cheow

S.M., Massachusetts Institute of Technology (2009)
B.S., Cornell University (2005)

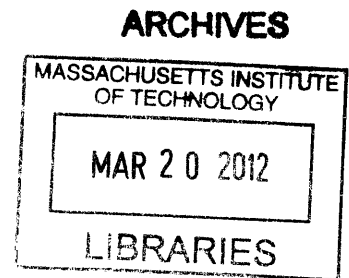
Submitted to the Department of Electrical Engineering and Computer Science
in Partial Fulfillment of the Requirements for the Degree of

Doctor of Philosophy

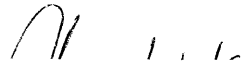
at the

Massachusetts Institute of Technology

February 2012




© 2012 Massachusetts Institute of Technology. All rights reserved

Signature of Author 

Department of Electrical Engineering and Computer Science
February 1, 2012

Certified by 

Jongyoon Han
Associate Professor of Electrical Engineering and Computer Science
Associate Professor of Biological Engineering
Thesis Supervisor

Accepted by 

Leslie A. Kolodziejski
Chairman, Department Committee on Graduate Students
Department of Electrical Engineering and Computer Science

Development of a Concentration-Enhanced Mobility Shift Assay Platform for
Aptamer-Based Biomarker Detection and Kinase Profiling

by

Lih Feng Cheow

Submitted to the Department of Electrical Engineering and Computer Science
on February 1, 2012 in Partial Fulfillment of the
Requirements for the Degree of Doctor of Philosophy
in Electrical Engineering and Computer Science

ABSTRACT

New methods to quantify rare biomarkers from patient samples are critical for developing point-of-care diagnostic platforms. To be compatible with resource limited settings, these assays have to provide fast and accurate results without sacrificing ease of use. Biosensing in homogeneous fashion is the preferred format which satisfies these criteria, but the lack of amplification method is a bottleneck that limits their use for sensitive applications. To address this issue, this thesis explores physical signal amplification means to increase the sensitivities of homogeneous assays. We identified several key applications where the use of these technologies could make a positive impact in improving medical diagnostics systems and advancing biological research.

We first outline the use of electrokinetic concentration to realize a continuous signal amplification scheme that increases the sensitivity of homogeneous mobility shift assays. By simultaneously concentrating and separating reacted and unreacted species (with different mobilities) in this device, we can perform sensitive, quantitative and ratiometric measurement of target biomarkers. Using this platform, we improved the sensitivity of aptamer affinity probe capillary electrophoresis to achieve pM detection limit of IgE and HIV-RT in simple buffer and serum sample. This work is timely and impactful as it directly addresses the sensitivity shortcomings of using aptamers as low cost and robust substitutes for antibodies in point-of-care applications.

Next, we presented a herringbone nanofilter array device which can perform continuous size-selective concentration of biomolecules based on their direct interaction with nanostructures with comparable critical dimensions. We demonstrated the use of this platform to perform a novel homogeneous immunoassay for detecting a cardiac biomarker, C-reactive protein, at clinically relevant concentrations.

Finally, we demonstrated that the concentration-enhanced mobility shift assay platform is a powerful tool for probing biological activities such as cellular kinase activities. We have developed technology to isolate, grow and lyse single cells, and used our platform to measure kinase activities from single cells. Through rational design of peptide substrates and spacers, this platform has the ability to simultaneously concentrate and separate multiple analytes. This enables users to obtain simultaneous measurements of multiple cellular kinase activities that could reveal important information about their functional relationships.

Thesis Supervisor: Jongyoon Han

Title: Associate Professor of Electrical Engineering and Computer Science and Associate Professor of Biological Engineering

Acknowledgements

I have been very fortunate to be surrounded by many friends and mentors over the course of my graduate studies. This thesis is a milestone that would not have been possible without their support and guidance.

First of all, I would like to thank Professor Jongyoon Han for being a great advisor and mentor. I truly appreciate his insightful guidance into the field of micro-nanofluidics. He encouraged me by giving me the freedom to try new ideas and listening to and trusting my opinions. His tenacity and enthusiasm for science will be a constant inspiration to me. I would also like to thank my other thesis committee members, Professor Joel Voldman and Professor Jacquin Niles for their constructive inputs and ideas.

I am indebted to my fellow group members in the Han Lab, who have made my graduate school life a delightful experience. I would like to specially thank Aniruddh Sarkar and Hansen Bow, who are my collaborators in this thesis work. I would also like to thank other present and past group members: Yong-Ak Song, Sung Jae Kim, Hiong Yap Gan, Chia-Hung Chen, Rohat Melik, Leon Li, Rhokyun Kwak, Sha Huang, Lidan Wu, Vincent Liu, Reto Schoch, Jeong Hoon Lee and Masumi Yamada for their help and friendship. I have learned a lot from them in different ways over the years. In addition, I also thank the visiting students who have worked with me: Sung Hee Ko and Hyuk-Seong Seo.

I would like to thank A*STAR Singapore for its generous scholarship support. I must also thank the agents that supported my work, including the National Institute of Health (CA 119402), Singapore-MIT Alliance-II CE programme and the CDP center grant. I also thank the staff members at the MIT Microsystems Technology Laboratories for their help in device fabrication.

Finally, I would like to express my deepest gratitude to my family for their unconditional love and support. Above all, I would like to thank my fiancée, Rui Zhen Tan, for her understanding, support, encouragement and love. I would like to dedicate this thesis to her.

Table of Contents

1. Introduction	13
1.1. Opportunities in micro/nano-fluidics for biomolecule analysis.....	13
1.2. New developments in biosensing	14
1.3. The issues of affinity capture agents	15
1.4. Signal amplification in homogeneous assays	17
1.5. Thesis outline and scope	18
1.6. References	21
2. Concentration enhanced mobility shift assay platform for aptamer-based biomarker detection	24
2.1. Aptamers as affinity agents in diagnostic platforms.....	24
2.2. Electrokinetic concentration as a signal amplification module for aptamer affinity probe electrophoresis assay	27
2.3. Principle of the assay	30
2.4. Experimental section	33
2.4.1.Reagents and chemicals	33
2.4.2.Microchip fabrication	33
2.4.3.Microchip operation	34
2.4.4.Measurement instrument and image analysis	35
2.5. Optimization of assay	36
2.6. Detection of IgE and HIV-1 RT from buffer	39
2.7. Detection of IgE from serum sample	44
2.8. Summary	47
2.9. References	48

3. Differential concentration of biomolecules using herringbone nanofilter array	50
3.1. Nanostructures for biomolecular sieving	51
3.2. Size based concentration of biomolecules using herringbone nanofilter array	55
3.3. Device fabrication	59
3.4. Concentration of short DNA molecules by Ogston sieving	60
3.5. Differential concentration of DNA-protein complex	62
3.6. Differential concentration of protein-protein complex	65
3.7. Differential concentration of antibody-antigen complex	68
3.8. Summary	73
3.9. References	74
4. Multiplexed single cell kinase activity assay	76
4.1. Antibody based method vs direct activity measurement	78
4.2. Single cell kinase activity assay	78
4.3. Electrokinetic concentration enhanced kinase activity assay	80
4.4. Experimental section	82
4.4.1. Reagents and chemicals	82
4.4.2. Microchip operations	83
4.4.3. Measurement instrument and image analysis	83
4.4.4. Recombinant kinase experiment	84
4.4.5. Substrate cross reactivity	87
4.4.6. Cell lysate experiment	89
4.5. Multi-substrate separation	92
4.6. Single adherent cell culture	103
4.7. Single cell lysis and kinase reaction	104
4.8. Concentration enhanced single cell kinase activity assay	109
4.9. Concentration enhanced single cell multiple kinase activity assay	116

4.10. Summary.....	118
4.11. References	119
5. Conclusion	121
5.1. Thesis contribution	121
5.2. Directions for future work	123
5.2.1. Concentration enhanced mobility shift assay	123
5.2.2. Size-based concentration of biomolecules using herringbone nanofilter array	124
5.2.3. Multiplexed single cell biological activity assay	125
5.3. References	126

List of Figures

Figure 2.1:	Structure of an aptamer	25
Figure 2.2:	Operating principle of the electrokinetic concentration enhanced aptamer affinity probe electrophoresis assay	32
Figure 2.3:	Effect of BSA on detection sensitivity of IgE	38
Figure 2.4:	Experimental results for multiplexed concentration enhanced aptamer affinity probe electrophoresis assay for detection of IgE in buffer	41
Figure 2.5:	Electropherogram and dose response curve for detection of IgE in buffer	42
Figure 2.6:	Electropherogram and dose response curve for detection of HIV-1 RT in buffer	43
Figure 2.7:	Effect of serum on detection of IgE	44
Figure 2.8:	Experimental results and dose response curve for detection of IgE in serum	46
Figure 3.1	Hydrophoresis device for continuous size based separation of particles	54
Figure 3.2:	Schematic and cross section of herringbone nanofilter array	58
Figure 3.3:	Fabrication process of the herringbone nanofilter array	59
Figure 3.4:	Size based concentration of short double-stranded DNA in herringbone nanofilter array device	61
Figure 3.5:	Size based concentration of DNA-protein complex in herringbone nanofilter array device	64
Figure 3.6:	Size based concentration of protein-protein complex in herringbone nanofilter array device	66
Figure 3.7:	Size based concentration of protein-protein complex in herringbone nanofilter array device under reversed electric field polarity	67
Figure 3.8:	A homogeneous immunoassay for C-Reactive Protein using the herringbone nanofilter	

	array device	70
Figure 3.9:	Dose response curve for detection of C-Reactive Protein using the herringbone nanofilter array	72
Figure 4.1:	Diagram showing the cellular signal transduction network	77
Figure 4.2:	Operating principle of the electrokinetic concentration enhanced kinase activity assay	81
Figure 4.3:	Multiplexed electrokinetic concentration enhanced mobility shift assay for detection of recombinant AKT activity	85
Figure 4.4:	Dose response curve for detection of recombinant MK2 and PKA activity	86
Figure 4.5:	Pair-wise cross-reactivity between kinases and substrates	88
Figure 4.6:	Detection of AKT and PKA activity in stimulated and unstimulated HepG2 cell lysates	91
Figure 4.7:	Principle of electrofocusing and depletion zone isotachopheresis to simultaneously concentrate and separate two species	93
Figure 4.8:	Strategy to simultaneously separate and concentrate multiple analytes by utilizing intermediate mobility spacer molecules	95
Figure 4.9:	Creation of extended separation zone by ampholyte additives	97
Figure 4.10:	Separation behavior of two kinase substrates with ampholyte additives	98
Figure 4.11:	Complete separation of two kinase substrates and their products using ampholytes and MES as intermediate mobility spacer	99
Figure 4.12:	Predicted mobility of kinase substrates and synthetic peptide spacers according to the Offord Model	101
Figure 4.13:	Simultaneous concentration and baseline separation of substrates and products	

	corresponding to PKA, AKT and MK2 using rationally designed synthetic peptide spacers	102
Figure 4.14:	Complete process flow for the cell culture, lysis, reaction and fluidic transfer operations	107
Figure 4.15:	Figure showing release of intracellular contents from adherent HepG2 cells after ultrasonic lysis	108
Figure 4.16:	Detection of AKT activity from single HepG2 cell.....	110
Figure 4.17:	MK2 activity vs cell number	112
Figure 4.18:	Linear relationship between kinase activity and total cell volume	114
Figure 4.19:	MK2 activity vs cell number after normalizing by the average cell volume, showing single cell sensitivity and resolution	115
Figure 4.20:	Concentration-enhanced mobility shift assay for detection of multiple kinase activity from single cell	117

List of Tables

Table 4.1:	Buffer recipes	81
-------------------	----------------------	----

Chapter 1

Introduction

1.1 Opportunities in micro/nano-fluidics for biomolecule analysis

One of the most pressing issues in analytical chemistry is detecting low abundance analytes from complex samples such as blood, saliva and urine. Tests for low abundance biomarkers are routinely used for disease diagnostics, to monitor patient response during therapy, and to help detect recurrence following treatment. Therefore, there is significant clinical relevance to increase the sensitivity of these tests to facilitate early detection of the onset of diseases, since these biomarkers get diluted significantly in biofluids, especially in the early stages of disease progression.

The traditional workflow of biomarker analysis involves taking a sample from a patient, sending the sample to a laboratory where the analysis is performed with sophisticated equipments, and getting the results several days later. Several problems associated with this model are the need of good infrastructure for sample transport, possibility of sample deterioration during storage, and long turnaround time leading to patient anxiety. In order to address these problems, there has been tremendous interest in developing point-of-care diagnostic systems, which aims to bring medical testing to near patient care in the form of portable test kits. Commercial examples of point-of-care diagnostic systems include the over-the-counter pregnancy test strip, which uses lateral-flow-immunoassays to provide test results in minutes. However, these tests are usually qualitative and have limited sensitivities. At the same time, certain clinical applications, such as cancer diagnostics, requires assay sensitivities that are beyond the capabilities of existing point-of-care diagnostic devices. This calls for a new breed of technology that could perform more sophisticated operations to achieve better assay sensitivity and specificity.

An answer to this challenge is micro total analysis systems (μ TAS), which aims at integrating multiple biological and chemical analyses in a single chip. Leveraging on the microfabrication techniques developed for semiconductor manufacturing, microfluidics technology have matured considerably in the

last few decades to deliver performances that are on-par or often better than conventional benchtop techniques. Various microchip-based processes including sample filtration^{1, 2}, dilution^{3, 4}, mixing⁵, polymerase chain reaction^{6, 7}, sample preconcentration⁸⁻¹⁰ and separation techniques^{6, 7} have been demonstrated. The seamless integration of these functionalities into a single microchip platform have enabled complex multi-step chip-based bioanalysis¹¹ such as immunoassays^{12, 13}, DNA analysis^{6, 7, 14}, and chemical detection^{15, 16} to be performed from raw sample with minimal user intervention. These lab-on-chip systems could change the current healthcare paradigm as sensitive tests could now be performed at a doctor's office or from a portable device in resource-poor regions. Instant access to this important test information would help healthcare providers in making a better diagnosis and prescribing the appropriate treatment at much lower overall cost.

Aside from the versatile integration in lab-on-chip systems, microfluidic devices could make use of the novel physics associated with the micro/nano structures to realize new capabilities. As we can now fabricate structures with critical dimension comparable to biomolecules, we can directly manipulate biomolecules based on their size-dependent interactions with the solid-state nanostructures. This had led to applications such as biomolecular separation in nanochannel arrays¹⁷⁻¹⁹ as well as ultrasensitive biosensing using nanowires^{20, 21} and nanopores²²⁻²⁵. Besides, interesting phenomena such as concentration polarization at the micro-nano interface has been used successfully for sample preconcentration⁹ and increasing the sensitivity of various biomarker assays²⁶⁻²⁸.

1.2 New developments in biosensing

The sensitivity and application of biosensing depends critically on the methods used for detection. Thanks to recent advances in material science, fabrication technology and discovery of new physics, several notable ultrasensitive biosensors have been developed and reported in the literature. Enzyme-linked immunosorbent assays²⁹⁻³¹ (ELISA), which use enzymes-conjugated antibodies to continuously convert a substrate to a detectable product, are still the gold standard in many assays such as detection of HIV due to their high sensitivities. Other variants of ELISA, such as use of quantum dot-conjugated antibodies³², polymerase chain reaction (PCR) amplification^{33, 34} and reduction of silver to enhance the output signal³⁵.

³⁶, have been demonstrated to detect target analytes with exquisite sensitivities. Ultrasensitive assays using electrochemical stripping³⁷ also share some similarities with ELISA in using a built-in signal amplification mechanism. There have also been several notable label-free detection methods including platforms using silicon nanowires^{20, 21}, whispering-gallery mode optical sensors^{38, 39}, suspended microchannel resonator^{40, 41} and surface enhanced raman scattering (SERS)⁴². The common features among these ultrasensitive assays are the various signal amplification mechanisms including enzymatic/chemical amplification²⁹⁻³⁷, field-effect enhancement^{20, 21}, as well as optical^{38, 39, 42} and mechanical resonance^{40, 41}. These assays are also examples of heterogeneous assays, where the target molecules are detected by selectively capturing them onto capture agents immobilized on a solid-phased support. For portable lab-on-chip applications, heterogeneous assays present many challenges such as the requirement for multiple washing steps and slow binding kinetics. Moreover, immobilizing specific antibodies to the solid-phase support while maintaining the activity and specificity of the antibodies is a non-trivial task and often a source of error in heterogeneous biosensors.

On the other hand, in homogeneous assays, no immobilization step is required as reaction between the target molecule and capture agent is carried out in solution phase. Reacted molecules are detected by a change in physical property such as fluorescence signal^{43, 44}, fluorescence polarization⁴⁴, size-dependent light scattering⁴⁵, magnetic relaxation⁴⁶ and electrophoretic mobility⁴⁷. Homogeneous assays are attractive from a point-of-care diagnostic viewpoint due to the fast reaction kinetics and simple mix-and-use operation which does not require labor intensive washing steps. However, they are usually less sensitive than their heterogeneous assay counterpart because of the lack of signal amplification. A signal amplification method that could be generally applied to homogeneous assays would combine the best of both worlds – ease of use of a homogeneous assay coupled with the sensitivity of a heterogeneous enzyme-linked assay.

1.3 The issues of affinity capture agents

Due to their high affinity and specificity, antibodies have been used extensively as capture agents in diagnostic tools⁴⁸. The use of antibodies in detecting analytes became widespread in the 1970s with

polyclonal antisera derived from immunized animals. In 1975, the development of monoclonal antibodies from hybridoma cells was a major milestone that allowed the production of a unique antibody in large quantity⁴⁹. Today, the antibody discovery process starts with immunizing an animal with the antigen of interest over a course of several weeks, followed by isolating antibody-producing cells from the spleen of the animal, fusing these cells with immortalized myeloma cells to form hybridoma cells, and finally screening for cell lines that produce high affinity and specificity antibodies. These cells are continuously cultured to harvest monoclonal antibodies. Due to the laborious process, identification and production of antibodies could be very time consuming and expensive especially when searching for rare antibodies that require screening of a large number of colonies. As such, this could lead to a prohibitively high cost when using antibodies as affinity reagents. Furthermore, antibodies have limited shelf life and the performance of the same antibody tends to vary from batch to batch. These are major roadblocks in developing robust, affordable and standardized point-of-care diagnostic platforms.

Several alternative affinity capture agents, including oligonucleotide aptamers⁵⁰⁻⁵³, phage-display peptides⁵⁴ and multiligand protein capture ligand⁵⁵, have been proposed to be replacements for antibodies for diagnostic applications. Unlike antibodies, these capture agents are selected through in-vitro processes such as phage display⁵⁴, systematic evolution of ligands by exponential enrichment (SELEX)⁵⁶, and one bead one compound (OBOC) method⁵⁵. Therefore, identification of a suitable capture agent is fast (days) and miniaturization could further reduce the reagent cost. Due to the well defined chemical synthesis, they could be produced with extreme accuracy and reproducibility, and various functional groups can be attached to these molecules during synthesis. Finally, these synthetic capture agents are also more resistant to denaturation and hence compatible with the use in point-of-care diagnostic devices. Compared to antibodies, however, these capture agents often have lower binding strengths. This could limit their use in heterogeneous assays, where stringent washing steps could detach the target molecules. Their lower binding affinities also necessitate higher sensitivity methods to detect the comparatively lesser target molecules that are bound at equilibrium.

1.4 Signal amplification in homogeneous assays

Signal amplification techniques are essential in order to boost the sensitivities of biosensors to detect low abundant analytes. This aspect is especially important in portable lab-on-chip systems where the optical path length is short and when the integrated detection system has limited sensitivity. ELISA or other chemical amplification techniques can be routinely implemented in heterogeneous assays, but it is much more challenging to achieve this in homogeneous assays.

There have been a few reports of enzyme amplification in homogeneous assays, such as the enzyme-multiplied immunoassay technique (EMIT)⁵⁷, enzyme channeling⁵⁸ and enzyme complementation immunoassay⁵⁹. These techniques are based on the principle that when the target molecule binds to the enzyme-linked antibody, the enzyme activity is altered due to steric effects. Such altered activities can be read out via observing the accumulation of reaction products, as in ELISA. However, since these assays are based on changes in the three-dimensional conformation of the enzymes upon target binding, considerable amount of selection and optimization is required to identify the effective capture agent conjugate for each target. Therefore, they are seldom used in real applications.

Physical (instead of enzymatic or chemical) signal amplification methods have also been demonstrated in the context of homogeneous assays. These are usually achieved by concentrating molecular probes/substrates which undergo fluorescence change upon reaction with the target. Examples include electrokinetic concentration of special substrates for proteases²⁷ and kinases⁶⁰ which become fluorescent upon reaction with their target molecule, as well as isotachopheresis concentration of molecular beacons which undergo strong fluorescence enhancement upon binding to a target RNA⁶¹. Physical signal amplification in these cases greatly improved the sensitivities of each assay. Nevertheless, it should be noted that the molecular probes/substrates for these assays are specially customized and designed for detection of these target molecules. It is an exception rather than a norm that such probes are available for a given target molecule.

Another strategy for amplifying signal in homogeneous assay is to preconcentrate all the biomolecules in the reaction mixture before separating them for detection. Unlike the above two classes

of methods, these techniques can be applied to a very large class of assays as most biological reaction or binding result in changes in size or charge that can be detected in a mobility shift assay. Various preconcentration techniques such as membrane preconcentration^{8, 62, 63}, field-amplified sample stacking (FASS)⁶⁴, isotachopheresis (ITP)⁶⁵ and electrokinetic trapping^{9, 66} have been used in conjunction with downstream electrophoretic separation to improve detection sensitivity. As the preconcentration and separation steps were carried out sequentially in these methods, band dispersion and complex dissociation during separation would ultimately reduce the sensitivity enhancement. Field gradient focusing methods such as electric field gradient focusing (EFGF)⁶⁷⁻⁶⁹, bipolar electrode focusing^{70, 71} and temperature gradient focusing (TGF)⁷²⁻⁷⁵ are able to simultaneously concentrate and separate analytes of different mobilities. However, these techniques involve the use of special buffers, electrodes in microchannels that cause bubble generation, complicated temperature control setups and nonstandard fabrication. Furthermore, most of these techniques were only demonstrated for concentration and separation of model fluorescent protein and not for real biological assays. Therefore, despite many efforts, there is still no general platform that can be used to provide signal amplification in homogeneous assays.

1.5 Thesis outline and scope

The lack of amplification method in homogeneous assays is a bottleneck that limits their use for sensitive measurements. In recognizing the comparative advantages of homogeneous assays over heterogeneous assays for lab-on-chip systems, we aimed to increase the sensitivities of homogeneous assays by implementing physical signal amplification methods. In this thesis, we have developed two different techniques to simultaneously concentrate and separate reacted from unreacted target molecules by electrophoretic mobility and size differences. The general applicability of these platforms for point-of-care diagnostics is demonstrated in the context of improving the sensitivity of aptamer-based affinity probe electrophoresis assay and homogeneous immunoassay for clinically relevant biomarkers. Finally, we show that this homogeneous amplification platform is a powerful tool that enables measurements of biological activities in single cells that were previously very difficult to obtain.

Electrophoretic mobility shift assays are the workhorse of molecular biology and have been widely used to measure various biomolecular interactions and enzymatic reactions. In Chapter 2, we developed a microfluidic electrokinetic concentration device to realize a continuous signal amplification scheme for homogeneous mobility shift assays. This is demonstrated in the context of an electrokinetic concentration-enhanced aptamer affinity probe electrophoresis assay to achieve highly sensitive and quantitative detection of protein biomarkers. We reported the lowest detection limit for two biomarkers, human immunoglobulin E (IgE) and human immunodeficiency virus 1 reverse transcriptase (HIV-1 RT), in a multiplexed microfluidic platform using low voltages and gravitational induced flow without the need of periphery equipments (syringe pumps, temperature blocks) or multiple buffers. This work is timely and impactful because it directly addresses the sensitivity shortcomings of using aptamers as low cost and robust substitutes for antibodies in point-of-care applications.

There are some cases where biomolecular interactions do not lead to an appreciable mobility change. In those instances, a size difference between reacted and unreacted biomolecules can often be used as a measure for the degree of interaction. In Chapter 3, we developed a herringbone nanofilter array which allows continuous flow size-selective concentration of biomolecules. This is enabled by precise microfabrication of solid-state nanostructures that facilitates size-dependent interactions with biomolecules with comparable critical dimensions. As a proof of concept, we demonstrated the utility of this platform to perform a sensitive homogeneous immunoassay for C-reactive protein, a biomarker for cardiac disease, at clinically relevant concentrations. The continuous flow format also makes this device an attractive sample preparation tool to continuously purify and concentrate target molecules based on size from a sample before performing downstream analysis.

In Chapter 4, we explored how we could adapt the concentration-enhanced mobility shift assay platform developed in Chapter 2 as a tool for basic biological studies. Kinases are important enzymes in the cellular signaling pathways that affect cell fate, yet little is known about how individual cells in different states of intracellular processing respond differently to external stimuli, since most conventional techniques provide only a population-averaged measurement of the signals within the regulatory pathway.

A platform technology that can reliably assay for kinase activity from single cells is a valuable tool for biologists to study how individual cells develop into different cell fates and correlate with their phenotype. In Chapter 4, we first outlined the use of concentration-enhanced mobility shift assay platform to measure cellular kinase activity with high sensitivity. We also developed a new capability to separate multiple species in the concentration-enhanced mobility shift assay platform by using ampholytes or rational design of peptide substrate and spacers. This capability enables users to perform multi-kinase profiling using different substrates. To enable single cell kinase assay, we have developed technology to first grow, isolate and observe single adherent cells, followed by parallel cell lysis and enzyme reaction in confined nanoliter chambers, and lastly methods to recover reaction products and transfer to a separate chip for analysis. By combining these methods, we demonstrated kinase activity assay with single cell sensitivity and resolution. We also demonstrated multiple-kinase activity assay from single cells that could provide vital clues about the functional relationships between different pathways in the signal transduction network.

Finally, Chapter 5 summarizes the thesis contribution and presents future directions.

1.6 References

- (1) Broyles, B. S.; Jacobson, S. C.; Ramsey, J. M. *Analytical Chemistry* **2003**, *75*, 2761-2767.
- (2) Yamada, M.; Seki, M. *Lab Chip* **2005**, *5*, 1233-1239.
- (3) Jacobson, S. C.; McKnight, T. E.; Ramsey, J. M. *Analytical Chemistry* **1999**, *71*, 4455-4459.
- (4) Pihl, J.; Sinclair, J.; Sahlin, E.; Karlsson, M.; Petterson, F.; Olofsson, J.; Orwar, O. *Analytical Chemistry* **2005**, *77*, 3897-3903.
- (5) Johnson, T. J.; Ross, D.; Locascio, L. E. *Analytical Chemistry* **2002**, *74*, 45-51.
- (6) Khandurina, J.; McKnight, T. E.; Jacobson, S. C.; Waters, L. C.; Foote, R. S.; Ramsey, J. M. *Analytical Chemistry* **2000**, *72*, 2995-3000.
- (7) Lagally, E. T.; Simpson, P. C.; Mathies, R. A. *Sensors and Actuators B: Chemical* **2000**, *63*, 138-146.
- (8) Foote, R. S.; Khandurina, J.; Jacobson, S. C.; Ramsey, J. M. *Analytical Chemistry* **2005**, *77*, 57-63.
- (9) Wang, Y. C.; Stevens, A. L.; Han, J. *Analytical Chemistry* **2005**, *77*, 4293-4299.
- (10) Yu, C.; Davey, M. H.; Svec, F.; Fréchet, J. M. J. *Analytical Chemistry* **2001**, *73*, 5088-5096.
- (11) Erickson, D.; Li, D. *Analytica Chimica Acta* **2004**, *507*, 11-26.
- (12) Herr, A. E.; Hatch, A. V.; Throckmorton, D. J.; Tran, H. M.; Brennan, J. S.; Giannobile, W. V.; Singh, A. K. *Proceedings of the National Academy of Sciences* **2007**, *104*, 5268.
- (13) Fan, R.; Vermesh, O.; Srivastava, A.; Yen, B. K. H.; Qin, L.; Ahmad, H.; Kwong, G. A.; Liu, C. C.; Gould, J.; Hood, L. *Nature Biotechnology* **2008**, *26*, 1373-1378.
- (14) Waters, L. C.; Jacobson, S. C.; Kroutchinina, N.; Khandurina, J.; Foote, R. S.; Ramsey, J. M. *Analytical Chemistry* **1998**, *70*, 158-162.
- (15) Duffy, D. C.; Gillis, H. L.; Lin, J.; Sheppard Jr, N. F.; Kellogg, G. J. *Analytical Chemistry* **1999**, *71*, 4669-4678.
- (16) Moser, I.; Jobst, G.; Urban, G. A. *Biosensors and Bioelectronics* **2002**, *17*, 297-302.
- (17) Han, J.; Craighead, H. G. *Science* **2000**, *288*, 1026.
- (18) Fu, J.; Mao, P.; Han, J. *Applied Physics Letters* **2005**, *87*, 263902-263902-263903.
- (19) Fu, J.; Schoch, R. B.; Stevens, A. L.; Tannenbaum, S. R.; Han, J. *Nature Nanotechnology* **2007**, *2*, 121-128.
- (20) Cui, Y.; Wei, Q.; Park, H.; Lieber, C. M. *Science* **2001**, *293*, 1289.
- (21) Zheng, G.; Patolsky, F.; Cui, Y.; Wang, W. U.; Lieber, C. M. *Nature Biotechnology* **2005**, *23*, 1294-1301.
- (22) Clarke, J.; Wu, H. C.; Jayasinghe, L.; Patel, A.; Reid, S.; Bayley, H. *Nature Nanotechnology* **2009**, *4*, 265-270.
- (23) Liang, X.; Chou, S. Y. *Nano Letters* **2008**, *8*, 1472-1476.
- (24) Karnik, R.; Castelino, K.; Fan, R.; Yang, P.; Majumdar, A. *Nano Letters* **2005**, *5*, 1638-1642.
- (25) Schoch, R. B.; Cheow, L. F.; Han, J. *Nano Letters* **2007**, *7*, 3895-3900.
- (26) Wang, Y. C.; Han, J. *Lab Chip* **2008**, *8*, 392.
- (27) Lee, J. H.; Song, Y. A.; Tannenbaum, S. R.; Han, J. *Analytical Chemistry* **2008**, *80*, 3198-3204.
- (28) Cheow, L. F.; Ko, S. H.; Kim, S. J.; Kang, K. H.; Han, J. *Analytical Chemistry* **2010**, *82*, 3383-3388.
- (29) Sato, K.; Tokeshi, M.; Otake, T.; Kimura, H.; Ooi, T.; Nakao, M.; Kitamori, T. *Analytical Chemistry* **2000**, *72*, 1144-1147.
- (30) Sato, K.; Tokeshi, M.; Kimura, H.; Kitamori, T. *Analytical Chemistry* **2001**, *73*, 1213-1218.
- (31) Yakovleva, J.; Davidsson, R.; Lobanova, A.; Bengtsson, M.; Eremin, S.; Laurell, T.; Emnéus, J. *Analytical Chemistry* **2002**, *74*, 2994-3004.
- (32) Park, J. S.; Cho, M. K.; Lee, E. J.; Ahn, K. Y.; Lee, K. E.; Jung, J. H.; Cho, Y.; Han, S. S.; Kim, Y. K.; Lee, J. *Nature Nanotechnology* **2009**, *4*, 259-264.

- (33) Schweitzer, B.; Wiltshire, S.; Lambert, J.; O'Malley, S.; Kukanskis, K.; Zhu, Z.; Kingsmore, S. F.; Lizardi, P. M.; Ward, D. C. *Proceedings of the National Academy of Sciences* **2000**, *97*, 10113.
- (34) Nam, J. M.; Thaxton, C. S.; Mirkin, C. A. *Science* **2003**, *301*, 1884.
- (35) Park, S. J.; Taton, T. A.; Mirkin, C. A. *Science* **2002**, *295*, 1503.
- (36) Taton, T. A.; Mirkin, C. A.; Letsinger, R. L. *Science* **2000**, *289*, 1757.
- (37) Hansen, J. A.; Wang, J.; Kawde, A. N.; Xiang, Y.; Gothelf, K. V.; Collins, G. *Journal of the American Chemical Society* **2006**, *128*, 2228-2229.
- (38) Armani, A. M.; Kulkarni, R. P.; Fraser, S. E.; Flagan, R. C.; Vahala, K. J. *Science* **2007**, *317*, 783.
- (39) Vollmer, F.; Arnold, S. *Nature Methods* **2008**, *5*, 591-596.
- (40) Burg, T. P.; Manalis, S. R. *Applied Physics Letters* **2003**, *83*, 2698.
- (41) Burg, T. P.; Godin, M.; Knudsen, S. M.; Shen, W.; Carlson, G.; Foster, J. S.; Babcock, K.; Manalis, S. R. *Nature* **2007**, *446*, 1066-1069.
- (42) Lu, Y.; Liu, G. L.; Kim, J.; Mejia, Y. X.; Lee, L. P. *Nano Letters* **2005**, *5*, 119-124.
- (43) Kuningas, K.; Ukonaho, T.; Pääkkilä, H.; Rantanen, T.; Rosenberg, J.; Lövgren, T.; Soukka, T. *Analytical Chemistry* **2006**, *78*, 4690-4696.
- (44) Tachi, T.; Kaji, N.; Tokeshi, M.; Baba, Y. *Lab Chip* **2008**, *9*, 966-971.
- (45) Liu, X.; Dai, Q.; Austin, L.; Coutts, J.; Knowles, G.; Zou, J.; Chen, H.; Huo, Q. *Journal of the American Chemical Society* **2008**, *130*, 2780-2782.
- (46) Chemla, Y. R.; Grossman, H. L.; Poon, Y.; McDermott, R.; Stevens, R.; Alper, M. D.; Clarke, J. *Proceedings of the National Academy of Sciences* **2000**, *97*, 14268.
- (47) Bromberg, A.; Mathies, R. A. *Analytical Chemistry* **2003**, *75*, 1188-1195.
- (48) Borrebaeck, C. A. K. *Immunology Today* **2000**, *21*, 379-382.
- (49) Köhler, G.; Milstein, C. *Nature* **1975**, *256*, 495-497.
- (50) Cox, J. C.; Hayhurst, A.; Hesselberth, J.; Bayer, T. S.; Georgiou, G.; Ellington, A. D. *Nucleic Acids Research* **2002**, *30*, e108-e108.
- (51) McCauley, T. G.; Hamaguchi, N.; Stanton, M. *Analytical Biochemistry* **2003**, *319*, 244-250.
- (52) Gold, L.; Ayers, D.; Bertino, J.; Bock, C.; Bock, A.; Brody, E. N.; Carter, J.; Dalby, A. B.; Eaton, B. E.; Fitzwater, T. *PLoS ONE* **2010**, *5*, e15004.
- (53) Proske, D.; Blank, M.; Buhmann, R.; Resch, A. *Applied Microbiology and Biotechnology* **2005**, *69*, 367-374.
- (54) Smith, G. P.; Petrenko, V. A. *Chemical Reviews* **1997**, *97*, 391-410.
- (55) Agnew, H. D.; Rohde, R. D.; Millward, S. W.; Nag, A.; Yeo, W. S.; Hein, J. E.; Pitram, S. M.; Tariq, A. A.; Burns, V. M.; Krom, R. J. *Angewandte Chemie International Edition* **2009**, *48*, 4944-4948.
- (56) Tuerk, C.; Gold, L. *Science* **1990**, *249*, 505.
- (57) Rubenstein, K. E.; Schneider, R. S.; Ullman, E. F. *Biochemical and Biophysical Research Communications* **1972**, *47*, p1972.
- (58) Litman, D. J.; Hanlon, T. M.; Ullman, E. F. *Analytical Biochemistry* **1980**, *106*, 223-229.
- (59) Dieter Engel, W.; Khanna, P. L. *Journal of Immunological Methods* **1992**, *150*, 99-102.
- (60) Lee, J. H.; Cosgrove, B. D.; Lauffenburger, D. A.; Han, J. *Journal of the American Chemical Society* **2009**, *131*, 10340-10341.
- (61) Bercovici, M.; Kaigala, G. V.; Mach, K. E.; Han, C. M.; Liao, J. C.; Santiago, J. G. *Analytical Chemistry* **2011**, *83*, 4110-4117.
- (62) Khandurina, J.; Jacobson, S. C.; Waters, L. C.; Foote, R. S.; Ramsey, J. M. *Analytical Chemistry* **1999**, *71*, 1815-1819.
- (63) Hatch, A. V.; Herr, A. E.; Throckmorton, D. J.; Brennan, J. S.; Singh, A. K. *Analytical Chemistry* **2006**, *78*, 4976-4984.
- (64) Lichtenberg, J.; Verpoorte, E.; de Rooij, N. F. *Electrophoresis* **2001**, *22*, 258-271.
- (65) Jung, B.; Bharadwaj, R.; Santiago, J. G. *Analytical chemistry* **2006**, *78*, 2319-2327.

- (66) Astorga-Wells, J.; Swerdlow, H. *Analytical Chemistry* **2003**, *75*, 5207-5212.
- (67) Koegler, W. S.; Ivory, C. F. *Journal of Chromatography A* **1996**, *726*, 229-236.
- (68) Petsev, D. N.; Lopez, G. P.; Ivory, C. F.; Sibbett, S. S. *Lab Chip* **2005**, *5*, 587-597.
- (69) Kelly, R. T.; Woolley, A. T. *Journal of Separation Science* **2005**, *28*, 1985-1993.
- (70) Laws, D. R.; Hlushkou, D.; Perdue, R. K.; Tallarek, U.; Crooks, R. M. *Analytical Chemistry* **2009**, *81*, 8923-8929.
- (71) Mavré, F.; Anand, R. K.; Laws, D. R.; Chow, K. F.; Chang, B. Y.; Crooks, J. A.; Crooks, R. M. *Analytical Chemistry* **2010**, *82*, 8766-8774.
- (72) Ross, D.; Locascio, L. E. *Analytical Chemistry* **2002**, *74*, 2556-2564.
- (73) Balss, K. M.; Ross, D.; Begley, H. C.; Olsen, K. G.; Tarlov, M. J. *Journal of the American Chemical Society* **2004**, *126*, 13474-13479.
- (74) Balss, K. M.; Vreeland, W. N.; Phinney, K. W.; Ross, D. *Analytical Chemistry* **2004**, *76*, 7243-7249.
- (75) Munson, M. S.; Meacham, J. M.; Ross, D.; Locascio, L. E. *Electrophoresis* **2008**, *29*, 3456-3465.

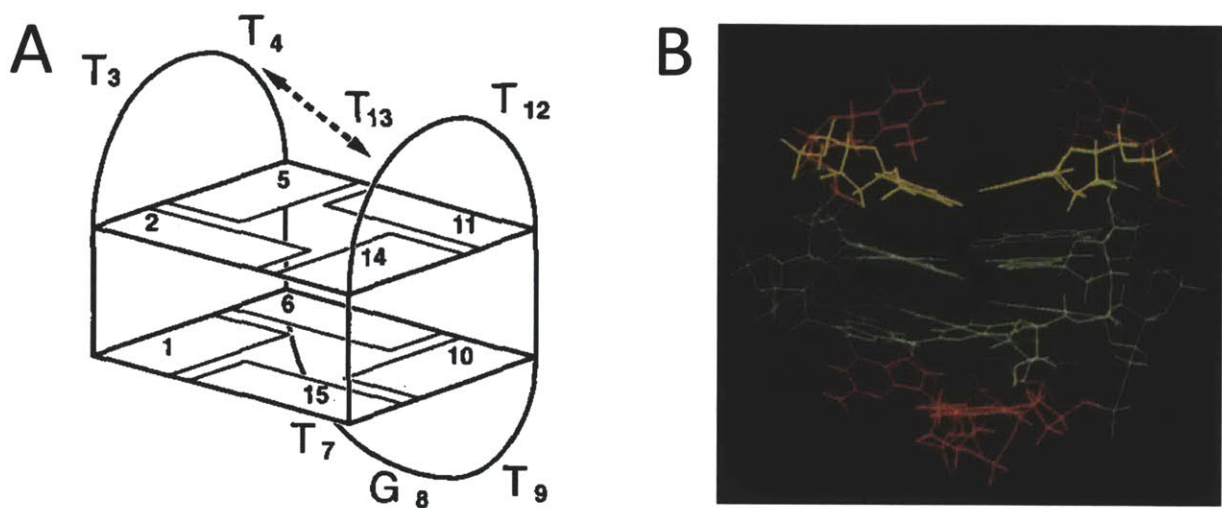
Chapter 2

Concentration-Enhanced Mobility Shift Assay Platform for Aptamer-Based Biomarker Detection

In this chapter, we describe a continuous signal amplification scheme for homogeneous mobility shift assays. This is achieved by simultaneously concentrating and separating bound and unbound molecules (with different electrophoretic mobilities) in a microfluidic device. The utility of this platform is demonstrated in the context of an electrokinetic concentration-enhanced aptamer affinity probe electrophoresis assay to achieve highly sensitive and quantitative detection of protein biomarkers. The key weaknesses of aptamer as a binding agent (weak binding strength/fast target dissociation) were counteracted by continuous injection of fresh sample while band-broadening phenomena were minimized due to self-focusing effects. Within 30 minutes of continuous signal enhancement, we can detect 4.4 pM human Immunoglobulin E (IgE) and 9 pM Human Immunodeficiency Virus 1 Reverse Transcriptase (HIV-1 RT), which are among the lowest limits of detection (LOD) reported. IgE was detected in serum sample with a LOD of 39 pM due to nonspecific interactions between aptamers and serum proteins.

2.1 Aptamers as affinity agents in diagnostics platforms

The issue of affinity agent is a bottleneck in developing robust, affordable and standardized diagnostic platforms. For decades, antibody-based immunoassays have been used for disease diagnosis that requires highly specific and sensitive recognition elements. However, production of antibodies is an expensive and laborious process that involves immunizing host animals and developing hybridoma cell lines. Antibodies are also prone to denaturing at ambient conditions and often subjected to batch-to-batch variations, thus complicating their use in point-of-care diagnostic platform.



Thrombin binding aptamer: 5'-GGTTGGTGTGGTTGG-3'

Figure 2.1: a) Schematic model, and b) 3-dimensional structure of the thrombin binding aptamer. The highlighted bases form the G-quadruplex secondary structure. (Adapted from works of Schultze *et al.*¹)

Recently, aptamers are emerging as an increasingly popular alternative to antibodies as affinity probe in analytical applications. Aptamers are single-stranded oligonucleotides that have undergone multiple round of *in vitro* selection to bind specifically to various molecular targets^{2,3}. **Figure 2.1** shows an example of a 15 base pair DNA aptamer with secondary G-quadruplex structures that binds to human thrombin protein¹. As binding agents, aptamers can rival antibodies in terms of sensitivity and selectivity. A major advantage of aptamers compared to antibodies is the low cost, since aptamers are synthesized chemically whereas antibodies are produced from animals or hybridoma cell lines⁴. Unlike protein-based binding agents, aptamers can also be stored in harsh environment without permanently denaturing⁴. Finally, various functional groups can be easily attached to aptamers during synthesis with excellent batch-to-batch uniformity. With these features, aptamers are very attractive candidates for developing point-of care biosensors. Recently, more than 800 aptamers have been generated against proteins that are potential biomarkers⁵. These are promising signs that aptamer biosensors will find widespread applications.

Various kinds of aptamer-based biosensors, both homogeneous and heterogeneous assays, have been reported in the literature. In heterogeneous assays, aptamers are immobilized on a solid surface to selectively capture target molecules from the sample. These include electrochemical assays^{6, 7} and sandwich assays⁸ where the captured target protein is detected by a secondary fluorescent or enzyme labeled aptamer. Label-free detection is also possible with surface-plasmon resonance^{9, 10} or quartz crystal microbalance¹¹ techniques. On the other hand, aptamers and target molecules react in solution phase in homogeneous assays. These include assays using structure-switching aptamers that change fluorescence when they bind to the target^{12, 13}, electrophoresis based methods which can separate bound and unbound aptamers^{14, 15}, and techniques which rely on polymerase chain reaction (PCR) such as proximity ligation assays¹⁶.

Comparing between heterogeneous and homogeneous aptamer biosensors, the heterogeneous aptamer assays are usually very sensitive because the signal can be amplified by enzymes. However, these sensors require multiple washing steps and binding kinetics of target molecules to surface bound aptamers is slow. There is also potential loss of aptamer binding activity after surface immobilization and the inherent difficulty of generating two aptamers against distinct epitopes on a target biomarker to be used in a sandwich assay format. On the other hand, the homogeneous assays are very easy to use and have fast binding kinetics, but usually have lower sensitivity and many of the structure-switching type assays require customization for each aptamer-target binding pair. The homogeneous aptamer assays are attractive candidates as point-of-care biosensor platforms because they are fast and simple to use. However, the bottleneck that prevents their widespread application is the limited sensitivity. A general signal amplification scheme that can increase the sensitivity of homogeneous aptamer assays would greatly expand their utility.

2.2 Electrokinetic concentration as a signal amplification module for aptamer affinity probe electrophoresis assay

Among the homogeneous aptamer biosensors, capillary electrophoresis (CE) based methods which can separate bound and unbound aptamers have been widely used to detect specific target proteins such as IgE^{14, 17, 18}, thrombin^{14, 19}, ricin¹⁵, and HIV-1 reverse transcriptase (HIV-1 RT)^{17, 20, 21}. Unlike heterogeneous immunoassay methods such as ELISA that require several hours and multiple washing steps, the homogeneous CE assay is performed in one step with only a short incubation time (≤ 30 minutes). However, CE assays are generally less sensitive than ELISA due to the ability of enzymes in ELISA to continuously convert a substrate to visible product over time. Furthermore, band dispersion and complex dissociation when using lower affinity (high K_d) aptamers limits their applicability to detect low abundance biomarkers.

As described in Chapter 1, the readout sensitivity of homogeneous assays can be improved by physically preconcentration. In the context of aptamer-based CE analysis, sample preconcentration has been reported in the forms of sample sweeping¹⁹, preconcentration using a size-exclusion membrane¹⁸, transient isotachopheresis (t-ITP)²², and temperature gradient focusing (TGF)²³. Preconcentration and separation were carried out sequentially in the first two cases, thus the detection sensitivity was limited by band-broadening during the separation step. The t-ITP method required multiple buffer arrangements and concentration factor was limited by injected plug volume. In the TGF example, special temperature sensitive buffer was needed and higher limit of detection (LOD) was expected since detection was based on monitoring a small decrease in the large free aptamer peak. In all these examples, high voltages of ≥ 1 kV are required.

The Han group has previously reported on nanofluidic electrokinetic concentration devices that can continuously collect negatively charged molecules in a given sample into a much smaller volume, thereby increasing local concentration significantly²⁴. Electrokinetic concentration is particularly amenable to lab-on-chip applications as it has been demonstrated to accomplish very high concentration

factors and does not require complicated setup such as high voltage, multiple buffer arrangements and temperature control schemes. This principle has been used successfully in several approaches to realize ultra-high sensitivity immunoassays. In the first instance, by using an electrokinetic concentrator to increase the local concentration of target molecules around antibody-conjugated beads, the primary immunobinding kinetics and assay sensitivity are greatly improved²⁵. In another method, an electrokinetic concentrator is used to enhance the readout sensitivity of ELISA by accumulating the fluorescent turnover products from target-bound enzymes²⁶. Both these platforms, however, are examples of heterogeneous immunoassays. Continuous physical amplification for homogeneous binding assays has not been demonstrated to date as it would require the additional capability of separating bound from unbound analytes in solution phase at the same time.

In this chapter, we describe an electrokinetic concentration device that can simultaneously concentrate and separate biomolecules based on mobility differences. This device is used to improve the sensitivity of an aptamer affinity probe electrophoresis assay. This scheme features three simultaneous processes: 1) continuous injection, 2) focusing, and 3) separation of the free aptamers and aptamer-protein complexes. One of the significant disadvantages of aptamer affinity probe CE is that complex may dissociate during long migration times, leading to weak or even absence of signal²⁷. Decreasing the time spent on column, either by applying very high electric fields or utilization of hydrodynamic flow was often necessary to achieve reliable detection of the aptamer-protein complex²⁷. In this new scheme, we counteract dissociation of the aptamer-protein complex by continuous injection and accumulation of fresh sample from the inlet reservoir. Band broadening phenomena commonly encountered in CE are also minimized due to the self-focusing effect. When a continuous flux of sample from the equilibrium mixture in the reservoir is subjected to simultaneous focusing and separation the signal-to-noise ratio increases with time. A good signal enhancement scheme is the key to highly sensitive assays such as ELISA. The scheme presented here presents an opportunity to enhance the signal in homogeneous mobility shift assay for better sensitivity.

As a proof of concept, we demonstrate the use of electrokinetic concentration-enhanced aptamer affinity probe electrophoresis assays for two different disease biomarkers, namely human Immunoglobulin E (IgE) and Human Immunodeficiency Virus 1 Reverse Transcriptase (HIV-1 RT). IgE is the least abundant class of antibodies produced in human, and plays an important role in generating allergic response as well as defending against parasites^{28, 29}. Some recent studies have suggested the use of serum IgE as a predictive biomarker for diseases such as asthma and peanut allergy^{29, 30}. On the other hand, HIV-1 RT is a key diagnostic and therapeutic target of HIV-1^{31, 32}. Many aptamer based sensor have been used to detect IgE with different LOD, these include methods based on fluorescence enhancement (57 pM)^{33, 34}, carbon nanotube field effect transistors (250 pM)³⁵, surface plasmon resonance (18.5 pM)¹⁰, CE (46 pM)^{14, 17, 18} and aptamer microarray using labeled IgE (10 pM)^{36, 37}. Meanwhile, for detection of HIV-1 RT, the methods reported are predominantly based on CE (100 pM)^{17, 20, 21}, temperature gradient focusing (84 pM), transient isotachopheresis (<1 pM) and CE followed by PCR (30 fM). It is worth noting that the LOD reported is dependent on detection instruments and the affinity of the particular aptamers, and that coupling separation with amplification step often leads to dramatic increase in sensitivity.

Using our platform, we obtained LOD of 4.4 pM and 9 pM for human IgE and HIV-RT respectively in simple buffer after 30 minutes preconcentration, compared to LOD of 46 pM¹⁴ and 100 pM¹⁷ obtained with conventional CE methods. These are the lowest assay LOD reported in the literature for aptamer affinity probe capillary electrophoresis in spite of the inferior detector used for our assays (arc lamp and CCD camera) versus Laser Induced Fluorescence and Photomultiplier Tube for CE. To demonstrate the applicability of this assay to complex sample analysis, we performed the assay in 10-fold diluted donkey serum. Initial experiments showed significant nonspecific interaction between DNA aptamers and serum proteins. However, we found that addition of nonspecific and nonfluorescent oligonucleotides largely suppresses the matrix interference, thus enabling us to detect IgE in 10% donkey serum with a LOD of 39 pM.

2.3 Principle of the assay

Figure 2.2 shows the key operation of the poly(dimethylsiloxane) (PDMS) microfluidic electrokinetic concentration chip. The basic device consists of two microchannels connected by a cation selective channel that allows the flow of positively charged ions (cations) but impedes the flow of negatively charged ions (anions). Cation selective channels in microfluidics systems have been realized in the form of glass nanochannels where the overlap between Debye layers can exclude coions, or in the form of ion-selective membranes such as Nafion where the presence of highly negatively charged chemical side groups strongly impedes the flow of anions. Under the voltage configuration shown in **Figure 2.2a**, cations can electromigrate from the top to bottom microchannel, but the passage of anions from the bottom to top microchannel is blocked. As a result, a region depleted of both anions and cations is created in the top microchannel at the vicinity of the cation selective channel in a process known as concentration polarization. The conductivity gradient at the boundary of the ion depletion zone gives rise to a stable electric field gradient. When a sample is injected into this microchannel with a constant bulk flow (due to hydrodynamic pressure or electroosmotic flow), the negatively charged biomolecules will experience an opposing electromigration velocity proportional to the electric field and their electrophoretic mobilities. As shown schematically in **Figure 2.2b**, the biomolecules stop moving and focus at the location where the electrophoretic velocity balances the bulk velocity. Free aptamers, which have very high electrophoretic mobilities due to the highly negative-charged backbone of the oligonucleotide, are concentrated at the low electric field region. On the other hand, the aptamer-protein complex has a lower mobility due to its larger mass; therefore it concentrates nearer to the cation selective membrane where the electric field is higher. In this way, bound and unbound aptamers can be simultaneously separated and concentrated to facilitate sensitive measurement of the target protein in the sample.

Conventional aptamer affinity probe CE operate in a nonequilibrium condition, since there are no targets in the run buffer that allow for rebinding of aptamers that have dissociated from their initial target during separation. A unique advantage of this platform is that the free target protein molecules are able to travel downstream beyond the concentrated aptamer-protein complex band (an even higher electric field

is needed to stop the low mobility free protein). Therefore, aptamers that have dissociated from their target in the complex band can quickly rebind with free proteins in the run buffer and regenerate the complex, akin to the Equilibrium Capillary Electrophoresis of Equilibrium Mixtures (ECEEM)³⁸ where a plug of equilibrium aptamer-target mixture is injected and separated in a capillary prefilled with target. This is an important advantage which allows even aptamers with relatively high K_d 's to be used in this platform with good sensitivity. Using this device, we realized a multiplexed microfluidic platform where homogeneous aptamer affinity probe electrophoresis assays can be performed with low voltages (30V) and gravitation-induced flow without the need of periphery equipments (syringe pumps, temperature blocks) or multiple buffers.

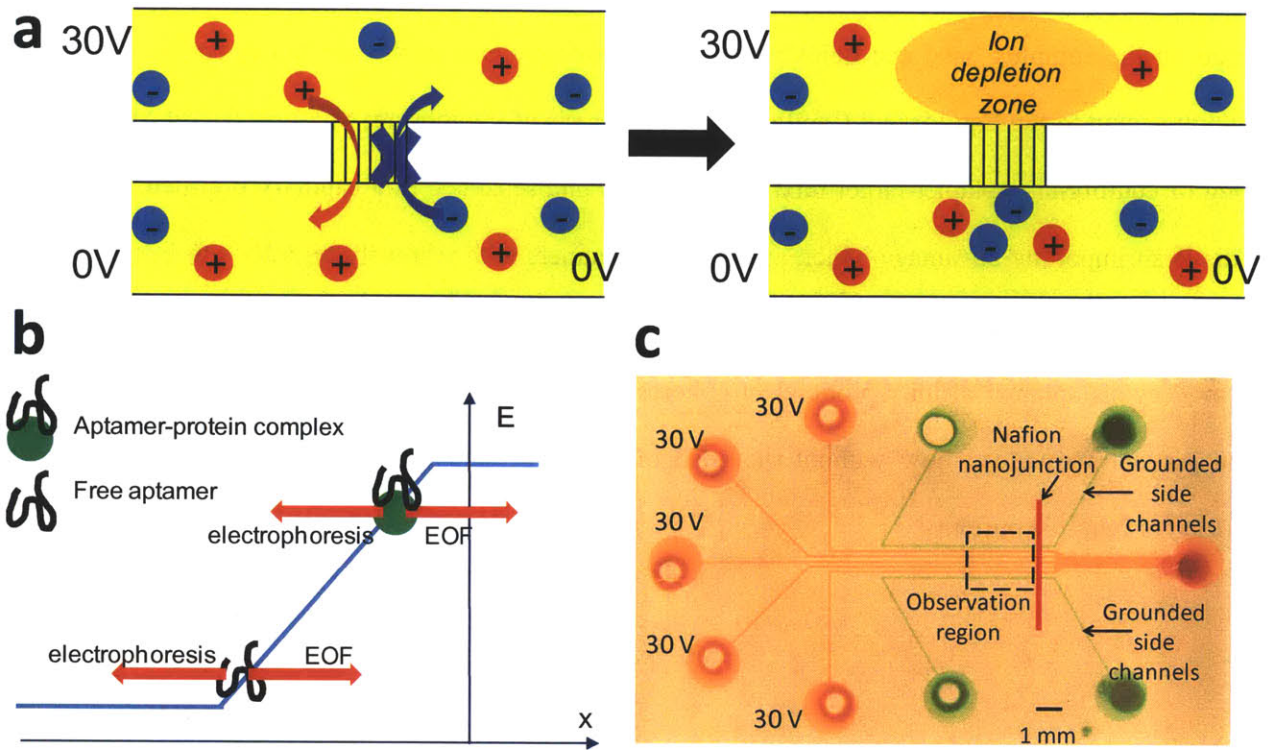


Figure 2.2: a) Ion selective membrane creates a local ion depletion zone with high electric field upon applying a voltage, b) Free aptamers and aptamer-protein complex concentrate at different locations on the electric field profile due to their different electrophoretic mobility, c) Optical image of multiplexed PDMS device with 200 μm wide surface patterned Nafion thin film on glass substrate. Sample channels and side channels are filled with red and green dyes respectively. Experimental images are taken at the observation region.

2.4 Experimental section

2.4.1 Reagents and chemicals

Unless stated otherwise, all chemicals used in the experiments were purchased from Sigma (St. Louis, MO). Human myeloma IgE was purchased from Athens Research and Technology, Inc. (Athens, GA). Recombinant HIV-1 reverse transcriptase (HIV-1 RT) was purchased from Worthington Biochemical Corporation (Lakewood, NJ). Oligonucleotides were synthesized and fluorescently labeled by Integrated DNA Technologies, Inc. (Coralville, IA). IgE-binding aptamer (5'-GGG GCA CGT TTA TCC GTC CCT CCT AGT GGC GTG CCC C-3') was labeled with 6-carboxyfluorescein (FAM) during synthesis at the 5' end using ethylene glycol linker¹⁴. HIV-1 RT-binding aptamer (5'-AT CCG CCT GAT TAG CGA TAC TCA GAA GGA TAA ACT GTC CAG AAC TTG GA-3') was labeled directly at the 5' end with FAM¹⁷. Nonfluorescent nonspecific oligonucleotides (5'-TGG TCT TGT GTG GCT GTG GCT ATG TCT GAT CTT AAT CCA CGA AGT CAC C-3')¹⁷ were also obtained from the same source. Donkey serum was purchased from Innovative Research (Novi, MI). All solutions were made with deionized water (18.2M Ω) by Fluid Solutions (Lowell, MA).

2.4.2 Microchip fabrication

The microchip was fabricated using poly(dimethylsiloxane) PDMS (Sylgard 184, Dow Corning Inc., Midland, MI) irreversibly bonded on a glass slide. Microchannels were molded in PDMS by replica molding technique¹⁶. To obtain the positive master mold, the desired design was photolithographically patterned onto a silicon wafer using positive photoresist. Next, the wafer was etched to a depth of 6 μ m via a reactive ion etching (RIE) process. The silicon master was further treated with trichlorosilane (T2492, UCT Specialties, Bristol, PA) in a vacuum desiccator overnight to prevent adhesion to PDMS.

We fabricated the ion-selective nanoporous structures by using the microflow patterning technique to obtain a thin strip of Nafion film on a standard glass slide^{17, 18}. A 50 μ m deep and 200 μ m wide PDMS microchannel was used to define the flow path of the Nafion solution (20 wt% solution in lower aliphatic alcohol/H₂O mix, Sigma Aldrich, St. Louis, MO). The PDMS chip with microchannels was irreversibly bonded on top of the glass slide by standard plasma bonding.

Figure 2.2c showed the top view of the actual PDMS device used in the experiments. 0.1-10 μL pipette tips (USA Scientific, Ocala, FL) were cut at the tip end with a razor blade and inserted into the punched PDMS holes to act as fluid reservoirs. There were five separate inlets connecting to one outlet, allowing five samples to be preconcentrated simultaneously. Two side channels flanked the inlet channels to provide symmetrical electrical ground. The ion-selective nanojunction was fabricated at the center of the device to concentrate sample molecules by electrokinetic trapping when voltages are applied. The channels were filled with dyed solution for visualization purpose.

2.4.3 Microchip operation

Before the experiment, the PDMS device channels were passivated with 1% bovine serum albumin (BSA) for 10 minutes to reduce nonspecific binding of the sample to channel walls. After that, the channels were flushed with DI water 3 times and filled with buffer solution (10 mM Tris-HCl, pH 7.4) until the samples were ready to be loaded. Sample was prepared by mixing 5 nM of fluorescently labeled aptamer with different concentrations of analyte in buffer solution (10 mM Tris-HCl, 1 mM MgCl_2 , 200 $\mu\text{g}/\text{mL}$ BSA, pH 7.4 (IgE)/ pH 8(HIV-1 RT)).

After 30 minutes incubation at room temperature, 30 μL of sample was loaded into each of the five inlet reservoirs and drawn into the microchannel by applying a brief suction at the outlet reservoir. The liquid height difference between the inlet reservoir and the empty outlet reservoir caused a well-controlled gravitational flow of sample solution from inlet to outlet, without any need for external pump.

Electrodes were inserted into the inlet and buffer reservoirs on the chip and connected to a power supply (Stanford Research Systems, Sunnyvale, CA). To initiate the concentration-enhanced affinity probe electrophoresis assay, we applied 30 V at the inlet reservoirs while grounding the side channels. An ionic concentration gradient was induced near the ion-selective membrane by concentration polarization effect. Meanwhile, charged sample molecules are continuously separated and stacked at the location where its electrophoretic velocity equals the bulk flow velocity. Within the experimental duration of 30 minutes, the fluorescent intensity of the stacked molecules increases linearly with time while background noise remained constant, resulting in a high signal-to-noise ratio. To study the reproducibility of the

assay, we repeated the experiment in the same device after removing the contents in the inlet reservoirs and replacing them with new samples.

2.4.4 Measurement instrument and image analysis

An inverted epifluorescence microscope IX 71 (Olympus, Center Valley, PA) equipped with a cooled CCD camera (SensiCam, Cooke Corp., Romulus, MI) was used for fluorescence imaging. A mechanical shutter which only opens for 100 ms every 5 s when images are taken was used to prevent photobleaching of the fluorescent molecules. The images were analyzed using the NIH ImageJ software. Flat-field correction was performed by dividing a reference image of the device taken before each experiment. Concentrations of bound and unbound aptamers were assumed to be directly proportional to the focused peak height as demonstrated in previous work²³. Complex peak heights are normalized by the sum of complex peak height and free aptamer peak height. Dose response curves were fitted using a four-parameter logistic model. Origin 7 software (OriginLab Corp., Northampton, MA) was used for curve fitting.

2.5 Optimization of assay

We first determined the optimal conditions that promote stable aptamer-protein complex formation in free solution. The presence of divalent cations such as Mg^{2+} has been reported to be necessary for certain aptamer-protein complex formation³⁹. Without Mg^{2+} , no aptamer-IgE complex was formed while the aptamer-HIVRT complex band was only weakly fluorescent. Addition of 1 mM of $MgCl_2$ greatly improved the interaction between the species. We have also found that complex stability is a sensitive function of buffer pH. Best results were obtained in 10 mM Tris-HCl buffer at pH 7.4 and pH 8.0 for IgE and HIV-1 RT assays respectively.

In initial experiments, aptamer and target proteins (IgE and HIV-1 RT) were simultaneously concentrated and separated in bare PDMS-glass devices. We observed no complex bands until high concentrations (> 10 nM) of target proteins are added. Precoating the microchannels with 1% BSA for 10 minutes enabled us to clearly visualize the complex band corresponding to 750 pM of IgE (**Figure 2.3a**), suggesting that prevention of nonspecific adsorption of proteins to the microchannel surface is important to increase sensitivity. Precoating microchannel with 5% BSA did not lead to additional improvement in sensitivity. Interestingly, as shown in **Figure 2.3**, adding BSA into the sample increases sensitivity of the assay. Adding 50 $\mu\text{g/mL}$ of BSA led to a clear complex band corresponding to 75 pM of IgE, while addition of 100 $\mu\text{g/mL}$ of BSA to the sample enabled detection of 7.5 pM of IgE. No further sensitivity improvement was obtained when more than 200 $\mu\text{g/mL}$ of BSA was added to the sample. Similar trends were observed with the HIV-1 RT assays. This observation is thought to be due to BSA stabilizing the aptamer-protein complex⁴⁰. Based on previous reports, it has been suggested that the presence of BSA in solution helps maintain the correct aptamer and target protein conformation for optimal binding⁴⁰. Presence of BSA in the solvent could also maintain the ratio of hydrophobic and hydrophilic regions on the target protein, thus preventing it from denaturation⁴¹. Both the IgE and HIV-1 RT specific aptamers did not interact with BSA, as the negative controls containing BSA but no target proteins did not form a visible complex band. In all our subsequent experiments, the microchannel surfaces were passivated with 1% BSA for 10 minutes and 200 $\mu\text{g/mL}$ of BSA were added to the samples to obtain the best sensitivities.

We also observed that the separation distance between the bound and free aptamers increased with the addition of high concentrations of BSA into the sample. We believe that this is due to an isotachopheresis-like effect where preconcentration of an intermediate mobility species (BSA) results in a broadening electric-field plateau that separates the bound and unbound aptamer bands⁴². This suggests a method whereby the separation resolution between two species can be independently tuned by adding a spacer molecule with intermediate mobility in the sample.

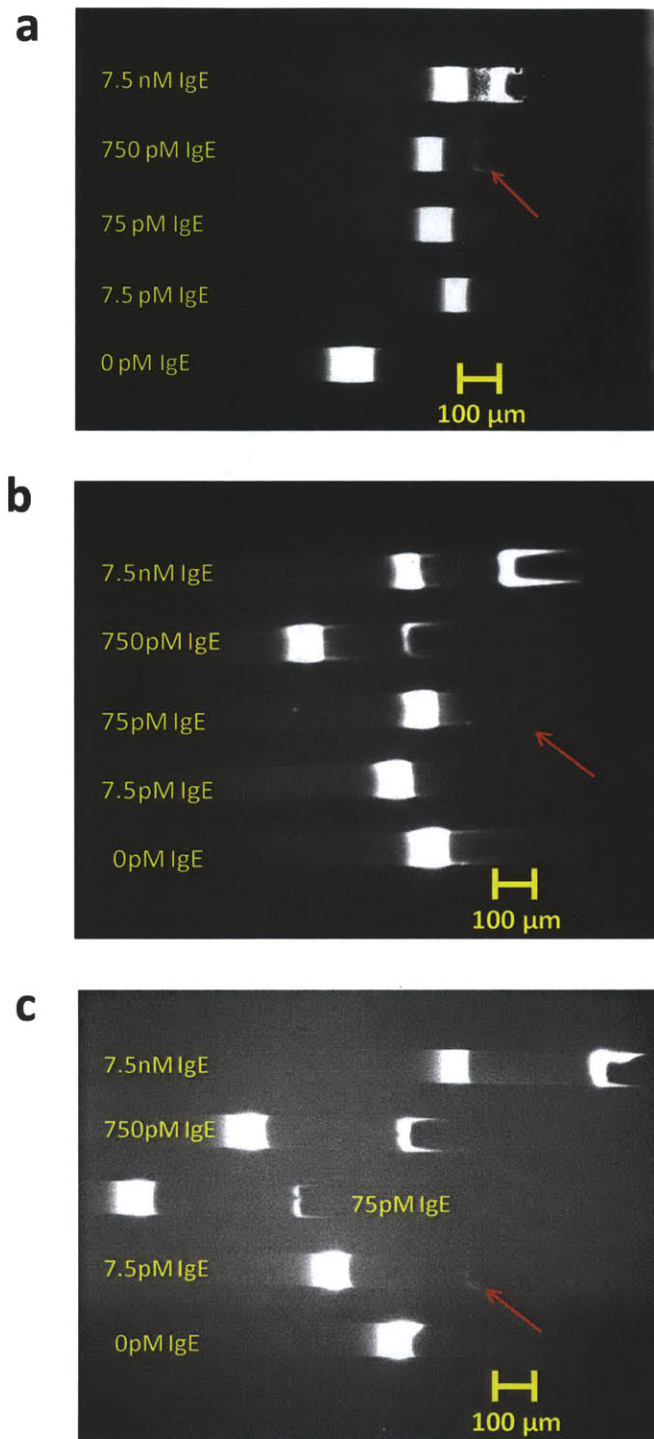


Figure 2.3: Addition of BSA improved detection of IgE in buffer using concentration-enhanced aptamer affinity probe electrophoresis assay. a) no BSA in sample (cannot detect 75 pM IgE), b) 50 μ g/mL BSA in sample (can detect 75 pM IgE), c) 100 μ g/mL BSA in sample (can detect 7.5 pM IgE).

2.6 Detection of IgE and HIV-1 RT from buffer

We first demonstrate electrokinetic concentration-enhanced affinity probe electrophoresis assay of IgE using a specific aptamer for this protein. Upon binding to IgE, the mobility of a free aptamer ($-2.81 \times 10^{-4} \text{ cm}^2 \text{ V}^{-1} \text{ s}^{-1}$) is expected to shift to $-0.58 \times 10^{-4} \text{ cm}^2 \text{ V}^{-1} \text{ s}^{-1}$ ¹⁷. **Figure 2.4** shows the representative results for electrokinetic concentration-enhanced affinity probe electrophoresis assay for human IgE using anti-IgE aptamer as affinity probe. Experiments were performed in optimized buffer conditions (10 mM Tris-HCl, pH 7.4, 1 mM MgCl₂, 200 μg/mL BSA) with constant aptamer concentration (5 nM) and varying concentrations of human IgE protein (5 pM to 75 nM). During the 30 minutes experiment, the fluorescent intensity of the bands increased linearly with time and achieved concentration factors of >1000. The aptamer and complex bands were well-resolved (resolution~3.9). The position of the aptamer-protein band was also remarkably stable; moving less than 200 μm after it reached an equilibrium position at around 2 minutes. Slight variations in the band locations are due to differences in gravitation-induced flow, but the ratiometric assay results are relatively insensitive to the exact band locations. As expected, with increasing target protein concentration, the free aptamer peak decreased and the complex peak increased. **Figure 2.5b** shows the aptamer-protein complex peak due to 4.92 pM of IgE. For comparison, no complex band was observed in the negative control experiment.

The full dynamic range of the assay is shown in **Figure 2.5c**. The dose response curve was fitted using the four-parameter logistic model. The average and standard deviation of the zero dose response was calculated by performing two separate experiments where the sample contains no IgE, and taking the peak ratios as described in the methods section. **Figure 2.5d** shows a linear relationship in the log-log plot obtained at low IgE concentrations (5 pM – 7 nM). The LOD for IgE, calculated to be the analyte concentration needed to produce a signal three standard deviations above the zero dose response, is 4.4 pM. This is the lowest LOD reported to date for detection of IgE using aptamers. Interestingly, the apparent K_d (1.85 nM) is found to be more than an order of magnitude lower than the reported dissociation constant for this aptamer (64 nM)¹⁴. One possible explanation for this binding enhancement is that aptamer-protein rebinding events in the electrokinetic concentration zone more than offset the

effect of dissociation during the experiment. Given that aptamers generally have higher K_d compared to antibodies, this scheme could significantly increase the sensitivity and utility of aptamer based assay.

Similar experiments were performed using Human Immunodeficiency Virus 1 Reverse Transcriptase (HIV-1 RT) and an aptamer against this protein to demonstrate that this method is general and can be applied to multiple analytes. Upon binding to IgE, the mobility of a free aptamer ($-2.81 \times 10^{-4} \text{ cm}^2 \text{ V}^{-1} \text{ s}^{-1}$) is expected to shift to $-0.50 \times 10^{-4} \text{ cm}^2 \text{ V}^{-1} \text{ s}^{-1}$ ^{14, 17}. The results (**Figure 2.6**) showed a LOD of 9 pM, which is also among the lowest LOD reported to date for this aptamer-protein pair.

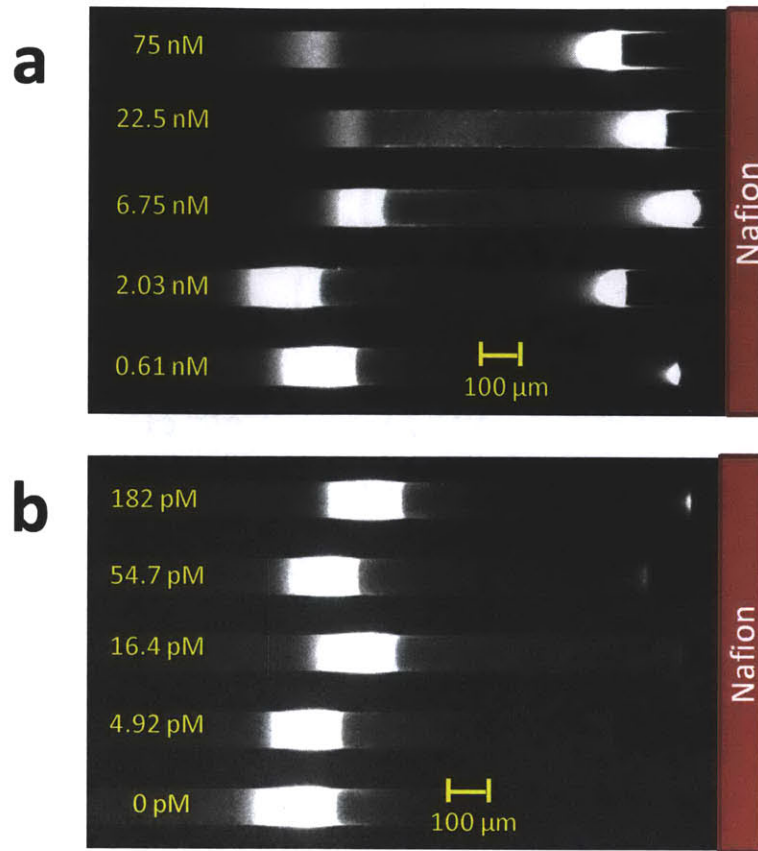


Figure 2.4: Experimental results for multiplexed concentration enhanced aptamer affinity probe electrophoresis assay for detecting a) high concentrations, and b) low concentrations of IgE in buffer solution after 30 minutes of concentration.

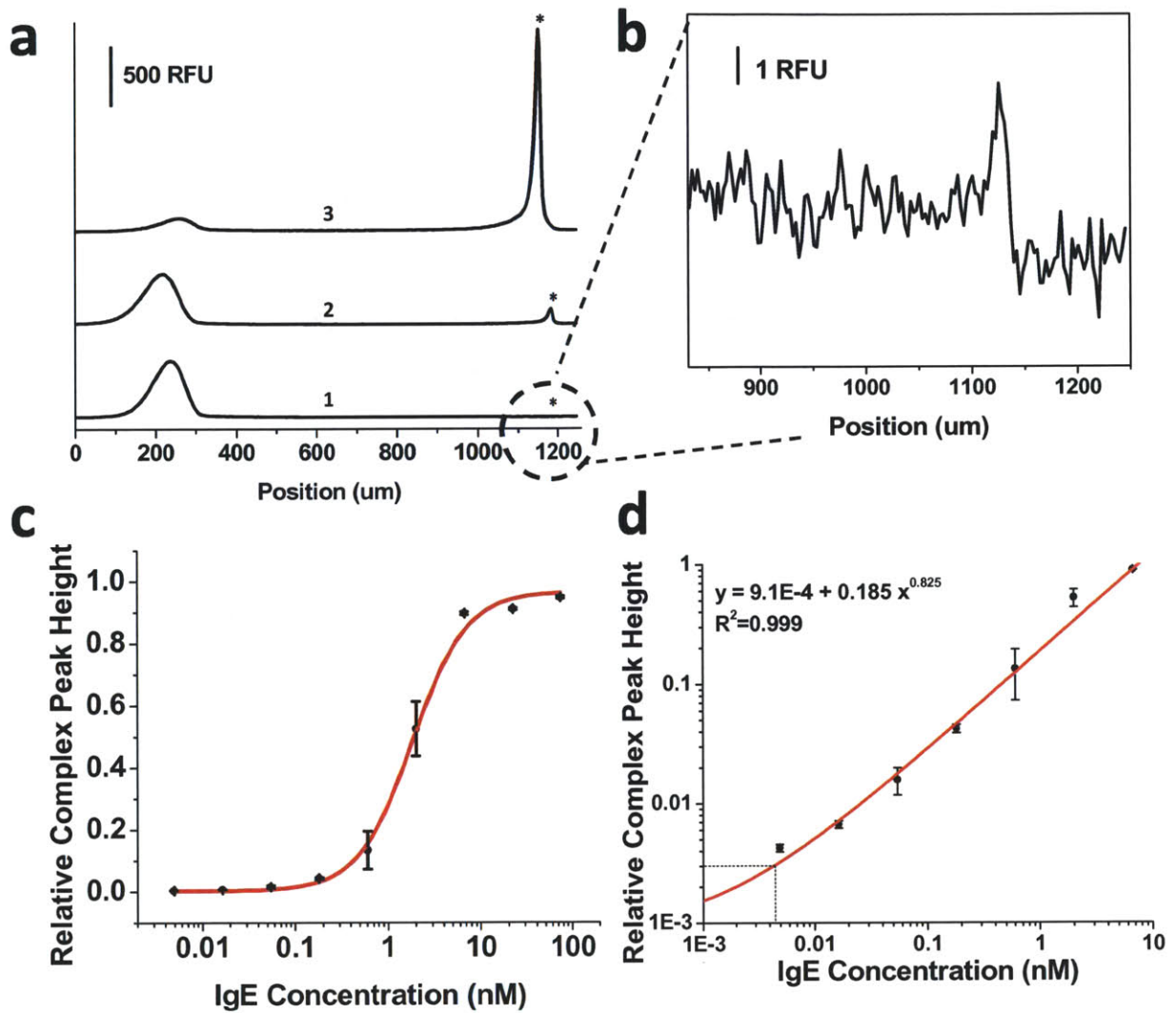


Figure 2.5: a) Electropherogram for optimized electrokinetic concentration and separation of IgE aptamer (5 nM) and different concentrations of IgE: (1) 4.92 pM, (2) 0.6 nM, and (3) 6.75 nM IgE. The complex band is labeled with an asterisk, b) Inset demonstrates detection of 4.92 pM IgE in buffer, c) Dose-response curve of anti-IgE aptamer with IgE spiked in buffer, error bars represent standard error from duplicate experiments, d) Linear relationship in the log-log plot is obtained at low concentrations of IgE. The measured LOD is 4.4 pM IgE.

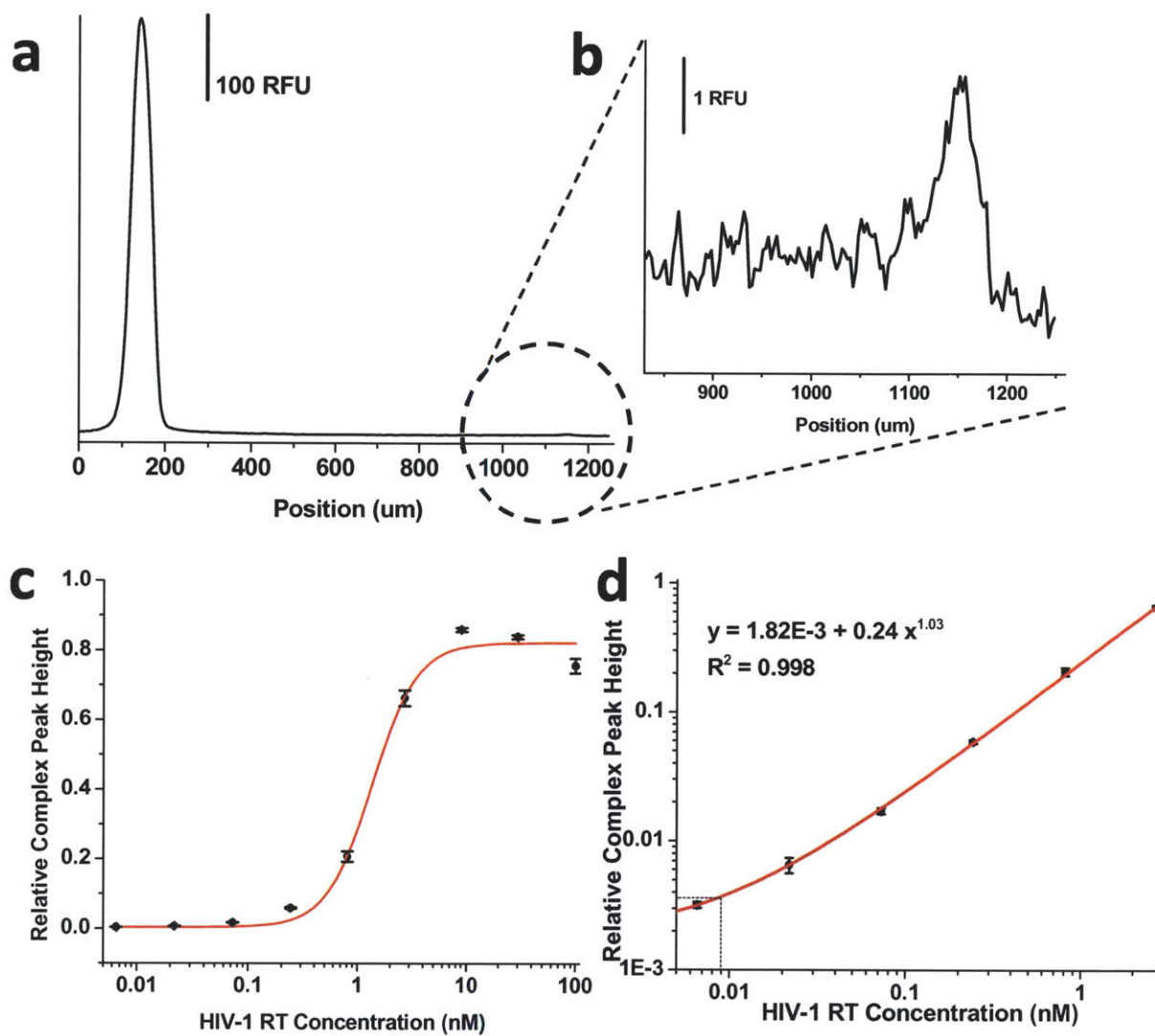


Figure 2.6: a,b) Electropherogram demonstrating detection of 6.5 pM HIV-1 RT in buffer, c) Dose response curve of anti-HIV-1RT aptamer with HIV-RT spiked in buffer, error bars represent standard error from duplicate experiments, d) Linear relationship in the log-log plot is obtained at low concentrations of HIV-1RT, measured LOD is 9 pM HIV-1 RT

2.7 Detection of IgE from serum sample

To demonstrate the applicability of this assay to complex sample analysis, we performed the IgE assay in a buffer that consists of diluted donkey serum. Initial experiments showed significant interactions of serum components with the aptamers. **Figure 2.7** showed a representative IgE assay performed in 1% donkey serum. We observed fluorescent precipitation in the sample solution. Moreover, there is formation of an extra fluorescent band in between the free aptamer and aptamer-protein band. Interestingly, the extra band is well defined and baseline-separated from the other two bands. This suggests that the aptamer is interacting with a particular species in serum, such as DNA binding proteins found in mammalian serum⁴³. Although this interference did not interfere with the formation and determination of the free aptamer and the aptamer-protein complex (they are all baseline separated), the fluorescent precipitation in the sample solution caused large spikes in the electrophoregram.

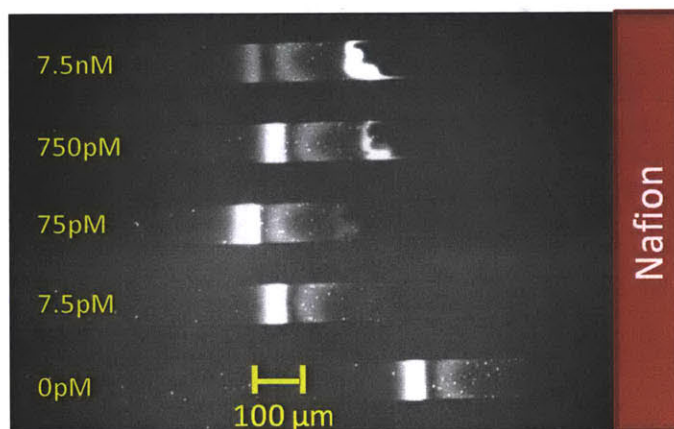


Figure 2.7: Concentration enhanced aptamer affinity probe electrophoresis assay for detecting IgE in sample containing 1% donkey serum. Aptamer binding to serum components gave rise to a third fluorescent band in between the free aptamer and aptamer-target protein band. Fluorescent precipitation is also observed in solution.

It has been reported that serum matrix interference on aptamer affinity probe capillary electrophoresis can be suppressed by addition of nonspecific oligonucleotides that bind competitively to the interfering serum proteins¹⁷. We found that addition of 10 μM of a nonspecific and nonfluorescent 49-mer oligonucleotide¹⁷ eliminated the extra band and fluorescent precipitation in a sample solution containing 10% donkey serum.

Figure 2.8 shows the experimental results for IgE assay in 10% donkey serum after 1 minute preconcentration, with addition of 10 μM of nonspecific oligonucleotide to suppress matrix interference. Due to the high total protein concentration in the sample, preconcentration leads to a rapid broadening of electric field plateau between the free aptamer and the aptamer-protein complex as discussed in the previous section. We can only perform experiments for 2 minutes before the separation distance exceeds the microscope field of view. Due to the shorter preconcentration time, there is less sensitivity enhancement. We obtained a LOD of 39 pM for IgE assay in 10% donkey serum.

The LOD using this scheme is ultimately restricted by the specificity, rather than the affinity (K_d) of the aptamers against the target protein. Experiments in the serum sample showed that two bands were observed even in the case of the negative control (**Figure 2.8b**), which indicated that nonspecific binding was not completely eliminated by addition of nonspecific oligonucleotides. On the other hand, experiments in simple buffer showed that signal-to-noise ratio increased with time. We can obtain better sensitivities at the expense of longer assay time. The key advantage of this technique is a continuous influx of sample that counteracts the effects of dissociation and a self-focusing ability that minimizes band dispersion, so even aptamers with relatively high dissociation constant can be used in this assay.

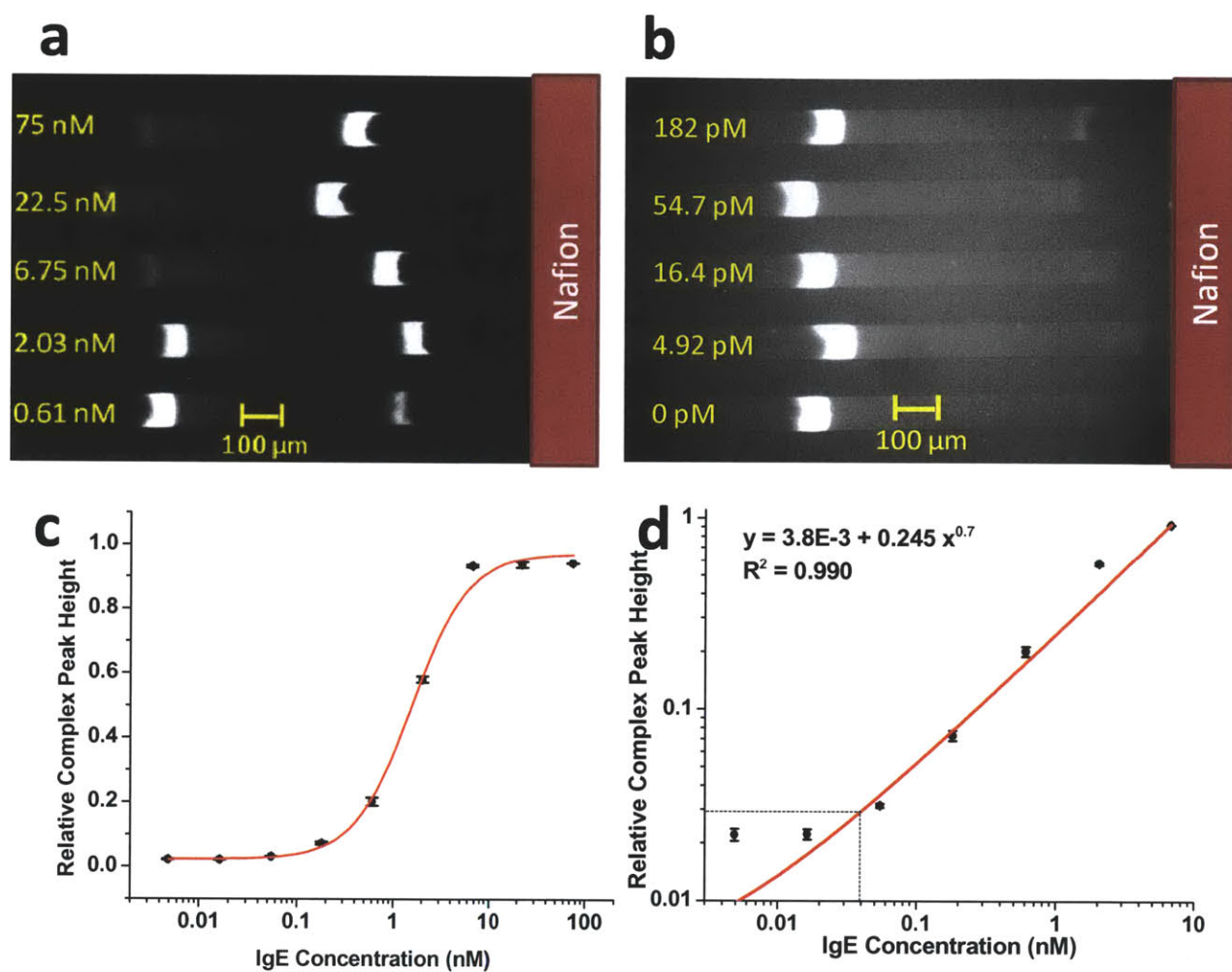


Figure 2.8: a,b) Experimental results for multiplexed concentration enhanced aptamer affinity probe electrophoresis assay for detecting IgE in 10% donkey serum, c) Dose response curve of anti-IgE aptamer with IgE spiked in 10% serum, error bars represent standard error from duplicate experiments, d) Log-log plot at low concentrations of IgE in serum showing effects of nonspecific binding on sensitivity. The measured LOD is 39 pM IgE.

2.8 Summary

In conclusion, this chapter demonstrates the use of electrokinetic concentration to realize a continuous signal amplification scheme that increases the sensitivity of homogeneous mobility shift assay. Aptamers are attractive alternatives to antibodies for point-of-care diagnostics purposes due to their stability, low cost, and homogeneity. Our aptamer based affinity probe electrophoresis assay in a lab-on-chip device could detect 4.4 pM and 9 pM of IgE and HIV-RT in simple buffers, and detect 39 pM of IgE in 10% serum sample. These are among the lowest LOD obtained for aptamer affinity probe capillary electrophoresis experiments. Furthermore, this method has an advantage over many other assays since it is rapid, uses low voltage, consumes very little sample, can be multiplexed, and is very user-friendly (no multiple processing steps required).

Miniaturized capillary electrophoresis devices are one of the first microfluidic systems that gained popular acceptance, and remains a mainstay in lab-on-chip platforms. The method presented in this chapter has broad applicability to improve the sensitivity of various capillary electrophoresis assays, such as those involving protein-protein interactions and enzymatic reactions.

2.9 References

- (1) Schultze, P.; Macaya, R. F.; Feigon, J. *Journal of Molecular Biology* **1994**, *235*, 1532-1547.
- (2) Ellington, A. D.; Szostak, J. W. *Nature* **1990**, *346*, 818-822.
- (3) Tuerk, C.; Gold, L. *Science* **1990**, *249*, 505.
- (4) Jayasena, S. D. *Clinical Chemistry* **1999**, *45*, 1628.
- (5) Gold, L.; Ayers, D.; Bertino, J.; Bock, C.; Bock, A.; Brody, E. N.; Carter, J.; Dalby, A. B.; Eaton, B. E.; Fitzwater, T. *PLoS ONE* **2010**, *5*, e15004.
- (6) Zuo, X.; Song, S.; Zhang, J.; Pan, D.; Wang, L.; Fan, C. *Journal of the American Chemical Society* **2007**, *129*, 1042-1043.
- (7) Lai, R. Y.; Plaxco, K. W.; Heeger, A. J. *Analytical Chemistry* **2007**, *79*, 229-233.
- (8) Kirby, R.; Cho, E. J.; Gehrke, B.; Bayer, T.; Park, Y. S.; Neikirk, D. P.; McDevitt, J. T.; Ellington, A. D. *Analytical Chemistry* **2004**, *76*, 4066-4075.
- (9) Wang, Z.; Wilkop, T.; Xu, D.; Dong, Y.; Ma, G.; Cheng, Q. *Analytical and Bioanalytical Chemistry* **2007**, *389*, 819-825.
- (10) Kim, Y. H.; Kim, J. P.; Han, S. J.; Sim, S. J. *Sensors and Actuators B* **2009**, *139*, 471-475.
- (11) Liss, M.; Petersen, B.; Wolf, H.; Prohaska, E. *Analytical Chemistry* **2002**, *74*, 4488-4495.
- (12) Hamaguchi, N.; Ellington, A.; Stanton, M. *Analytical Biochemistry* **2001**, *294*, 126-131.
- (13) Levy, M.; Cater, S. F.; Ellington, A. D. *ChemBioChem* **2005**, *6*, 2163-2166.
- (14) German, I.; Buchanan, D. D.; Kennedy, R. T. *Analytical Chemistry* **1998**, *70*, 4540-4545.
- (15) Haes, A. J.; Giordano, B. C.; Collins, G. E. *Analytical Chemistry* **2006**, *78*, 3758-3764.
- (16) Fredriksson, S.; Gullberg, M.; Jarvius, J.; Olsson, C.; Pietras, K.; Gústafsdóttir, S. M.; Östman, A.; Landegren, U. *Nature Biotechnology* **2002**, *20*, 473-477.
- (17) Zhang, H.; Li, X. F.; Le, X. C. *Journal of the American Chemical Society* **2008**, *130*, 34-35.
- (18) Hecht, A. H.; Sommer, G. J.; Durland, R. H.; Yang, X.; Singh, A. K.; Hatch, A. V. *Analytical Chemistry* **2010**, 2079-2090.
- (19) Gong, M.; Wehmeyer, K. R.; Limbach, P. A.; Heineman, W. R. *Journal of Chromatography A* **2006**, *1125*, 263-269.
- (20) Pavski, V.; Le, X. C. *Analytical Chemistry* **2001**, *73*, 6070-6076.
- (21) Fu, H.; Guthrie, J. W.; Le, X. C. *Electrophoresis* **2006**, *27*, 433-441.
- (22) Wang, H.; Lu, M.; Le, X. C. *Analytical Chemistry* **2005**, *77*, 4985-4990.
- (23) Munson, M. S.; Meacham, J. M.; Ross, D.; Locascio, L. E. *Electrophoresis* **2008**, *29*, 3456-3465.
- (24) Wang, Y. C.; Stevens, A. L.; Han, J. *Analytical Chemistry* **2005**, *77*, 4293-4299.
- (25) Wang, Y. C.; Han, J. *Lab Chip* **2008**, *8*, 392.
- (26) Cheow, L. F.; Ko, S. H.; Kim, S. J.; Kang, K. H.; Han, J. *Analytical Chemistry* **2010**, *82*, 3383-3388.
- (27) Buchanan, D. D.; Jameson, E. E.; Perlette, J.; Malik, A.; Kennedy, R. T. *Electrophoresis* **2003**, *24*, 1375-1382.
- (28) Gould, H. J.; Sutton, B. J.; Beavil, A. J.; Beavil, R. L.; McCloskey, N.; Coker, H. A.; Fear, D.; Smurthwaite, L. *Annual Review of Immunology* **2003**, *21*, 579.
- (29) Burrows, B.; Martinez, F. D.; Halonen, M.; Barbee, R. A.; Cline, M. G. *New England Journal of Medicine* **1989**, *320*, 271-277.
- (30) Roberts, G.; Lack, G. *Journal of Allergy and Clinical Immunology* **2005**, *115*, 1291-1296.
- (31) Fiscus, S. A.; Cheng, B.; Crowe, S. M.; Demeter, L.; Jennings, C.; Miller, V.; Respass, R.; Stevens, W. *PLoS Medicine* **2006**, *3*.
- (32) Osborne, S. E.; Matsumura, I.; Ellington, A. D. *Current Opinion in Chemical Biology* **1997**, *1*, 5-9.
- (33) He, J. L.; Wu, Z. S.; Zhang, S. B.; Shen, G. L.; Yu, R. Q. *Analyst* **2009**, *134*, 1003-1007.
- (34) Gokulrangan, G.; Unruh, J. R.; Holub, D. F.; Ingram, B.; Johnson, C. K.; Wilson, G. S. *Analytical Chemistry* **2005**, *77*, 1963-1970.

- (35) Maehashi, K.; Katsura, T.; Kerman, K.; Takamura, Y.; Matsumoto, K.; Tamiya, E. *Analytical Chemistry* **2007**, *79*, 782-787.
- (36) Cho, E. J.; Collett, J. R.; Szafranska, A. E.; Ellington, A. D. *Analytica Chimica Acta* **2006**, *564*, 82-90.
- (37) Stadtherr, K.; Wolf, H.; Lindner, P. *Analytical Chemistry* **2005**, *77*, 3437-3443.
- (38) Drabovich, A.; Berezovski, M.; Sergey, N. *Journal of the American Chemical Society* **2005**, *127*, 11224-11225.
- (39) Wiegand, T. W.; Williams, P. B.; Dreskin, S. C.; Jouvin, M. H.; Kinet, J. P.; Tasset, D. *Journal of Immunology* **1996**, *157*, 221.
- (40) Wang, H.; Lu, M.; Weinfeld, M.; Le, X. C. *Analytical Chemistry* **2003**, *75*, 247-254.
- (41) Melnikova, Y. I.; Odintsov, S. G.; Kravchuk, Z. I.; Martsev, S. P. *Biochemistry (Moscow)* **2000**, *65*, 1256-1265.
- (42) Quist, J.; Janssen, K. G. H.; Vulto, P.; Hankemeier, T.; van der Linden, H. J. *Analytical Chemistry* **2011**, *83*, 7910-7915.
- (43) Thoburn, R.; Hurvitz, A. I.; Kunkel, H. G. *Proceedings of the National Academy of Sciences* **1972**, *69*, 3327.

Chapter 3

Differential Concentration of Biomolecules using Herringbone Nanofilter Array

**The work presented in this chapter was done in collaboration with Hansen Bow, who designed and fabricated the devices*

In Chapter 2, we have described a method whereby simultaneous focusing and separation of bound and unbound molecules can lead to an ultrasensitive homogeneous aptamer-based biomarker detection method¹. Separation of the analytes of interest is based on electrophoretic mobility difference, which is significant when small, highly negatively charged aptamers bind to relatively larger target proteins. To our knowledge, the method presented is the first reported signal amplification technique applicable to a broad class of homogeneous electrophoretic mobility shift assays.

However, not all biomolecular interactions lead to detectable and predictable changes in their electrophoretic mobility. For example, the free solution electrophoretic mobility of DNA is essentially size independent², while the interactions of near-neutral biomolecules often result in negligible mobility shifts. To extend the concept of signal amplification to a broader range of homogeneous biological assays, we are also interested in exploring alternative physical principles that can lead to simultaneous fractionation and concentration of analytes.

In this chapter, we introduce a microfabricated anisotropic sieving structure consisting of a herringbone nanofilter array (HNA). The structural anisotropy of the HNA causes different sized biomolecules to follow different migration trajectory. In addition, the HNA also redirect large biomolecules to focus at particular positions in the device, leading to continuous flow biomolecule concentration. We will show how we make use of these phenomena to interrogate biomolecular interactions, including protein-DNA binding, protein-protein interaction and antibody-antigen binding.

The final example demonstrates a novel method to perform homogeneous immunoassay for biomarker detection at clinically relevant concentrations.

3.1 Nanostructures for biomolecular sieving

Standard techniques for biomolecular separation such as gel filtration chromatography and gel electrophoresis rely on random polymer gels to provide nanometer-sized pores that are suitable for molecular sieving. While gel-based systems are proven reliable, the separation resolution is poor in gel filtration chromatography and sample recovery is difficult in gel electrophoresis. Extensive sample preparation steps which involve expensive infrastructures and lengthy procedures are also required. Furthermore, the considerably sample and reagent consumption in these traditional methods is a bottleneck towards multiplexed measurements. These are formidable obstacles that limit their use in point-of-care diagnostic settings.

Recent advances in micro- and nanofluidic technologies have opened up exciting opportunities in sample preparation and analysis as they promise miniaturization, automation, low sample consumption and seamless integration into a lab-on-chip format³⁻⁵. For example, a recent integrated microfluidic system⁶ has been demonstrated to perform on-chip blood separation and measurement of a dozen biomarkers within 10 minutes from whole blood obtained from a finger prick. For on-chip biomolecular separation, conventional microfluidic platforms use gelatinous sieving materials contained in microfluidic channels⁷⁻⁹. However, these foreign sieving matrices pose intrinsic difficulties for the integration of the separation process with the automated multistep point-of-care (POC) diagnostic platform. Furthermore, additional steps are needed to remove the sieving material from the sample for downstream processing.

Over the last decades, there have been many efforts to develop regular nanofluidic structures as an alternative to disordered gel material for biomolecule separation in microfluidic systems¹⁰⁻¹². As we can now fabricate nanofluidic structures with critical dimension comparable to biomolecules, we can directly manipulate biomolecules based on their size-dependent interactions with the solid-state nanostructures.

Various fabrication techniques for regular nanostructures have been explored, these include bottom-up approaches such as self-assembled colloidal particle packing¹³⁻¹⁵, ultra-thin porous membranes¹⁶ and top-down approaches involving the use of semiconductor microfabrication tools to pattern nanostructures with precise control of channel dimensions^{11, 17, 18}. Among these techniques, the top-down approaches are easy to integrate with other microfluidic systems. They also offer tremendous design flexibilities – by tailoring the shape and sizes of the nanostructures, we can exploit various nanofluidic phenomena to achieve functionalities that would not be possible in macro- or even microscale systems.

Microfabricated nanostructures that separate long DNA based on size have been realized in the forms of pillar arrays that mimic gel fibers¹⁹⁻²³, channels with alternating deep and shallow regions that act as entropic trap arrays^{17, 24, 25}, and asymmetric obstacles that act as Brownian ratchet²⁶⁻²⁹. These devices operate by either separating long DNA molecules based on their differences in conformational entropy, or rectifying lateral Brownian motion to deflect biomolecules based on their diffusivity. Separation of smaller molecules such as proteins and short oligonucleotides has also been demonstrated in devices consisting of nanofilter arrays^{30, 31}. However, the mechanism of separation is attributed to Ogston sieving instead of entropic trapping for the case when the biomolecules are smaller than the nanopores.

Recently, a two dimensional anisotropic nanofilter array (ANA) device has been implemented for continuous-flow separation of different sized DNA and protein³⁰. The designed structural anisotropy of the ANA causes biomolecules of different sizes and charges to follow distinct trajectories, leading to efficient continuous-flow separation. The continuous-flow operation of the ANA allows the separation process to be performed in-line with other continuous-flow processes, thus facilitating the integration of the separation step with upstream and downstream sample preparation or analysis steps. This unique operational characteristic provides a great advantage over other microfluidic batch separation techniques for the easy integration of the device into a common point-of-care diagnostic platform. As a step towards this direction, this device has been utilized to perform quantitative analysis of disease-marker proteins by continuously separating the larger antibody-protein immunocomplexes from the unbound antibodies³².

Finally, a method that continuously separate particles based on size using slanted obstacles in a microchannel has been reported³³ (**Figure 3.1**). The trajectory of the suspended particles is determined by hydrophoresis, which is the movement of particles under the microstructure-induced pressure field. Particle wall interaction will steer large particles with sizes comparable to the gap size of the slanted obstacles to focus near the sidewall of the device. On the other hand, small particles follow the streamline and exhibit a zig-zag trajectory motion, separate from the large particles. Using this method, the authors completely separated polystyrene microbeads with 9 μm and 12 μm diameters. In a separate paper, the same authors demonstrated continuous separation of red blood cells and white blood cells population this concept³⁴. In a later paper, hydrophoretic separation of micron and submicron particles (0.5 μm – 1.1 μm) and DNA molecules (radius of gyration 0.86 μm and 1.4 μm) was demonstrated using devices with obstacle gaps down to 1.2 μm ³⁵. DNA with radius of gyration greater than the obstacle gap had to change their conformation to pass through the gap. Hence, unlike smaller DNA which could immediately pass through the gap, they followed a different trajectory along the slanted obstacles until they acquire the right conformation that allows them to enter the gap. This mode of sieving share some similarities with the microfabricated entropic trap for long DNA separation¹⁷, but the structural anisotropy (slanted obstacles) enables continuous flow operation.

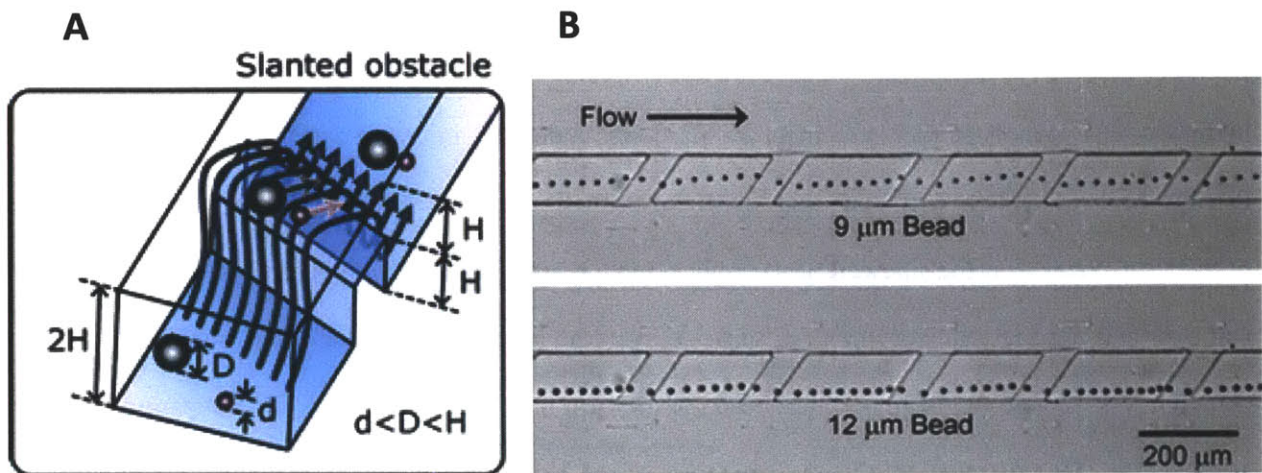


Figure 3.1: a) Example of a hydrophoresis device that can continuously separate particles based on size using slanted obstacles in a microchannel. b) Optical micrographs showing trajectories of 9 and 12 μm beads passing 19 μm-height slanted obstacles at $0.1 \mu\text{L min}^{-1}$. While the 9 μm bead was deviated from the focused position (the lower side of the channel), the 12 μm bead stayed in the focused position. (Adapted from works of Choi *et al.*³³)

3.2 Size based concentration of biomolecules using herringbone nanofilter array

In Chapter 2, we saw that coupling biomolecular concentration with the separation step could greatly improve the assay sensitivity. The need for biomolecular concentration step is even greater in micro/nanofluidic systems, where the low optical path length reduces detection sensitivity. Conventionally, size-based concentration of biomolecules in microfluidic devices is achieved by trapping large molecules in front of nanoporous gels and releasing them for analysis³⁶⁻³⁹. These methods have proven useful for increasing the assay sensitivity. However, as mentioned earlier, integrating foreign gel material into microfluidic devices present fabrication challenges. Furthermore, these are batch processes, which presents throughput and sample recovery challenges for downstream modules.

With the ability to fabricate nanochannels on the size order of biomolecules, one can explore the possibility of continuously fractionation and concentration, utilizing the biomolecule-nanofilter sieving interactions as a way to 'steer' molecules in a channel. In this section, we will introduce the HNA device, which could differentially concentrate small biomolecules based on size. The device consists of a periodic nanofilter array shaped like a herringbone (**Figure 3.2a**). The nanofilter array has shallow regions with gap thickness of d_s and deep regions with gap thickness of d_d . The design of the HNA device is similar to the periodic array of slanted obstacles used for hydrophoresis separation of particles and long DNAs. However, the HNA device is designed to utilize a different sieving mechanism (Ogston sieving)³¹. In the hydrophoretic separation of particles, the rotational flow induced by anisotropic obstacles redirect different sized particles into different trajectory³³. For the separation of long DNA, the obstacle gap size was smaller than the radius of gyration, and sieving involves molecules deforming to pass through the gap³⁵. On the other hand, Ogston sieving is the relevant mechanism when separating biomolecules whose sizes are smaller than the pore size in the herringbone nanofilter array.

Figure 3.2b illustrates the cross-section of the herringbone nanofilter array. An electric field drives the movement of the biomolecules (electrophoresis or electroosmosis) through the shallow and deep regions of the nanofilter array. Biomolecules experience a steric hindrance effect when they jump

across a nanofilter. Smaller molecules will have less resistance to jump across the nanofilter, thus will be more likely to be driven to flow across the nanofilter array in a straight line (path of least resistance) without altering their trajectory. On the other hand, larger sized biomolecules encounter a larger configurational entropic energy barrier while they transition from the deep to shallow region³¹, hence they have less frequency to jump across the nanofilters and become more likely to be driven towards the center of the herringbone structure. In this way, differently sized biomolecules are differentially concentrated in a continuous flow manner.

The concentration ability of this device is achieved by the design geometry of the herringbone nanostructure. The centerline of a herringbone structure represents a symmetric boundary condition, as large molecules from both sides are directed towards the center. Under such circumstances, the center region becomes a sink where large biomolecules accumulate. The only way for the trapped molecule to exit the local sink is by jumping over the shallow region. The concentration factor of large biomolecules in the center would be a function of its diffusion coefficient, trapping life time and the magnitude of the forces that drive the molecules to the center. For the most effective Ogson sieving of biomolecules, we should design the pore size to be comparable to the molecules to be analyzed⁴⁰. For the biomolecular complexes that we are interested in (most oligonucleotides and globular proteins have radii of gyration about 1-10 nm), we designed two depth for the nanofilter shallow region (53 nm and 80 nm) and the corresponding depth for the deep regions are 80 nm and 173 nm.

One of the immediate applications for such a platform is the ability to perform rapid quantification of biomarkers by separating free antibodies from the larger antibody-antigen complex. In previous work the ANA is used for continuous flow size-based immunoseparation³². However, detection sensitivity is poor as molecular dispersion reduces the signal at the detection region. With the concentration ability of the proposed device, we hope to improve the detection sensitivity by homogeneous signal amplification. Another application that we envisioned for this platform is for sample preparation, where we can simultaneously enrich and purify a target molecule based on size. As the

presence of high-abundance serum proteins (mostly albumin and immunoglobulin) present significant limitation to biomarker detection specificity and sensitivity, size-based removal of these compound prior to detection could improve the specificity and sensitivity of the assay. The continuous flow operation of the proposed device is ideally suitable for point-of-care formats such as lateral flow immunoassays.

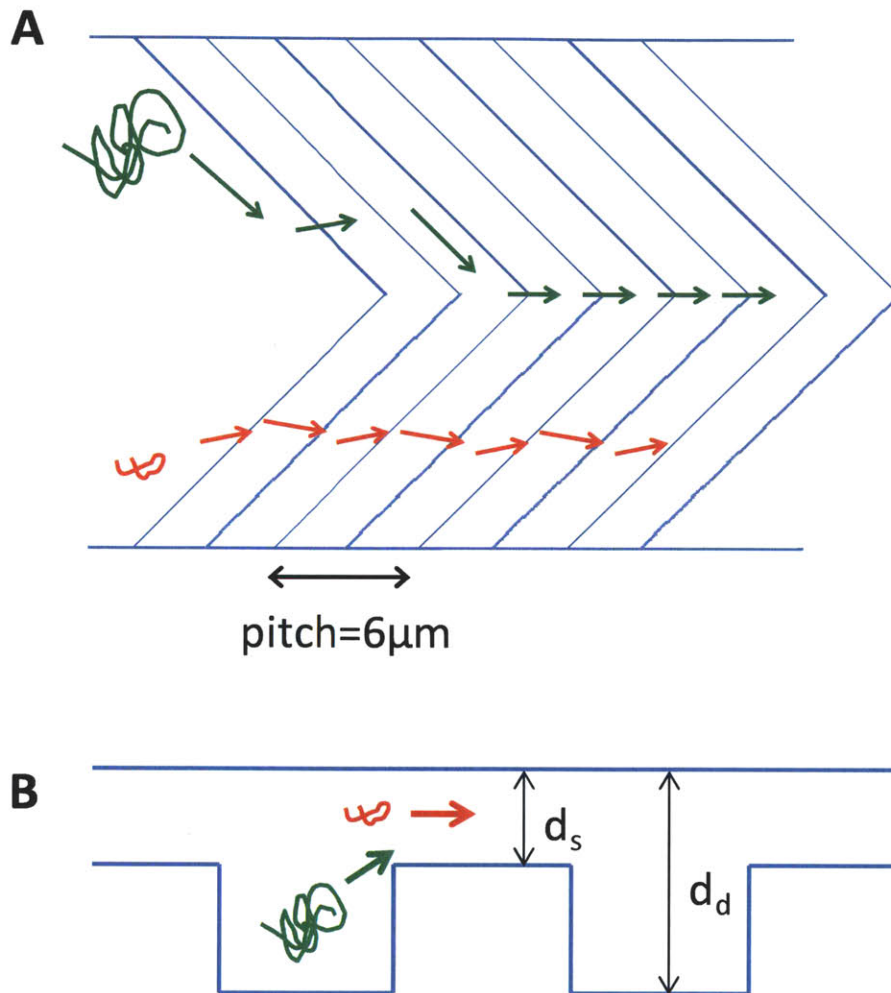


Figure 3.2: a) Schematic of the HNA device consisting of periodic nanofilter array shaped like a herringbone. An electric field drives the movement of the biomolecules through the nanofilter array. b) Cross-section of the HNA device showing shallow regions with gap thickness of d_s and deep regions with gap thickness of d_d . Small molecules (red) can migrate across the nanofilter array in a straight line without altering their trajectory. Large biomolecules (green) encounter a larger configurational entropic energy barrier while they transition from the deep to shallow region, hence they have less frequency to jump across the nanofilters and become more likely to be driven towards the center of the herringbone structure.

3.3 Device fabrication

The detailed fabrication process flow for this device has been reported elsewhere³¹. Briefly, structural patterning and RIE etching is done on silicon wafer using a 3-mask process. A potassium hydroxide etch was performed to etch a hole through the entire silicon wafer to create a buffer access hold. After thermal oxidation to provide electrical isolation between the buffer and the conductive silicon substrate, the herringbone nanofilter array was sealed by anodic bonding to a Pyrex wafer. A schematic of the key steps in this fabrication process flow is shown in **Figure 3.3**.

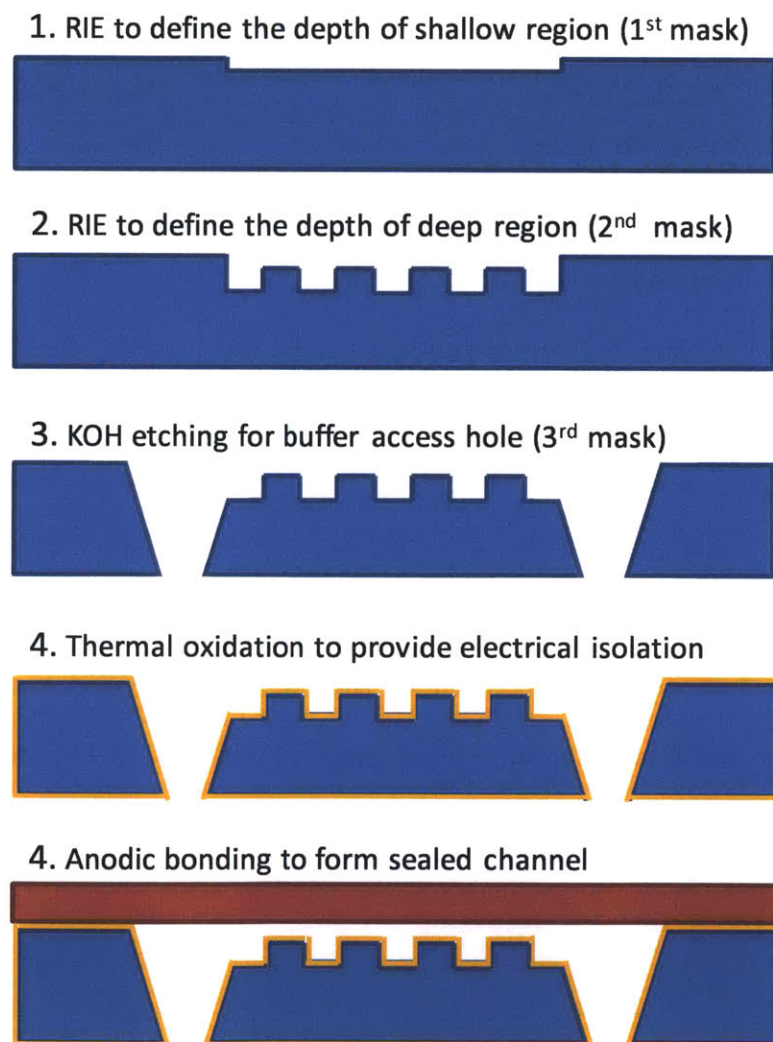


Figure 3.3: Fabrication process of the herringbone nanofilter array device.

3.4 Concentration of short DNA molecules by Ogston Sieving

We first demonstrate concentration of short double stranded DNA in the herringbone nanofilter array. Double stranded PCR markers (50-766 bp, New England Biolabs, Beverly, MA) was labeled with YOYO-1 intercalating fluorescent dye (Molecular Probes, Eugene, OR) with a dye to DNA base pair ratio of 1:10. The final DNA concentration in the sample solution was 10 $\mu\text{g/mL}$ in $1\times$ Tris Borate EDTA (TBE) buffer. Before the experiment, the device was equilibrated with the run buffer for 1 hour by applying 100 V across the nanofilter array.

Figure 3.4 shows the experimental results in a $d_s = 53$ nm device when the fluorescently labeled PCR marker was injected. Since the DNA molecules were highly negatively charged, migration of dsDNA followed the direction of electrophoresis. When 200 V was applied across the device, the DNA molecules focused into a tight band in the center of the herringbone structure. This phenomena is reversible, once the electric field is turned off, the focused band in the center of the channel quickly disperse, resulting in a uniform fluorescence distribution in the entire device. The PCR marker contains 5 different DNA fragments of sizes ranging from 50 bp to 766 bp. Since the persistence length of DNA is about 50 nm (about the contour length of 150 bp DNA), the PCR marker fragments are relatively straight, rigid rodlike molecules with end-to-end distance of about 16 nm to 150 nm. As the shallow region of the nanofilter is 53 nm, DNAs can enter these regions only in certain orientation. These differences in *configurational entropy* between the shallow and deep region leads to Ogston sieving effects^{41, 42}. It is important to note that the smallest dimensions of these rod-like molecules are less than the gap size of the shallow region, so the DNA molecules do not need to deform and change their conformational entropy as in the entropic trapping regime for long DNA^{17, 43}.

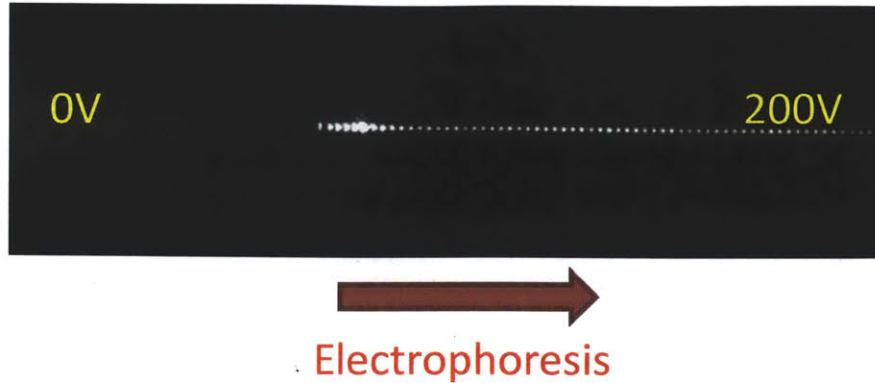


Figure 3.4: Size based concentration of YOYO-1 labeled PCR markers (50 – 766 bp) in the center of the HNA device ($d_s = 53\text{nm}$).

A potential application for this simple operation is to concentrate and focus DNA molecules from a sample prior to launching them for electrophoretic sizing. By doing so, we can obtain electropherograms with much higher signal and better resolution. Without any changes in process flow, the herringbone nanofilter array could be implemented routinely as a sample preconcentration module before size-based separation of biomolecules in the 1-D nanofilter array. Finally, as a sample preparation tool, this device can be used to continuously purify and concentrate the larger target molecules (e.g. DNA and large proteins) from a sample before performing downstream analysis such as mass spectrometry. Depending on the application, it is also possible to increase the throughput of these devices by creating massively-parallel, ultra-high-aspect-ratio nanochannels as demonstrated previously¹⁸.

3.5 Differential concentration of DNA-protein complex

One class of important biomolecular interaction involves the binding of protein to DNA. In a cell, DNA-protein interaction such as binding of transcription factors onto specific DNA sequences controls the transcription of genetic information from DNA to mRNA. As described in Chapter 2, DNA aptamers that can bind to specific target proteins are also recently gaining popularity for use in detecting and quantifying biomarkers for clinical diagnostics⁴⁴.

The HNA device can be used as a platform to selectively concentrate larger DNA-protein complex in a continuous flow manner and achieve rapid quantification of the target protein. To demonstrate this, we performed experiment using biotinylated fluorescent single stranded DNA (15 bp, Integrated DNA Technologies) which can bind to streptavidin (target protein). **Figure 3.5** shows the experimental results in a $d_s = 53$ nm device. When $4 \mu\text{M}$ of the fluorescently labeled single stranded DNA (ssDNA) in TBE $5\times$ was injected, migration of ssDNA followed the direction of electrophoresis, but the fluorescent profile in the HNA device appeared uniform. This is because the ssDNA is very small (persistence length ~ 1.5 nm) compared to the size of the nanogap and Ogston sieving is not significant. However, as shown in **Figure 3.5b**, when $2 \mu\text{M}$ of the streptavidin was added to the DNA probes, we saw a focused band in the center of the herringbone channel. Streptavidin is a globular protein (~ 3.5 nm) that can bind a maximum of 4 biotin moieties, therefore the total size of the DNA-protein complex is about 8 nm. Ogston sieving could occur and lead to continuous concentration of larger DNA-protein complex. **Figure 3.5c** shows the experimental results when the polarity of the electric field is reversed. Instead of concentrating in the center of the herringbone nanofilter array, the DNA-protein complex now concentrated at the sides of the nanofilter array as expected.

Although focusing of the DNA-protein complex was observed, the concentration factor was not high. This is probably due to the relatively small size of the DNA-protein complex compared to the gap height. Also, smaller molecules tend to have higher diffusion constant, which contributes to more dispersion of the concentrated band. To optimize the performance of this assay, a nanofilter array with smaller gap size should be used in the future. The ability to detect DNA-protein complex formation

makes this device a useful tool to screen for transcription factors that bind to specific DNA sequences, or to detect target proteins that bind to a specific aptamer. By virtue of the continuous flow operation of this device, one could also envision using this to select and purify aptamers that bind to a target protein from a DNA library by collecting the concentrated DNA-protein complex.

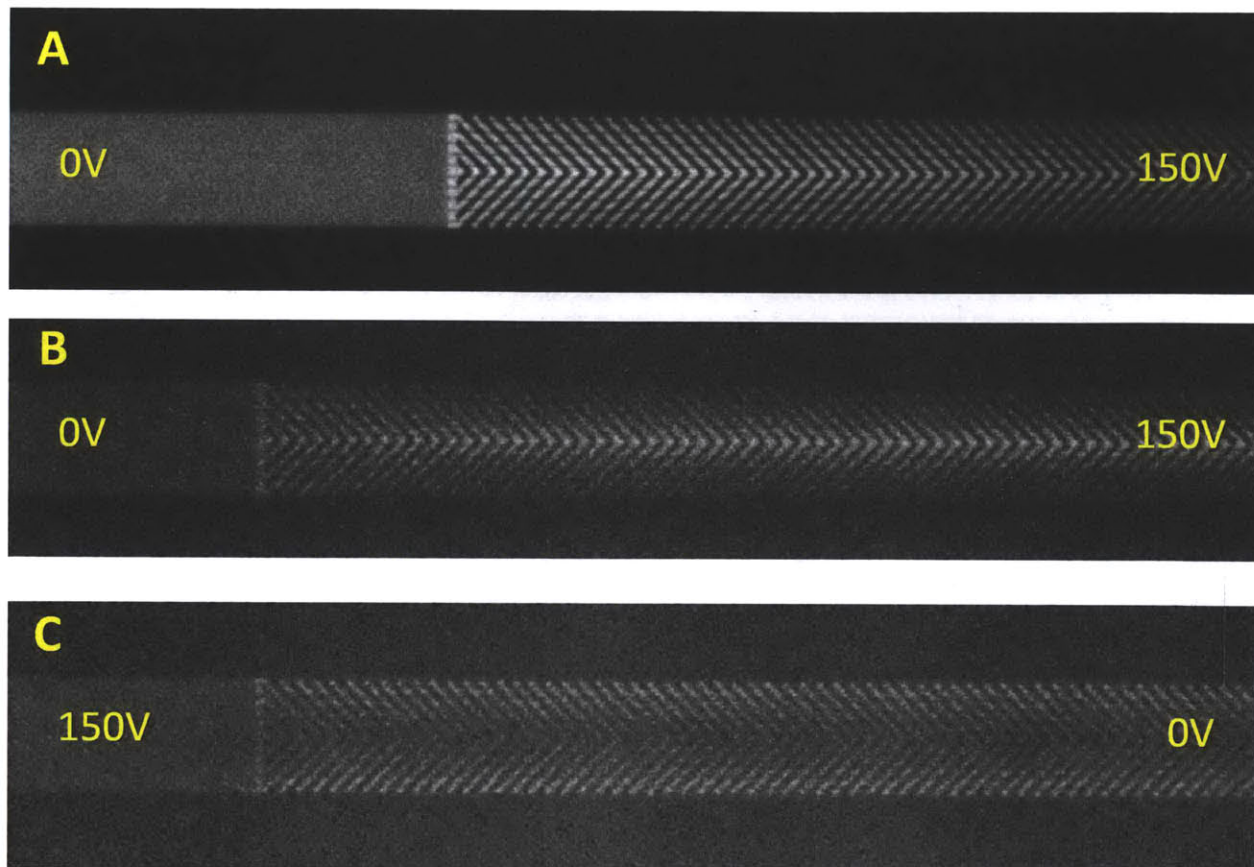


Figure 3.5: Size based concentration of DNA-protein complex in HNA device ($d_s = 53$ nm). a) Without any target protein, the fluorescent DNA does not concentrate in the HNA device, b) Upon adding the target protein, larger DNA-protein complex could concentrate in the center of the HNA device, c) Reversing the electric field polarity cause the DNA-protein complex to concentrate at the side of the HNA device.

3.6 Differential concentration of protein-protein complex

Protein-protein interactions that form complexes are important for the normal function of the cell. These range from simple receptor-ligand binding to complicated multi-protein assemblies such as ribosomes and proteosomes that perform essential cellular functions. Abnormal protein-protein interactions leading to large protein complex formation could cause diseases such as Alzheimers and encephalopathies⁴⁵.

The herringbone nanofilter array is also capable of performing size-based concentration of protein complexes under native conditions. As a proof of concept, we performed experiments using Alexa Fluor 488-conjugated streptavidin as a probe molecule to detect biotinylated BSA. The experiment is performed using a $d_s = 80\text{nm}$ device in TBE $1\times$ buffer. In the negative control, the fluorescent streptavidin migrated in the direction of electroosmosis but no concentration effect was observed due to its small size compared to the nanogap. However, as we add in the target protein, we observe a brighter band in the center of the channel, due to concentration of the larger streptavidin-biotinylated BSA complex (**Figure 3.6a**). **Figure 3.6b** is a plot of the fluorescence intensity profile across the herringbone nanofilter array for experiments with different concentrations of biotinylated BSA while the concentration of the fluorescent streptavidin probe molecule is kept constant at $20\ \mu\text{g/mL}$. The dose response curve in **Figure 3.6c** shows that the fluorescence peak height of the concentrated complexes initially increases with the addition of the target molecules, but when the target molecules are beyond a certain concentration, the fluorescence peak height starts to decrease. This is the well known high-dose Hook effect⁴⁶. When the concentration of the target molecules overwhelms the probe molecule, all the binding sites of the probe molecules are saturated and large complexes cannot form. The point when maximum large complex is formed is known as the *equivalence point*.

Figure 3.7 shows the experiments conducted in the same device with reversed electric field polarity. Instead of concentrating at the center of the herringbone nanofilter array, the protein-protein complexes focused near the sides of the nanofilter array. The dose response curves are similar for both cases. Quantitative detection of the target protein is possible in both device configurations.

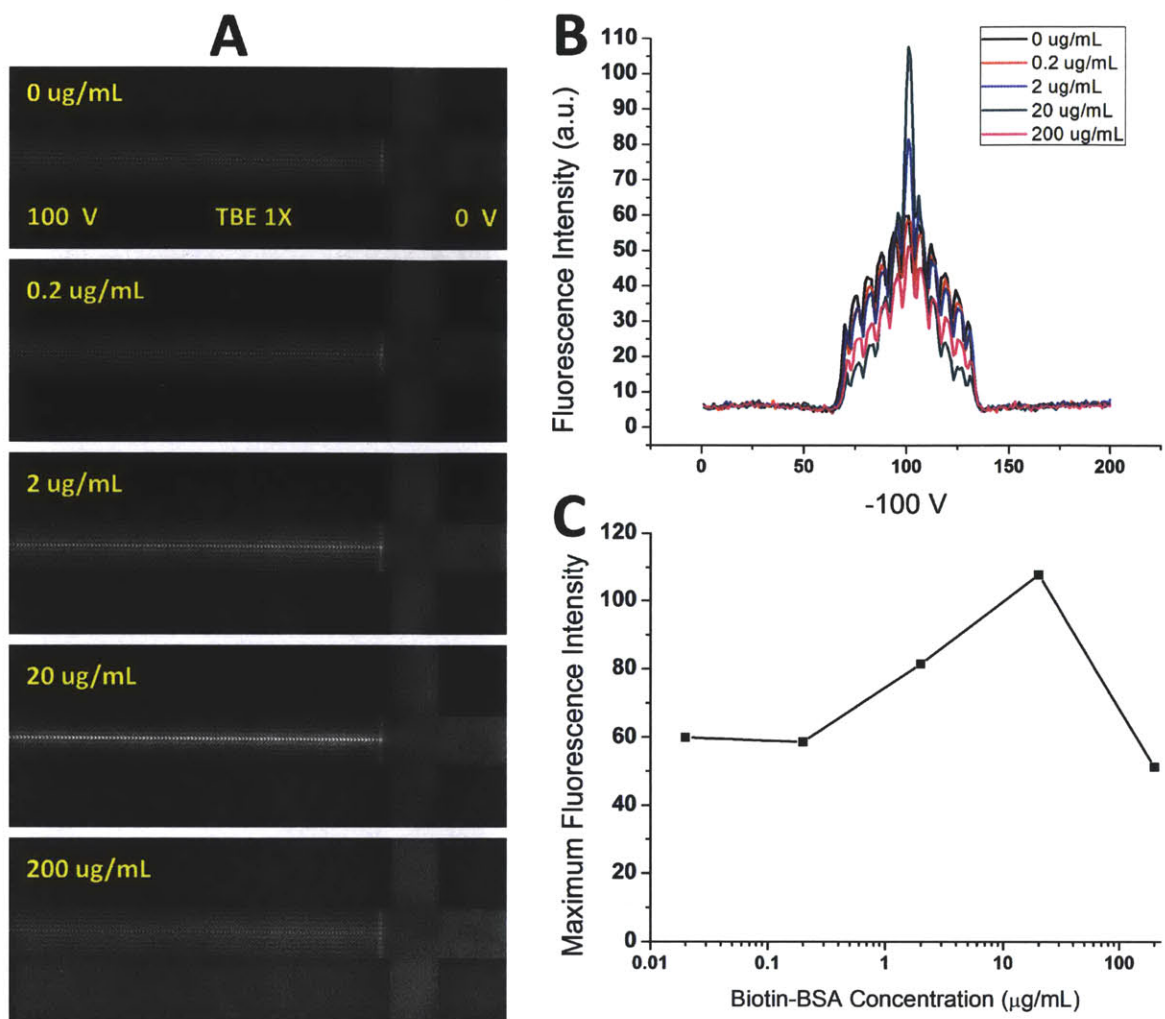


Figure 3.6: Size based concentration of protein-protein complex under native conditions in HNA device ($d_s = 80\text{nm}$). a) Experimental results showing behavior of protein-protein complex in HNA device at different target protein concentrations. b) Fluorescent intensity profile of the focused molecules at different target protein concentrations. c) Maximum peak height vs target protein concentration.

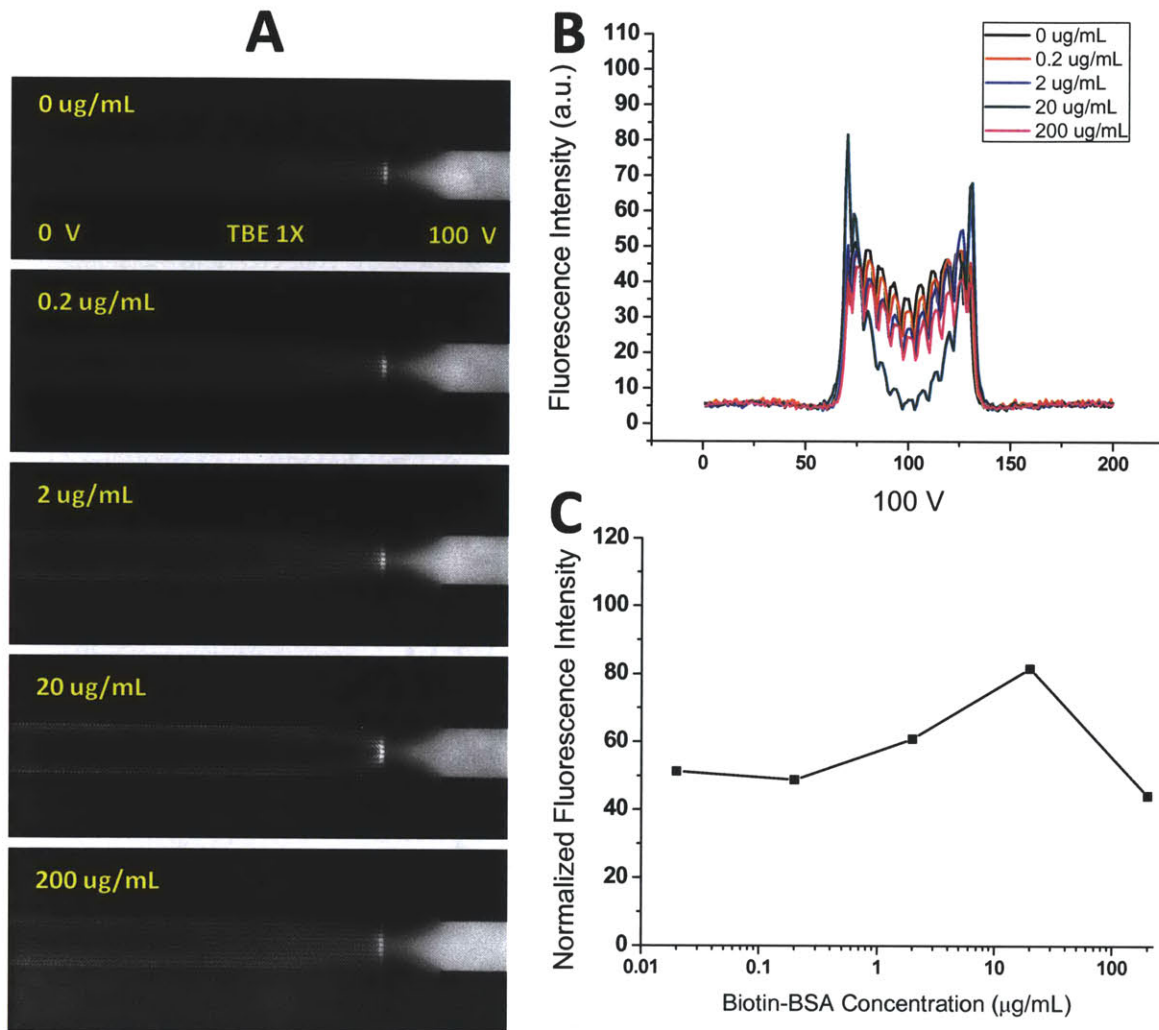


Figure 3.7: Size based concentration of protein-protein complex under native conditions in HNA device ($d_s = 80$ nm) under reversed electric field polarity. a) Experimental results showing behavior of protein-protein complex in HNA device at different target protein concentrations. b) Fluorescent intensity profile of the focused molecules at different target protein concentrations. c) Maximum peak height vs target protein concentration.

3.7 Differential concentration of antibody-antigen complex

Finally, we demonstrate the utility of the herringbone nanofilter array to perform a homogeneous immunoassay. Owing to their high sensitivity and specificity, immunoassays have been widely employed for clinical diagnostics and biochemical studies. Most of the common immunoassays feature a heterogeneous format, where antibodies are immobilized on a solid-phase support. The surface-bound antibodies selectively capture target molecules from the sample, which could then be detected by a second round of immunobinding and enzyme amplification. Although detection sensitivity is high, it is challenging to implement heterogeneous immunoassay in point-of-care diagnostic platforms due to the multiple washing steps, slow reaction kinetics, and the loss of antibody activity upon immobilization.

Homogeneous immunoassays, on the other hand, are ideally suited for point-of-care diagnostic platforms as they do not require any manual washing step and features very fast solution phase kinetics. The only requirement is a way to detect the antibody-antigen complex from free antibodies. This has been achieved by separating immunocomplexes from the unbound antibodies by gel electrophoresis and recently by using the ANA structure³². In these separation methods, there is always a tradeoff between signal and separation resolution as molecular dispersion inevitably reduces detection sensitivity. Here, using the HNA platform, we demonstrate that differential concentration of immunocomplexes allows us to quantitatively detect low abundance biomarkers. As this device concentrates immunocomplexes instead of letting them disperse as in normal separation methods, high signals are obtained which facilitates detection.

In the current study, we examined the human C-reactive protein (CRP) as a model biomarker. CRP is a pentameric serum protein with a molecular weight of ~115 kDa⁴⁷⁻⁴⁹. During acute inflammation such as cardiovascular diseases, CRP level in serum is upregulated, and the clinical cutoff value is 3-5 $\mu\text{g/mL}$. For our experiment, we used the $d_s = 80$ nm HNA device. CRP and 10 $\mu\text{g/mL}$ FITC-labeled antibody were mixed in $1 \times$ TBE containing 0.5% BSA off chip. After 30 minutes incubation for binding reaction to occur, the mixture was injected into the HNA device via applied voltage. Migration of the free antibodies and antibody-antigen complex followed the direction of electroosmosis. In the negative

control, there was a uniform fluorescence intensity profile throughout the HNA device, indicating that the free antibodies do not concentrate in the 80 nm device. With increasing concentration of CRP, a concentrated fluorescent band starts to appear in the center of the HNA device, indicating formation of large antigen-antibody complexes which undergo Ogston sieving (**Figure 3.8a**). In order to study the effects of electric field strength on the performance of this device, we performed the experiments at 4 different applied voltages (10 V, 20 V, 50 V and 100 V). The fluorescence intensity profiles across the HNA for different antigen concentrations and different applied voltages are plotted in **Figure 3.8b**.

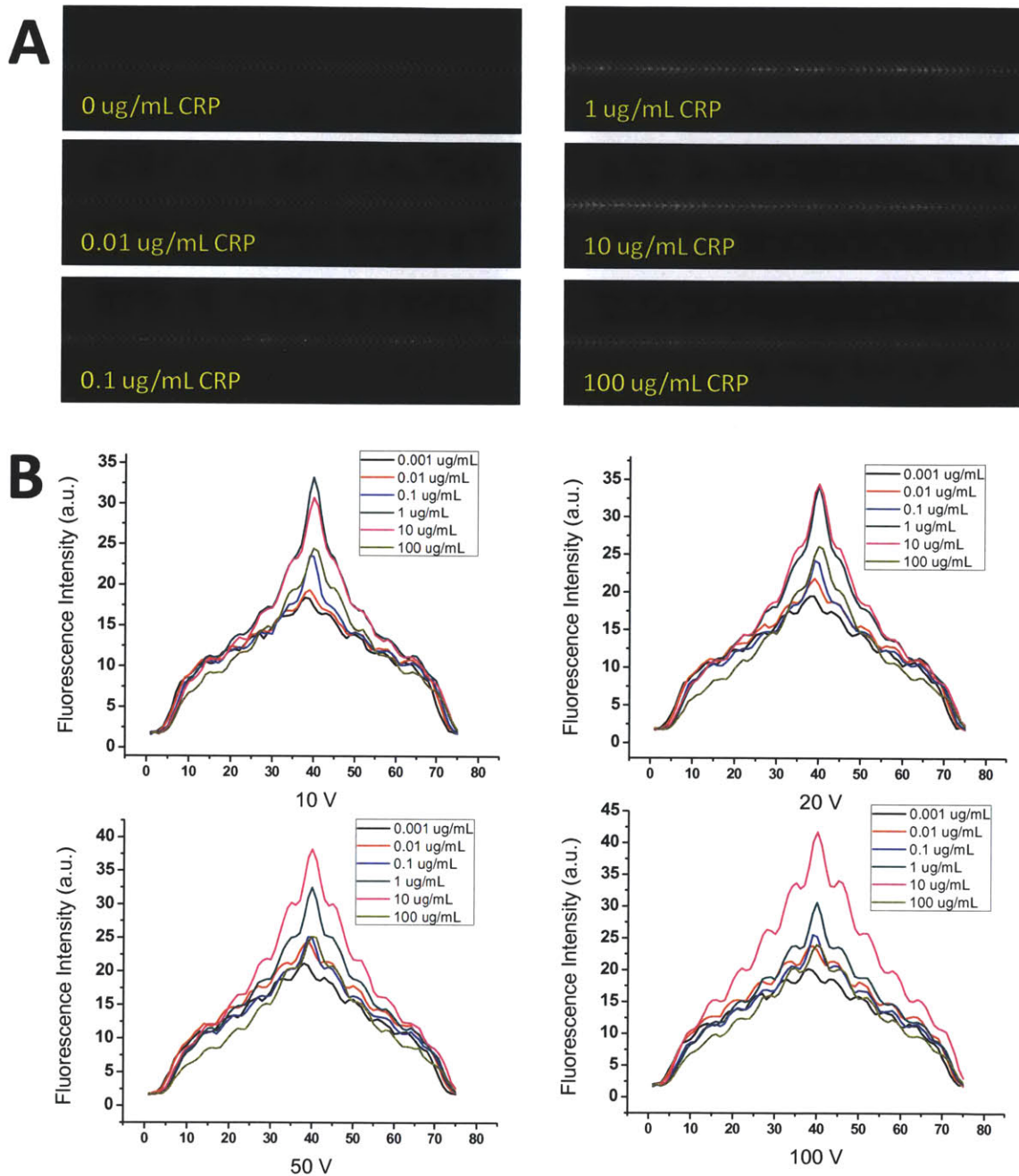


Figure 3.8: A concentration-enhanced homogeneous immunoassay using the HNA device. Quantitative measurement of biomarkers in a sample can be obtained by differential concentration of the antibody-antigen complex. a) Experimental results showing behavior of antibody-antigen complex in HNA device at different antigen concentrations when 20 V is applied across the device. b) Fluorescent intensity profile of the focused molecules at different target protein concentrations and applied voltage.

Figure 3.9 shows the dose response curve for detection of CRP molecules using the HNA device. As before, the fluorescence intensity of the concentrated band increases with the amount of CRP. At very high dose of CRP, however, the Hook effect was observed due to saturation of the antibody binding sites that prevent large complex formation.

The field strength (flow speed) affects different sized molecules differently in the HNA device. We can investigate this effect by looking at the dose response curve for experiments run at different applied voltages. The concentration factors in the center of the HNA depend on the amount of the biomolecular complexes c_{complex} that are accumulated within their trapping lifetime τ_{trap} . In **Figure 3.9** we see an interesting effect where the maximum concentration factor was around 1 $\mu\text{g/mL}$ CRP for low voltages operation (10 V), but the maxima became 10 $\mu\text{g/mL}$ CRP for high voltage operation (50 V and 100 V). We hypothesize that this crossover is due to the combined effects of trapping lifetime and accumulation rate of the complexes. At low voltage operation, the trapping lifetime is the dominant effect, thus the maximum concentration factor was achieved around 1 $\mu\text{g/mL}$ CRP when the largest biomolecular complexes are formed. At higher voltage operation, the Ogston sieving effect becomes less dominant⁵⁰. As the size dependence of trapping time is reduced, the accumulation rate of biomolecule complex becomes the dominant effect. There are more, albeit smaller, biomolecule complexes being formed at 10 $\mu\text{g/mL}$ CRP. Since the accumulation rate depends directly on the concentration of the biomolecule complex, the maxima in concentration factor shifts to 10 $\mu\text{g/mL}$ CRP at high voltage operation. The effect of field strength on size-dependent sieving is also apparent from the slope of the dose response curve. At low CRP concentrations, the slope of the dose response curve is highest at low voltage operation, indicating better size selectivity at low electric field conditions. Therefore, the optimum condition for operating the HNA device would be low electric field to best discriminate different sized biomolecule complexes. From the dose response curves, we can detect CRP concentrations as low as 10 ng/mL. This value is low enough to conduct clinical diagnosis of CRP (cutoff value 3-5 $\mu\text{g/mL}$).

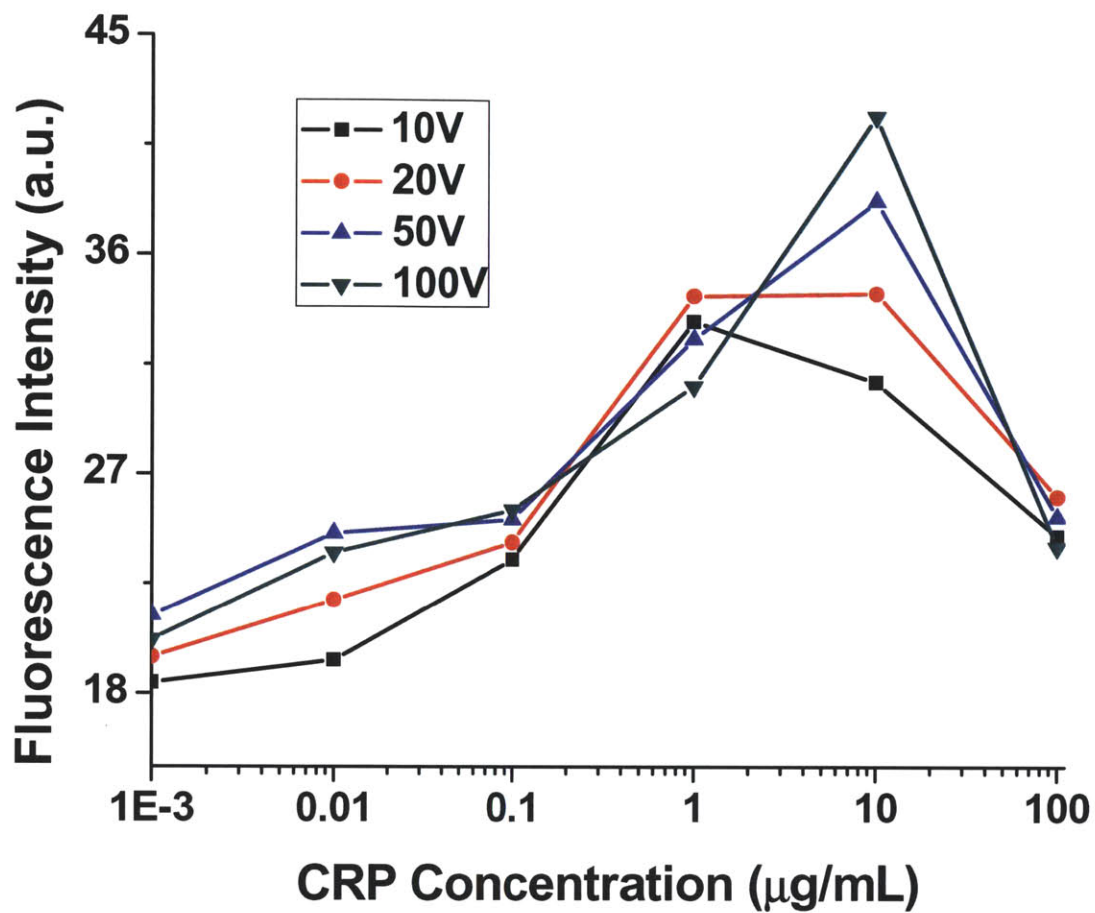


Figure 3.9: Dose response curve for detection of CRP molecules using the HNA device under different applied voltages.

3.8 Summary

In this chapter, we introduced the HNA device which allows continuous flow size-selective concentration of biomolecules. This is the first time that a continuous flow size-based concentration method has been realized, and it would be a useful technique to improve the sensitivities of various biological assays that utilize size-based fractionation. The concentration capability of this device is particularly useful in microfabricated lab-on-chip systems, where the low optical path length reduces detection sensitivity. The continuous flow format also makes this device an attractive sample preparation tool to continuously purify and concentrate target molecules based on size from a sample before performing downstream analysis.

In this work, we show how we make use of this device to interrogate biomolecular interactions, including protein-DNA binding, protein-protein interaction and antibody-antigen binding. The final example demonstrates a novel method to perform homogeneous immunoassay for biomarker detection at clinically relevant concentrations. In view of the rapid kinetics and ease of use, size based concentration could be a new paradigm for rapid quantification of biomarkers in point-of-care diagnostic systems.

3.9 References

- (1) Cheow, L. F.; Han, J. *Analytical Chemistry* **2011**, *83*, 7086-7093.
- (2) Stellwagen, N. C.; Gelfi, C.; Righetti, P. G. *Biopolymers* **1997**, *42*, 687-703.
- (3) Reyes, D. R.; Iossifidis, D.; Auroux, P. A.; Manz, A. *Analytical Chemistry* **2002**, *74*, 2623-2636.
- (4) Auroux, P. A.; Iossifidis, D.; Reyes, D. R.; Manz, A. *Analytical Chemistry* **2002**, *74*, 2637-2652.
- (5) Vilckner, T.; Janasek, D.; Manz, A. *Analytical Chemistry* **2004**, *76*, 3373-3386.
- (6) Fan, R.; Vermesh, O.; Srivastava, A.; Yen, B. K. H.; Qin, L.; Ahmad, H.; Kwong, G. A.; Liu, C. C.; Gould, J.; Hood, L. *Nature Biotechnology* **2008**, *26*, 1373-1378.
- (7) Viovy, J. L.; Duke, T. *Electrophoresis* **1993**, *14*, 322-329.
- (8) Yao, S.; Anex, D. S.; Caldwell, W. B.; Arnold, D. W.; Smith, K. B.; Schultz, P. G. *Proceedings of the National Academy of Sciences* **1999**, *96*, 5372.
- (9) Callewaert, N.; Contreras, R.; Mitnik-Gankin, L.; Carey, L.; Matsudaira, P.; Ehrlich, D. *Electrophoresis* **2004**, *25*, 3128-3131.
- (10) Mijatovic, D.; Eijkel, J. C. T.; Van Den Berg, A. *Lab Chip* **2005**, *5*, 492-500.
- (11) Fu, J.; Mao, P.; Han, J. *Trends in Biotechnology* **2008**, *26*, 311-320.
- (12) Han, J.; Fu, J.; Schoch, R. B. *Lab Chip* **2007**, *8*, 23-33.
- (13) Liu, L.; Li, P.; Asher, S. A. *Nature* **1999**, *397*, 141-144.
- (14) Nykypanchuk, D.; Strey, H. H.; Hoagland, D. A. *Science* **2002**, *297*, 987.
- (15) Zeng, Y.; Harrison, D. J. *Analytical Chemistry* **2007**, *79*, 2289-2295.
- (16) Sano, T.; Iguchi, N.; Iida, K.; Sakamoto, T.; Baba, M.; Kawaura, H. *Applied Physics Letters* **2003**, *83*, 4438.
- (17) Han, J.; Craighead, H. G. *Science* **2000**, *288*, 1026.
- (18) Mao, P.; Han, J. *Lab Chip* **2008**, *9*, 586-591.
- (19) Volkmuth, W. D.; Austin, R. H. *Nature* **1992**, *358*, 600-602.
- (20) Doyle, P. S.; Bibette, J.; Bancaud, A.; Viovy, J. L. *Science* **2002**, *295*, 2237.
- (21) Huang, L. R.; Tegenfeldt, J. O.; Kraeft, J. J.; Sturm, J. C.; Austin, R. H.; Cox, E. C. *Nature Biotechnology* **2002**, *20*, 1048-1051.
- (22) Baba, M.; Sano, T.; Iguchi, N.; Iida, K.; Sakamoto, T.; Kawaura, H. *Applied Physics Letters* **2003**, *83*, 1468.
- (23) Kaji, N.; Tezuka, Y.; Takamura, Y.; Ueda, M.; Nishimoto, T.; Nakanishi, H.; Horiike, Y.; Baba, Y. *Analytical Chemistry* **2004**, *76*, 15-22.
- (24) Han, J.; Turner, S. W.; Craighead, H. G. *Physical Review Letters* **1999**, *83*, 1688-1691.
- (25) Duong, T. T.; Kim, G.; Ros, R.; Streek, M.; Schmid, F.; Brugger, J.; Anselmetti, D.; Ros, A. *Microelectronic Engineering* **2003**, *67*, 905-912.
- (26) Ertas, D. *Physical Review Letters* **1998**, *80*, 1548-1551.
- (27) Duke, T. A. J.; Austin, R. H. *Physical Review Letters* **1998**, *80*, 1552-1555.
- (28) Chou, C. F.; Bakajin, O.; Turner, S. W. P.; Duke, T. A. J.; Chan, S. S.; Cox, E. C.; Craighead, H. G.; Austin, R. H. *Proceedings of the National Academy of Sciences* **1999**, *96*, 13762.
- (29) Van Oudenaarden, A.; Boxer, S. G. *Science* **1999**, *285*, 1046.
- (30) Fu, J.; Schoch, R. B.; Stevens, A. L.; Tannenbaum, S. R.; Han, J. *Nature Nanotechnology* **2007**, *2*, 121-128.
- (31) Fu, J.; Mao, P.; Han, J. *Applied Physics Letters* **2005**, *87*, 263902-263902-263903.
- (32) Yamada, M.; Mao, P.; Fu, J.; Han, J. *Analytical Chemistry* **2009**, *81*, 7067-7074.
- (33) Choi, S.; Park, J. K. *Lab Chip* **2007**, *7*, 890-897.
- (34) Choi, S.; Song, S.; Choi, C.; Park, J. K. *Lab Chip* **2007**, *7*, 1532-1538.
- (35) Choi, S.; Song, S.; Choi, C.; Park, J. K. *Analytical Chemistry* **2009**, *81*, 50-55.
- (36) Hatch, A. V.; Herr, A. E.; Throckmorton, D. J.; Brennan, J. S.; Singh, A. K. *Analytical Chemistry* **2006**, *78*, 4976-4984.
- (37) Hecht, A. H.; Sommer, G. J.; Durland, R. H.; Yang, X.; Singh, A. K.; Hatch, A. V. *Analytical Chemistry* **2010**, 2079-2090.

- (38) Meagher, R. J.; Hatch, A. V.; Renzi, R. F.; Singh, A. K. *Lab Chip* **2008**, *8*, 2046-2053.
- (39) Song, S.; Singh, A. K.; Kirby, B. J. *Analytical Chemistry* **2004**, *76*, 4589-4592.
- (40) Viovy, J. L. *Reviews of Modern Physics* **2000**, *72*, 813.
- (41) Giddings, J. C.; Kucera, E.; Russell, C. P.; Myers, M. N. *The Journal of Physical Chemistry* **1968**, *72*, 4397-4408.
- (42) Deen, W. M. *AIChE Journal* **1987**, *33*, 1409-1425.
- (43) Han, J.; Craighead, H. G. *Analytical Chemistry* **2002**, *74*, 394-401.
- (44) Gold, L.; Ayers, D.; Bertino, J.; Bock, C.; Bock, A.; Brody, E. N.; Carter, J.; Dalby, A. B.; Eaton, B. E.; Fitzwater, T. *PLoS ONE* **2010**, *5*, e15004.
- (45) Aguzzi, A.; Haass, C. *Science* **2003**, *302*, 814.
- (46) Heidelberg, M.; Kendall, F. E. *The Journal of Experimental Medicine* **1935**, *62*, 697.
- (47) Ramadan, M. A. M.; Shrive, A. K.; Holden, D.; Myles, D. A. A.; Volanakis, J. E.; DeLucas, L.; Greenhough, T. J. *Acta Crystallographica Section D: Biological Crystallography* **2002**, *58*, 992-1001.
- (48) Thompson, D.; Pepys, M. B.; Wood, S. P. *Structure* **1999**, *7*, 169-177.
- (49) Roberts, W. L.; Sedrick, R.; Moulton, L.; Spencer, A.; Rifai, N. *Clinical Chemistry* **2000**, *46*, 461.
- (50) Fu, J.; Yoo, J.; Han, J. *Physical Review Letters* **2006**, *97*, 18103.

Chapter 4

Multiplexed Single Cell Kinase Activity Assay

Kinases are an important family of proteins that regulate the majority of cell signaling pathways. They transmit information by catalyzing the phosphorylation of a specific substrate, thus modulating its activity. As the substrates of kinases are often kinases as well, information can be propagated through multiple signal transduction pathways, often with signal amplification. Interactions of multiple kinases in the signal transduction network lead to different outcomes in response to stimuli, which affects cell fate (**Figure 4.1**). Because of its importance in cell decision processing, there is tremendous interest in quantifying the dynamics of kinase activities in cells. Kinases are also receiving widespread attention in pharmacology industries, as they are important drug targets for diseases such as cancer. To test new targeted therapeutics, it is critical to develop sensitive analytical tools to detect abnormal activation of kinase pathways and to monitor their inhibition in response to treatment^{1,2}.

Recent studies have found that many anti-cancer drugs kill most but not all the cells in a tumor, often resulting in relapse of cancer³. It has been proposed that non-genetic cell-to-cell variability in protein activity, among other things, lead to this different response to drugs⁴. As most conventional techniques provide only a population-averaged measurement of the signals within the regulatory pathway, they do not reflect an accurate picture of a heterogeneous population of cells being in different states of intracellular processing⁵⁻⁷. A platform technology that can reliably assay for kinase activity from single cells is a valuable tool for biologists to study how individual cells develop into different cell fates and correlate with their phenotype.

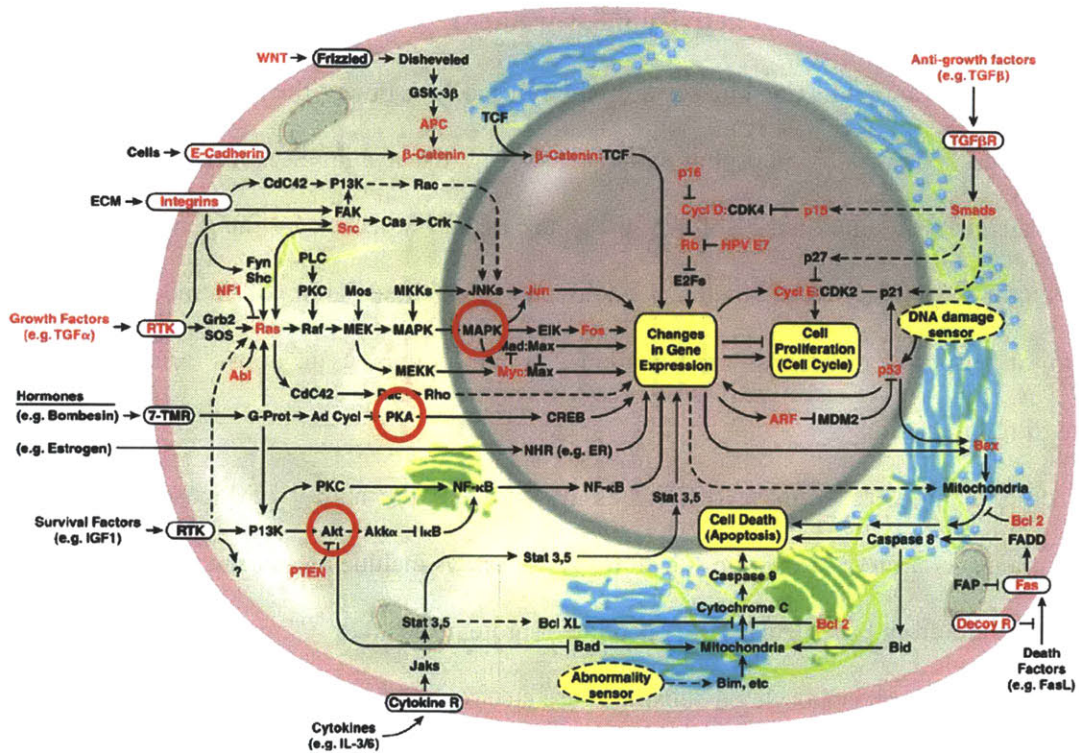


Figure 4.1: Diagram showing part of the cellular signal transduction network. Nodes in the network are protein kinases that transmit signal downstream by phosphorylating downstream kinases. Note the interconnectivity between different signaling pathways. Highlighted nodes (AKT, MK2, PKA) are important kinases that we measure in our assay. (Adapted from review of Hanahan and Weinberg⁸).

4.1 Antibody based method vs direct activity measurement

Currently, phosphospecific antibodies to kinases are widely used to estimate their activity, since many kinases are themselves activated by phosphorylation. However, the availability of specific and high affinity antibodies against different kinase isoforms presents a major bottleneck for the general use of this technique. Furthermore, antibody-based methods could not detect modulation of intracellular kinase activities due to other post-translational modifications, protein-protein associations such as protein scaffolds⁹⁻¹¹, and drug interaction¹².

On the other hand, direct kinase activity assays measure the ability of kinases to catalyze phosphorylation of a target protein or peptide substrate. These assays include measuring the incorporation of radiolabeled phosphate from [γ -³²P]ATP into a peptide or protein substrate^{13, 14}, mobility shift assays in which phosphorylated and unphosphorylated substrates are electrophoretically separated and quantified¹⁵,¹⁶, and a variety of fluorescence based methods including homogeneous time-resolved fluorescence¹⁷, fluorescence resonance energy transfer¹⁸ chelation-enhanced fluorescence¹⁹, and fluorescence polarization^{18, 20} techniques. A common limitation of direct kinase activity assay is the specificity of the enzyme towards the peptide substrate. Kinases often have overlapping substrate specificity leading to off-target cross-reactivity. Therefore, steps need to be taken to first isolate the target kinase from cell lysate by immunopurification. Otherwise, pharmacological inhibitors of off-target kinases are required to improve the specificity of the direct kinase activity assays.

4.2 Single cell kinase activity assay

In order to address the issues related to cellular heterogeneity in signal transduction, one would need measurement of various kinase activities at the single cell level. Currently, the most advanced methods for single cell level kinase measurement involve imaging live cells that are genetically encoded for a substrate molecule that can report the activity changes within the cytoplasm²¹⁻³³. These live-cell imaging methods are very powerful as they could yield spatio-temporal information about kinase activation; however they are limited in the number and types of enzymes that can be measured simultaneously in

single cells. In addition, expressing a reporter molecules involve laborious genetic engineering of a cell line to encode a fluorescent protein, and could alter the normal function of the cell line. Therefore, while useful for scientific studies of cell decision processes using cell cultures, it is generally not suitable for measuring kinase activity in primary cells such as patient-derived tumor samples. A second strategy that has been developed involves microinjecting fluorescent kinase substrates into single cells, lysing them and performing capillary electrophoresis to separate and quantify the phosphorylated and unphosphorylated substrate^{15, 34-36}. In this second method, it is possible to perform simultaneous measurements of several enzymes within the same cell, although it does not yield any spatial information about enzyme activation. However, in combination with techniques such as GFP-kinase translocation, enzyme activation and spatial location can be measured in the same cell¹⁵. In all the methods described above, substrate specificity would be an issue since there is significant substrate cross-reactivity among intracellular kinases. Since the living cell is a reaction vessel where the kinase catalyzed reaction takes place, strategies to improve substrate specificity such as addition of off-target kinase inhibitors cannot be implemented without perturbing the normal function of the cell. In addition, intracellular kinase substrate reporters are subjected to other cellular processes such as proteolysis and dephosphorylation during intracellular kinase reaction¹⁵, thus obfuscating the actual activity of the target kinase.

Ideally, to obtain single cell kinase activity measurement that can be comparable to conventional bulk lysate kinase activity measurement, it is preferable to rapidly lyse a single cell and allow the lysate to react with the substrate for a defined period of time, instead of loading substrate into the cell before lysing it. Substrate loading by microinjection could result in membrane or organelle damage, which in turn activates other undesirable stress response pathways in the cell¹⁵. Also, as mentioned above, injected substrates are subjected to intracellular off-target kinase reaction, proteolysis and dephosphorylation due to lack of kinase, protease and phosphatase inhibitors. On the other hand, lysing a cell first and then allowing the lysate to react with substrate preserves the snapshot of cell signaling state during rapid lysis, and various inhibitors can be added to the reaction mix to increase kinase specificity as well as prevent proteolysis and dephosphorylation. However, as the intracellular content of a single cell is released during

lysis, they immediately undergo a dilution factor proportional to the size of the reaction vessel. This necessitates an ultrasensitive assay in order to detect kinase activity at such low enzyme concentration.

4.3 Electrokinetic concentration enhanced kinase activity assay

Since the electrophoretic mobility of a kinase peptide substrate is modified upon phosphorylation, we could use the same concentration-enhanced mobility shift assay platform, described previously in Chapter 2, to increase the sensitivity of kinase activity assay. Furthermore, due to the separation capability of the concentration-enhanced mobility shift assay platform, it would be possible to simultaneously separate and concentrate two or more kinase substrates from their phosphorylated product at the same time. This would allow us to simultaneously monitor several kinase activities from the same sample, and enable users to measure the interactions between different nodes in the complex signal transduction network.

Figure 4.2 reiterates the key operation of the poly(dimethylsiloxane) (PDMS) microfluidic electrokinetic concentration chip. Under the voltage configuration shown in **Figure 4.2a**, ion depletion zones are created in the sample channels at the vicinity of the ion selective membrane due to concentration polarization phenomena. The conductivity gradient at the boundary of the ion depletion zone gives rise to a stable electric field gradient that can effectively focus negatively charged biomolecules at separate locations where electrophoretic velocity balances bulk flow velocity. In this work, fluorescently labeled peptides which contained the recognition sequences for specific kinases are used as substrates. Target kinases in the sample catalyze the phosphorylation of these peptides, leading to an increase in electrophoretic mobility (**Figure 4.2b**). Phosphorylated peptides, which have higher electrophoretic mobilities due to the negative-charged phosphoryl group, are concentrated at the low electric field region. On the other hand, unphosphorylated peptides have a lower mobility; therefore they concentrate nearer to the cation selective membrane where the electric field is higher (**Figure 4.2c**). In this manner, we can obtain good separation between phosphorylated and unphosphorylated substrates, while at the same time achieve continuous signal enhancement for greater sensitivity.

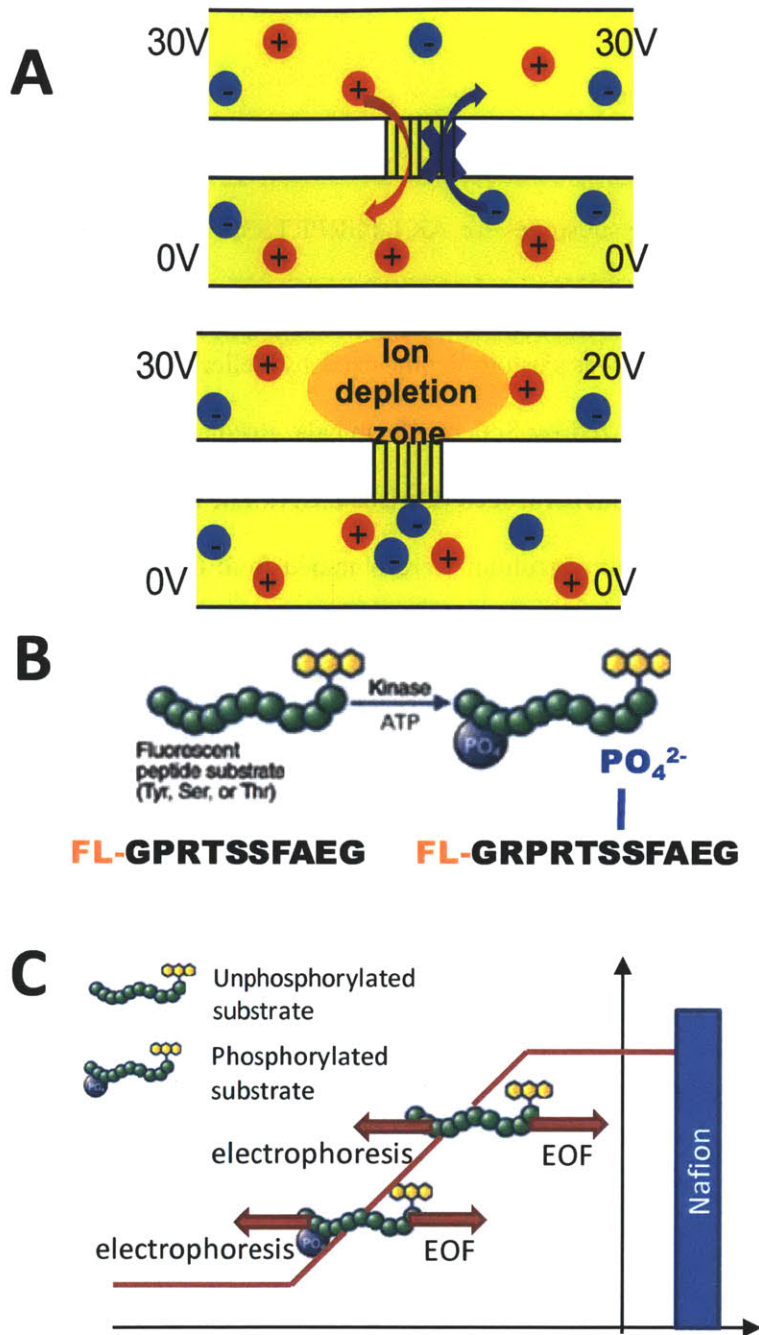


Figure 4.2: a) Ion selective membrane creates a local ion depletion zone with high electric field upon applying a voltage, b) Active kinases in the sample phosphorylates the specific fluorescent peptide substrates by adding a phosphoryl group on the serine/threonine residue, c) Unphosphorylated and phosphorylated peptide substrate concentrate at different locations on the electric field profile due to their different electrophoretic mobilities.

4.4 Experimental section

4.4.1 Reagents and chemicals

Unless stated otherwise, all chemicals used in the experiments were purchased from Sigma (St. Louis, MO). 5-FAM labeled peptide substrates for AKT (GRPRTSSFAEG, Crosstide³⁷) and PKA (LRRASLG, Kemptide³⁸) were obtained from Anaspec (Fremont, CA). 5-FAM labeled peptide substrate for MK2 (AHLQRQLSIA, MK2tide³⁹) was custom synthesized by Selleck Chemicals (Houston, TX). All other custom peptides were synthesized by Selleck Chemicals. Recombinant AKT, MK2 (MAPKAPK2) and PKA kinases were obtained from Invitrogen (Carlsbad, CA). The kinase inhibitors PKI-tide, GF109203X, PKC inhibitor peptide and Calmidazolium were obtained from Calbiochem (San Diego, CA). Protease inhibitors (protease inhibitor cocktail III) and phosphatase inhibitors (phosphatase inhibitor cocktail 1) were also obtained from Calbiochem. Ampholytes (Fluka) were purchased from Sigma (St. Louis, MO). **Table 1** lists the buffer recipes used in the experiments.

Buffer	Recipe
Buffer A	25 mM Tris-HCl (pH 7.5), 10 mM MgCl ₂ , 1 mM ATP, 1 mM DTT, 0.01% Triton X-100, 200 µg/mL BSA
Buffer B	5 mM Tris-HCl (pH 7), 100 µg/mL BSA
Buffer C	50 mM Tris-HCl (pH 7.5), 150 mM NaCl, 15 mM MgCl ₂ , 5 mM β-glycerolphosphate, 1 mM EGTA, 0.2 mM Na ₃ VO ₄ , 0.2 mM DTT, 200 µg/mL BSA
Buffer D	1% Triton X-100, 50 mM β-glycerolphosphate, 10 mM sodium pyrophosphate, 30 mM NaF, 1 mM benzamidine, 2 mM EGTA, 100 µM Na ₃ VO ₄ , 1 mM DTT, 10 µL/mL protease inhibitors, 10 µL/mL phosphatase inhibitors

Table 4.1: Buffer recipes

4.4.2 Microchip operation

The microchips were fabricated as described in Chapter 2. Before the experiment, the PDMS device channels were passivated with 1% BSA for 1 hour to reduce nonspecific binding of the sample to channel walls. After that, the channels were flushed with DI water 3 times and filled with buffer solution (5 mM Tris-HCl, pH 7) until the samples were ready to be loaded.

Samples were loaded into each of the five inlet reservoirs and drawn into the microchannel by applying a brief suction at the outlet reservoir. The liquid height difference between the inlet reservoir and the empty outlet reservoir caused a well-controlled gravitational flow of sample solution from inlet to outlet, without any need for external pump.

Electrodes were inserted into the inlet and buffer reservoirs on the chip and connected to a power supply (Stanford Research Systems, Sunnyvale, CA). To initiate the concentration-enhanced mobility shift assay, we applied 50 V at the inlet reservoirs while grounding the side channels. An ionic concentration gradient was induced near the ion-selective membrane by concentration polarization effect. Meanwhile, charged sample molecules are continuously separated and stacked at the location where its electrophoretic velocity equals the bulk flow velocity. The fluorescent intensity of the stacked molecules increases linearly with time while background noise remained constant, resulting in a high signal-to-noise ratio.

4.4.3 Measurement instrument and image analysis

An inverted epifluorescence microscope IX 71 (Olympus, Center Valley, PA) equipped with a cooled CCD camera (SensiCam, Cooke Corp., Romulus, MI) was used for fluorescence imaging. A mechanical shutter which only opens for 100 ms every 5 s when images are taken was used to prevent photobleaching of the fluorescent molecules. The images were analyzed using the NIH ImageJ software. Flat-field correction was performed by dividing a reference image of the device taken before each experiment. Concentrations of phosphorylated and unphosphorylated peptide substrates were assumed to be directly proportional to the focused peak height as demonstrated in previous work^{40, 41}. Phosphorylation ratio was calculated by dividing the peak height of the phosphorylated substrate by the sum of the peak heights of

the phosphorylated and unphosphorylated substrates. Dose response curves and statistical analysis was obtained using Origin 7 software (OriginLab Corp., Northampton, MA).

4.4.4 Recombinant kinase experiment

We first performed an experiment with recombinant AKT and its fluorescent peptide substrate Crosstide (5-FAM-GRPRTSSFAEG). We first diluted 0.5 μL of the recombinant kinase with 4.5 μL of the premixed assay buffer (Buffer A supplemented with 1 μM substrate) and incubated at room temperature for 60 minutes. After that, 1 μL of this mixture is diluted in 99 μL of run buffer (Buffer B) and 30 μL of this final sample is used for the concentration-enhanced mobility shift assay. **Figure 4.3a** shows the representative results for this experiment. During 15 minutes of electrokinetic concentration, two distinct bands corresponding to the phosphorylated substrate (left) and unphosphorylated substrate (right) were formed in each sample channel. The fluorescence intensities of these bands increased linearly with time and both bands were baseline resolved. Since this is a ratiometric assay, we can extract the fraction of phosphorylated substrate for each sample by dividing the fluorescence intensity of the phosphorylated substrate band by the total fluorescence intensity of both bands. Kinase reaction velocities can be directly calculated from these measurements without any need for calibrations. Besides, a ratiometric assay is relatively insensitive to external influences such as variable flow rate, light intensity etc., and thus is highly reproducible. **Figure 4.3b** showed a dose response curve for the recombinant AKT assay. The limit of detection for recombinant AKT was calculated to be 1 ng/mL.

To demonstrate the general applicability of this assay for activity measurement of other kinases, we performed a separate experiment with recombinant MK2 and PKA with their respective fluorescent peptide substrates MK2tide and Kemptide (MK2: 5-FAM-AHLQRQLSIA, PKA: 5-FAM-LRRASLG). Except for replacing the substrates, the recombinant MK2 and PKA assay was done with the same conditions as the recombinant AKT experiment. From the dose response curve in **Figures 4.4a** and **4.4b**, the LOD for recombinant MK2 and PKA were 1.2 ng/mL and 0.7 ng/mL respectively within 15 minutes of electrokinetic concentration.

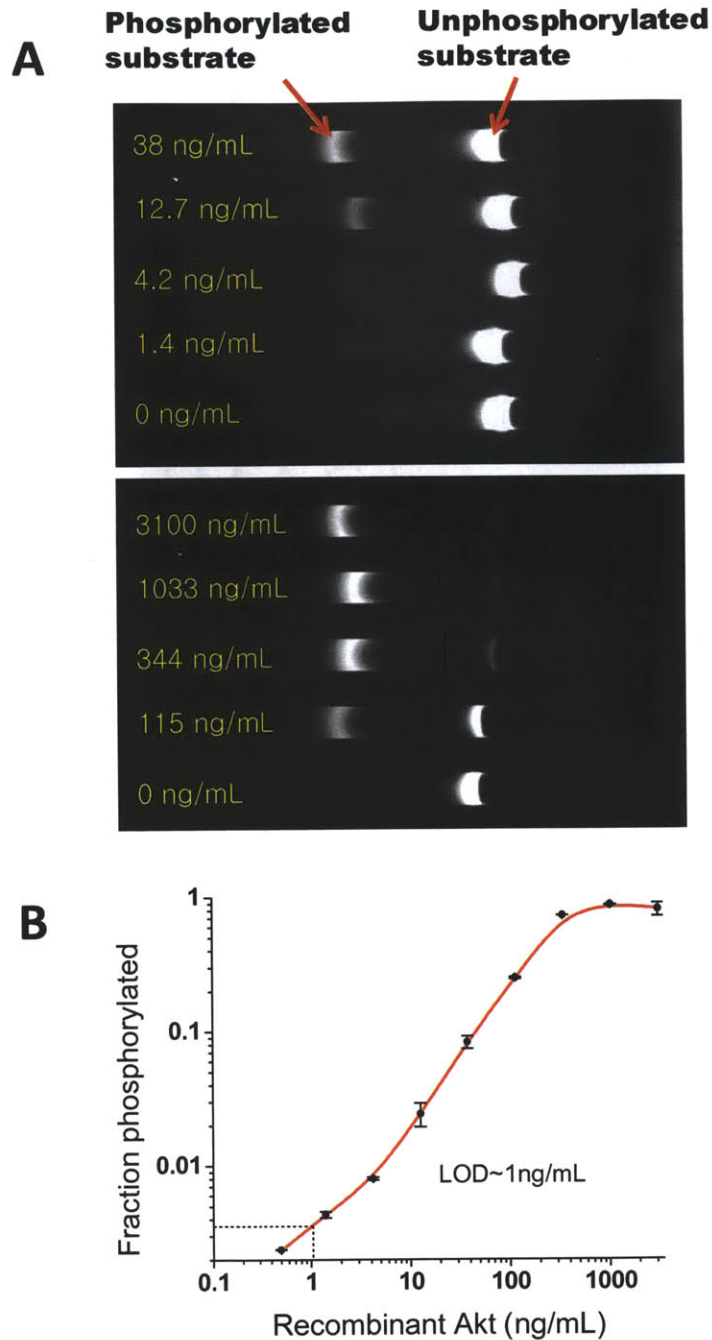


Figure 4.3: Multiplexed electrokinetic concentration-enhanced mobility shift assay for detection of recombinant AKT activity (a) With increasing recombinant AKT concentration, the phosphorylated substrate peak increases and the unphosphorylated substrate peak decreases, (b) Dose response curve for recombinant AKT activity assay. Plotted values indicate the mean \pm s.e.m. for duplicate measurements. The limit of detection was calculated to be 1 ng/mL.

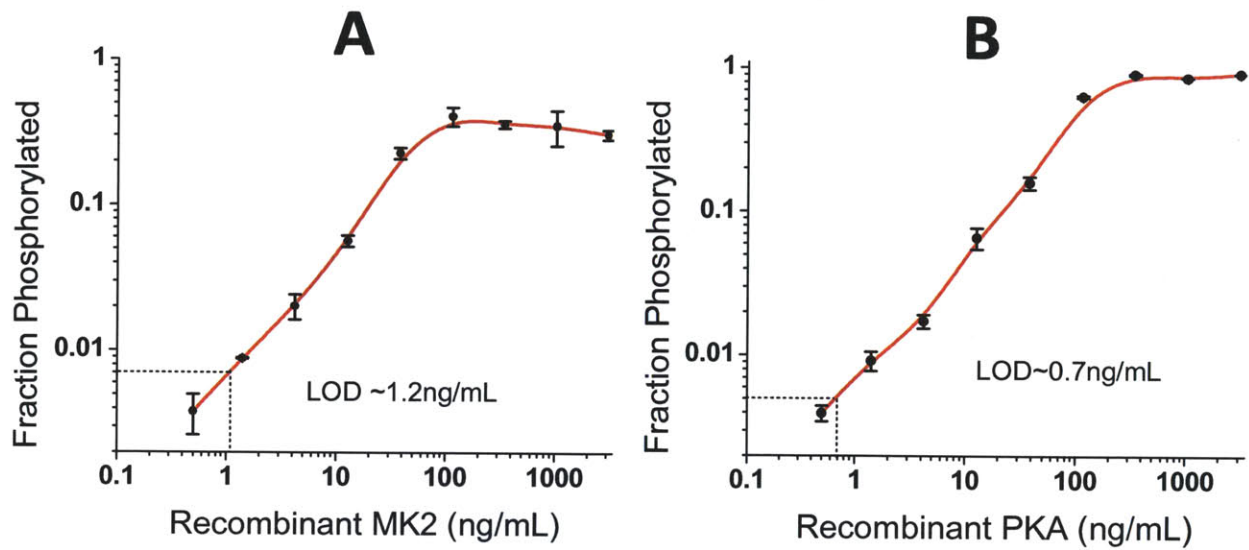


Figure 4.4: Dose response curves for a) Recombinant MK2 and b) Recombinant PKA activity assay. Error bars represent standard error from two replicates. Plotted values indicate the mean \pm s.e.m. for duplicate measurements. The limit of detections for recombinant MK2 and recombinant PKA were calculated to be 1.2 ng/mL and 0.7 ng/mL respectively.

4.4.5 Substrate cross-reactivity

In the experiments with recombinant kinases, the kinase activities can be unambiguously inferred by measuring the substrate phosphorylation fraction after a fixed amount of time. The concentration-enhanced mobility shift assay in this current format can be a useful platform in drug development applications, such as measuring the changes in recombinant kinase activities in the presence of novel small molecule drugs.

In order to assess the substrate specificity of our kinase of interest, we measured the pair-wise cross-reactivity between each substrate and kinase. Briefly, 1 μM of each substrate was separately reacted with a fixed amount (100 ng/mL) of each recombinant kinase in the assay buffer (Buffer A) for 1 hour at room temperature, and the phosphorylation fraction was measured on the concentration-enhanced mobility shift assay platform as described previously.

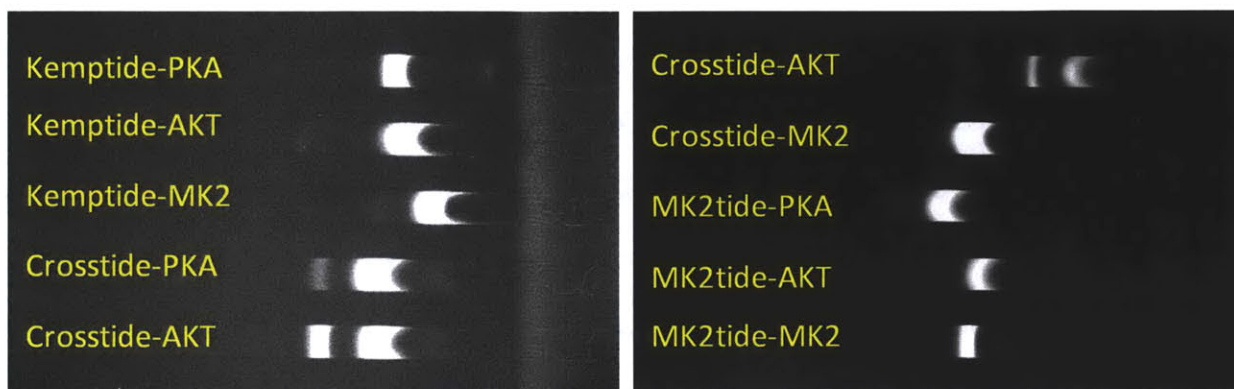
Figure 4.5 shows the results of this experiment. As expected, the degree of substrate phosphorylation is greatest when a kinase react with its target substrate (Kemptide for PKA, Crosptide for AKT, MK2tide for MK2). However, this assay also detected a small amount (<10%) of off-target phosphorylation. This is not surprising as kinases often have overlapping substrate specificity that could lead to off-target cross-reactivity.

Off-target kinase reactivity could present an accuracy problem when measuring specific kinase activities in complex samples such as crude cell lysates. Furthermore, the presence of other intracellular enzymes such as proteases and phosphatase could affect the stability and phosphorylation state of the substrates. This is one major limitation of many existing single cell kinase activity assays, where substrates that are microinjected into or expressed within the cell are subjected to the activity of other intracellular enzymes such as off-target kinases, proteases and phosphatases.

In order to improve the specificity of the kinase activity assays, inhibitors of off-target kinases, proteases and phosphatases can be added in the reaction buffer. It has been shown that these inhibitors can effectively suppress the activity of their target enzymes without affecting the activity of the kinase of interest¹⁹. In our subsequent experiments using bulk cell lysate and single cells, we adopted this strategy

of adding a cocktail of protease, phosphatase and off-target kinase inhibitors to improve our assay specificity.

A



B

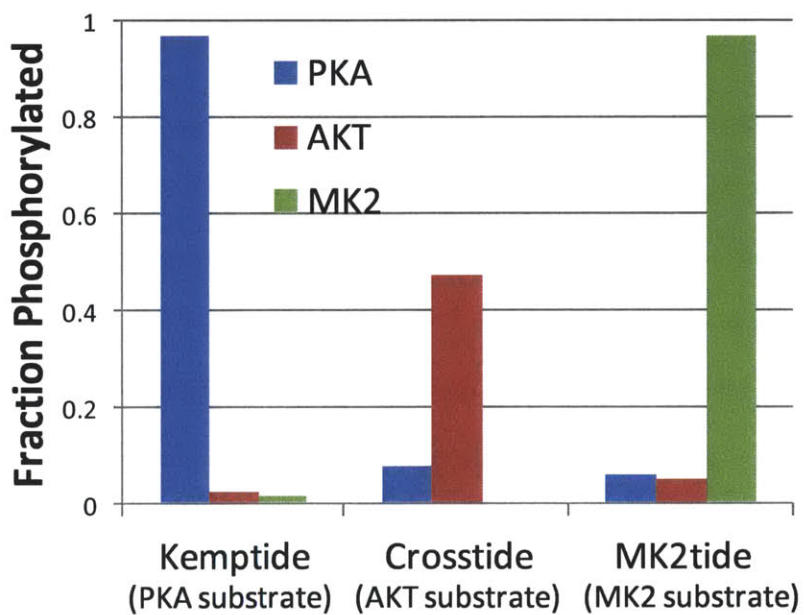


Figure 4.5: a) Experimental results, and b) Analysis showing the pair-wise cross-reactivity between three kinases (PKA, AKT, MK2) and their substrates (Kemptide, Crosstide, MK2tide).

4.4.6 Cell lysate experiment

To show the application of this assay with real samples, we repeated the kinase activity experiments with diluted HepG2 cell lysate. Cell culture, treatment, and lysis were conducted basically as in Shults et al¹⁹. HepG2 cells (a human hepatoblastoma cell line) were obtained from ATCC (Manassas, VA). HepG2 cells were seeded on 10-cm tissue culture-treated polystyrene plates at 1×10^5 cells/cm² in Eagle's minimum essential medium (EMEM; ATCC) supplemented with 10% fetal bovine serum (FBS; Hyclone, Logan, UT), 100 U/ml penicillin (Sigma, St. Louis, MO), and 100 µg/ml streptomycin (Sigma) and were incubated at 37°C in 5% CO₂. One day after seeding, medium was changed to fresh EMEM without FBS. One day after medium change, HepG2 cells reached confluence and were stimulated with 500 ng/mL insulin (Sigma) in EMEM (to activate AKT) or 25 µM forskolin (Sigma) in EMEM without FBS (to activate PKA), or left untreated (EMEM without FBS). For both conditions (activated and unactivated), cells were placed on ice 30 minutes following stimulation and culture medium was removed. Cells were lysed with lysis buffer (Buffer D, containing protease and phosphatase inhibitors) for 20 minutes at 4°C followed by scrapping. Lysates were clarified by centrifugation at 16,000g for 15 minutes at 4°C. Clarified lysates were analyzed using a bicinchoninic assay (Pierce, Rockford, IL) to determine the total cellular protein concentration. Stock lysates were divided into single-use aliquot and stored at -80°C.

We first demonstrate the results with AKT kinase activity assay. Insulin stimulation is known to increase the activity of AKT *in vivo*. Therefore, we compared the activity of serum starved HepG2 cell lysate and insulin stimulated HepG2 cell lysate. To perform the cell lysate kinase activity experiment, assay buffer (Buffer C with 4 µM PKC inhibitor, 4 µM calmidazolium, 1 µM fluorescent Crosstide, 1 mM DTT, 1 mM ATP, 0.4 µM PKI-tide, 5 µM GF109203X) was prepared in bulk and 18 µL volumes were aliquoted into separate microcentrifuge tubes. To begin each reaction, 10% (vol/vol) lysis buffer (Buffer D) or lysate (diluted in lysis buffer to stated concentrations) was added and the contents were mixed gently. Reaction was carried out at 37 °C for 60 minutes. After that, reaction was stopped by diluting 1 µL of this mixture in 99 µL of run buffer (Buffer B). 30 µL of this final sample was used for

the concentration-enhanced mobility shift assay. **Figure 4.6a** shows the results for this experiment. We observed no phosphorylated substrate band for the negative control samples (containing lysis buffer but not HepG2 cell lysate). For the same final cell lysate concentration (down to the lowest tested concentration of 2.16 $\mu\text{g/mL}$), the insulin stimulated sample consistently showed a higher fraction of phosphorylated substrate compared to the serum starved sample, confirming the utility of our assay to measure changes in cellular kinase activities in response to stimuli. The cells used in this experiment have about 1 ng of protein per cell. Detection from a final volume of 30 μL run buffer, after a total of 100-fold dilution of a 2.16 $\mu\text{g/mL}$ of cell lysate, represents kinase assay from ~ 0.6 cell. This demonstrates the sensitivity of our assay for single cell level studies of cell signaling pathways.

We also performed similar experiments measuring PKA activity from HepG2 cell lysate. Forskolin stimulation is known to increase the intracellular level of cAMP and upregulate PKA activity. The experimental procedure was similar to the cell lysate AKT activity measurement, except that the substrate was replaced by 1 μM fluorescent Kemptide and PKI-tide (which is a kinase inhibitor for PKA) was left out. **Figure 4.6b** shows that consistent with expectation, the forskolin stimulated sample consistently showed a higher fraction of phosphorylated PKA substrate compared to the serum starved sample. This shows that our platform can be generally applied to measure activities of different kinases with high sensitivity from physiological samples.

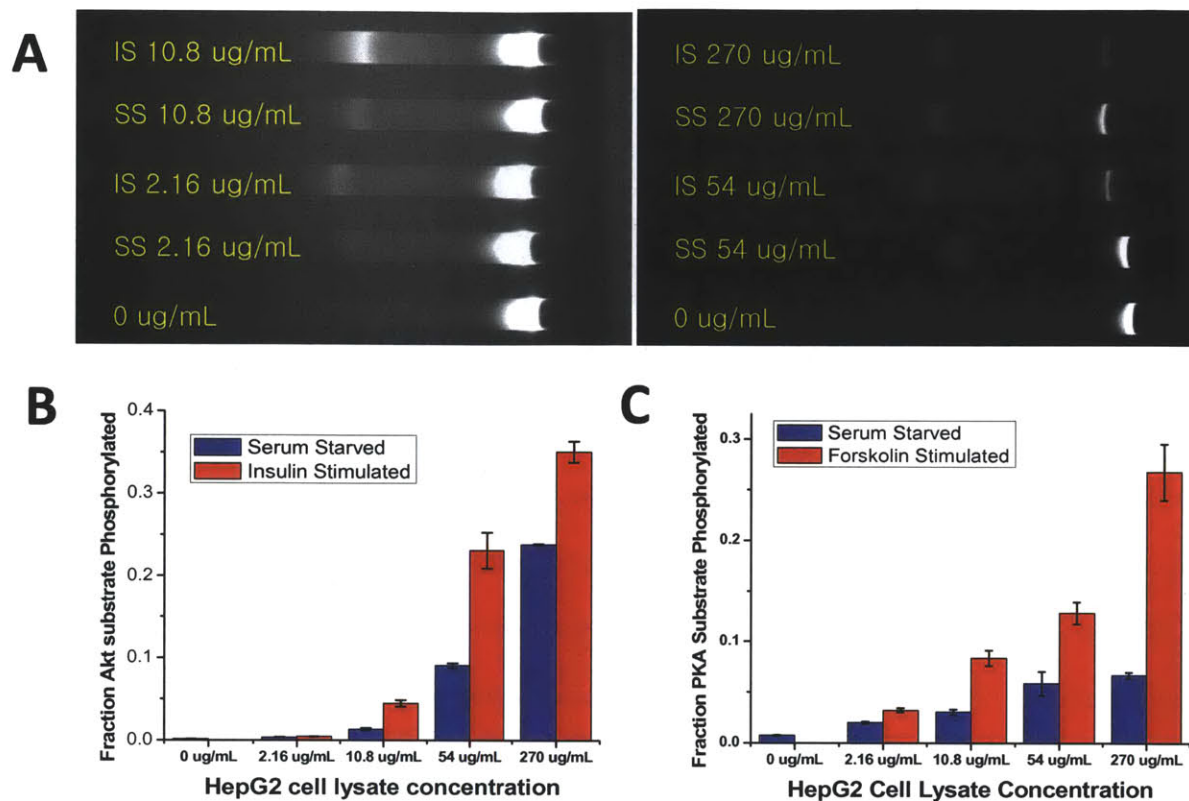


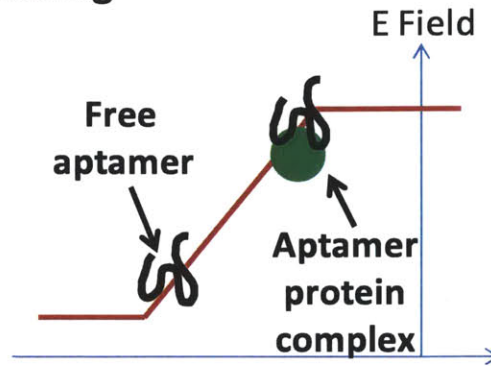
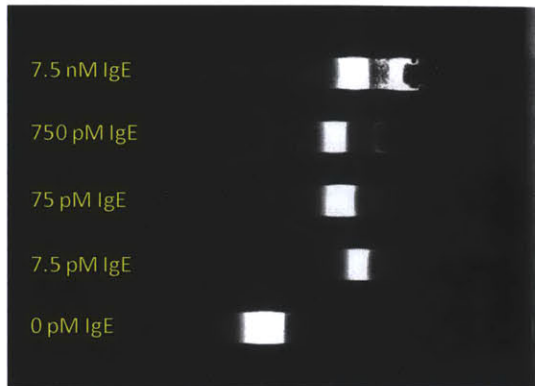
Figure 4.6: a) Representative experimental results showing multiplexed electrokinetic concentration-enhanced mobility shift assay for detection of AKT activity in serum-starved (SS) and 5 minutes 500 ng/mL insulin-stimulated (IS) HepG2 cell lysate, b) Dose response curve of AKT activity in different concentrations of serum starved and insulin treated HepG2 cell lysate showing upregulation of AKT activity by insulin, (c) Dose response curve of PKA activity in different concentrations of serum starved and forskolin (25 μ M, 30 mins) treated HepG2 cell lysate showing upregulation of PKA activity by forskolin. Plotted values indicate the mean \pm s.e.m. for duplicate measurements.

4.5 Multi-substrate separation

So far, in both the concentration-enhanced aptamer and kinase activity assays, we have demonstrated simultaneous concentration and separation of two species (free aptamer vs aptamer-protein complex, phosphorylated vs unphosphorylated peptide substrate). This phenomenon can be understood by considering the diagram in **Figure 4.7a**, which show electrofocusing of two species with different electrophoretic mobility at the electric field gradient formed around the ion depletion zone boundary. An examination of **Figure 4.7a**, which shows electrofocusing of free aptamer and aptamer-IgE complex in 5 mM Tris-HCl buffer without any additives, suggests that the spatial extent where the electric-field gradient is significant (distance between the two bands) spans only a short distance of the order of 100 μm . This is consistent with previous *in-situ* electric field measurements⁴², which shows a 30-fold amplified electric field in the ion depletion zone (width $\sim 200 \mu\text{m}$) compared to outside the depletion region. This sharp electric field gradient is key to the very high preconcentration factors⁴³ reported for this device as biomolecules experience a very high trapping force in this steep potential well. Given this situation, it would be difficult to observe clear separation of more than two analytes, since the region in which separation could occur is very short and molecular diffusion would cause closely-separated bands to merge and appear indistinguishable.

In studies related to the signal transduction network, investigators are often interested in understanding the functional relationship between activities of different kinases in the network. By measuring and comparing kinase activities between different signaling pathways, we could deduce how the different input stimuli are integrated and processed to produce different cellular response. Unfortunately, most current single cell kinase activity assays lack the capability of looking at more than one single kinase activity at a time.

A. Electrofocusing



B. Depletion zone isotachopheresis

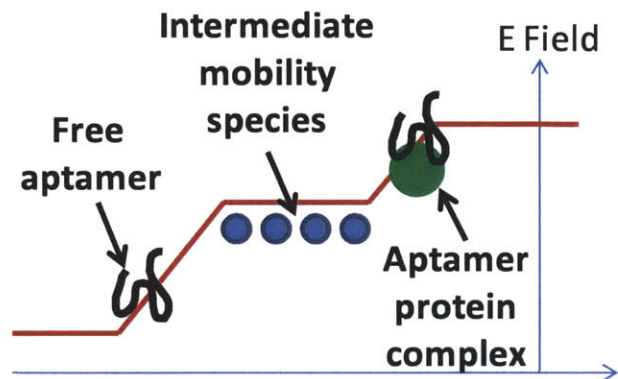
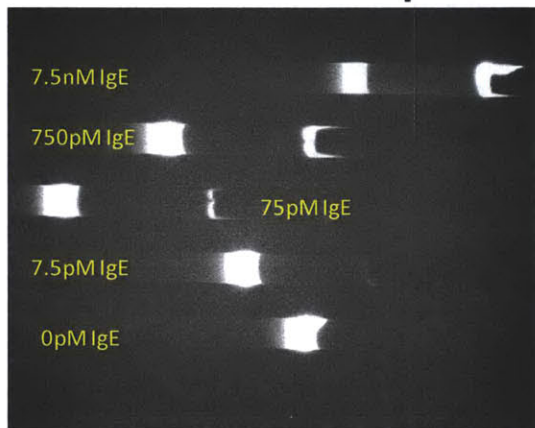


Figure 4.7: a) Experimental results and schematic showing simple electrofocusing of free aptamers and aptamer-IgE complex in 5 mM Tris-HCl buffer without any additives, b) Experimental results and schematic showing depletion zone isotachopheresis of free aptamers and aptamer-IgE complex in 5 mM Tris-HCl buffer with 100 $\mu\text{g}/\text{mL}$ BSA. Preconcentration of the intermediate mobility species creates an electric-field plateau which increases the separation distance between the two analytes of interest.

We discovered that addition of an appropriate high-abundant species in the buffer during the concentration-enhanced mobility shift assay result in a larger separation distance between the two fluorescent bands. The separation distance increases proportionally to the amount of the high-abundant species added. Interestingly, the peak width of the focused band remained narrow, suggesting that the electric field gradient is still very steep despite the larger separation distance. This phenomenon is shown in **Figure 4.7b**, where we observed a significant increase in separation distance between the free aptamer band and the aptamer-IgE complex band in buffer containing 100 $\mu\text{g/mL}$ BSA, all other conditions being the same.

This phenomenon is thought to be due to preconcentration of an intermediate mobility species (BSA in this case) to such high concentrations that it is capable of changing the electric field profile according to the Kohlraush Regulating Function (KRF), as is commonly observed in isotachopheresis (ITP) experiments. Other experiments and theoretical analysis strongly supports this hypothesis⁴⁴. Qualitatively, as preconcentration increases the local concentration of the intermediate mobility species (a co-ion), the high mobility co-ions in the same regions are displaced in order to maintain electroneutrality. This leads to a lower conductivity and sustains higher electric field in this region. Continuous preconcentration of the intermediate mobility species eventually expands the spatial extent of this low conductivity region, leading to a high electric field plateau.

Figure 4.7b shows the schematic of the electric field profile modulated by preconcentration of a high abundant intermediate mobility species. The electric field gradient remained steep where focusing of the free-aptamer and aptamer-protein complex occurs. Meanwhile, the region where the intermediate mobility BSA focuses forms an electric-field plateau which increases the separation distance. This staircase-like electric field profile is unique in the aspect that it could increase the spatial separation resolution between target analytes while still keeping the individual bands narrowly focused at local regions where the electric field gradient is steep. This suggests a method where we can simultaneously separate and focus multiple kinase substrates and products by “*adding more steps on the staircase*” - adding more *intermediate mobility species* between the analytes of interest as shown in **Figure 4.8**. By

adding suitable spacer molecules with appropriate mobilities at various concentrations, we can engineer an optimal electric field profile to perform a concentration-enhanced multiple kinase substrate mobility shift assay.

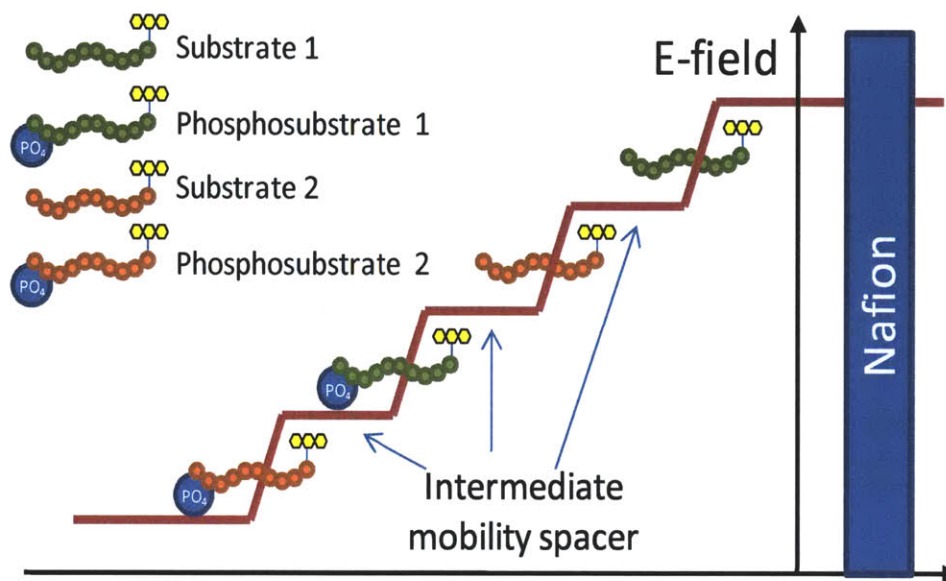


Figure 4.8: Schematic showing a strategy to simultaneously separate and focus multiple kinase substrates. Upon adding suitable spacer molecules with intermediate mobilities at various concentrations, depletion zone isotachopheresis results in a staircase-like electric field profile that increases the separation resolution between multiple kinase substrates.

The problem now reduces to how we would design a mixture of spacer molecules for optimal concentration and focusing. There are two main design considerations: 1) the spacer molecules should have electrophoretic mobilities in between the two analytes to be separated, 2) the concentration of the spacer molecules should be sufficient to provide the desired resolution, but not too high to avoid excessive voltage drop and therefore reduction of electric fields at the analyte focusing areas. In the absence of any knowledge about the actual analyte and spacer mobilities, one could turn to commercially available mixtures of compound which contains a wide range of molecules with different mobilities. Some compounds in this mixture are likely to have the appropriate mobility to act as a spacer for this purpose. One such mixture is commercially available ampholytes, which are a blend of zwitterionic compounds commonly used for isoelectric focusing (IEF). Ampholytes are designed to have a continuous range of isoelectric points and as such the compounds are expected to have a variety of different charges and mass (and thus different mobilities) at a particular pH. These compounds have also recently gained renewed interest for use in isotachopheresis as spacer molecules^{45, 46}. **Figure 4.9** illustrates the utility of ampholytes as spacer molecules in the concentration-enhanced mobility shift assay. According to the principle of depletion-zone isotachopheresis, compounds in the ampholyte stack in the order of their mobilities. This creates an extended separation zone where the equilibrium focusing position of individual fluorescent analytes are well resolved.

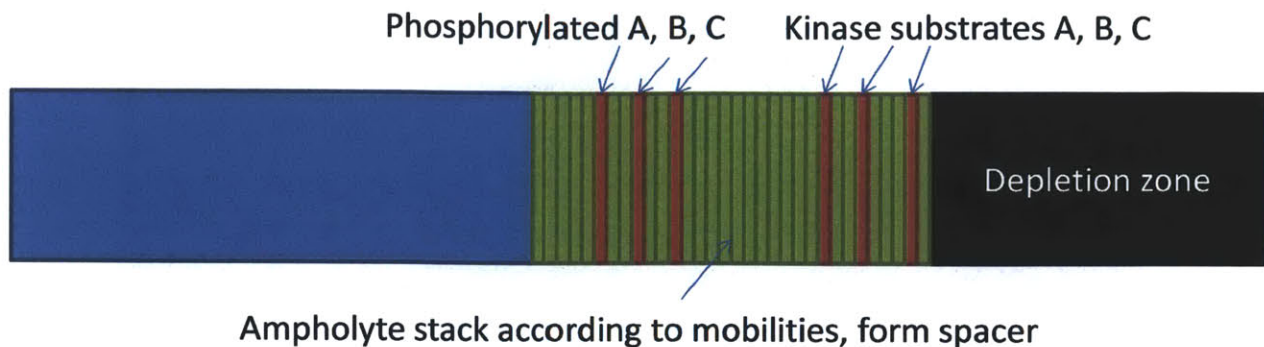


Figure 4.9: According to the principle of depletion-zone isotachopheresis, compounds in the ampholyte stack in the order of their mobilities. This creates an extended separation zone where the equilibrium focusing position of individual fluorescent analytes are well resolved.

We performed experiments in an attempt to two separate fluorescent peptide substrates (5-FAM-GRPRTSSFAEG for AKT and 5-FAM-LRRASLG for PKA kinases) and their products by adding different ampholytes (0.001%) to the buffer (5 mM Tris-HCl, pH7). As shown in **Figure 4.10**, three clear bands were observed in the channels containing ampholytes with isoelectric points (pI) values ranging from 5-7 and 3-10. This seem to suggest that ampholyte compounds with pI 8-10 have too low mobilities while compounds with pI 3-5 have too high mobilities to be appropriate spacers. Despite the complexities of the ampholyte compounds, it is seen that it could only provide good separation between the unphosphorylated substrates, since the phosphorylated substrates were still not clearly resolved. This means that there are no compounds in the ampholytes that are suitable spacers for separating the phosphorylated substrates.

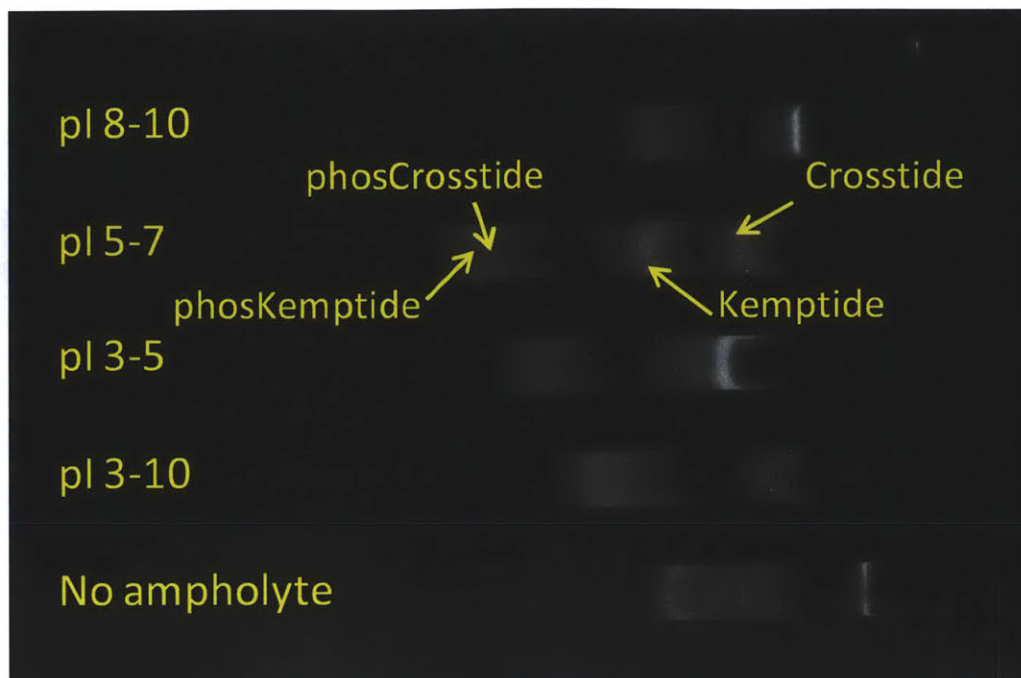


Figure 4.10: Experimental results showing separation of two kinase substrates (Crosstide for AKT, Kemptide for PKA) and their products by adding ampholytes with different pI ranges to the buffer. Ampholyte (0.001%, pI 5-7) was effective at separating the unphosphorylated kinase substrates but was not able to resolve the phosphorylated products from each other.

A similar situation was encountered when we attempted to separate the peptide substrates for MK2 (5-FAM-AHLQRQLSIA) and PKA from their products by adding ampholytes with pI ranging from 5-7 to the buffer. **Figure 4.11** (top two channels) shows that the unphosphorylated MK2 and PKA substrates were well resolved from each other and from the phosphorylated peptides, but the phosphorylated MK2 and PKA substrates were not well resolved from each other. We tried a number of other compounds and found that 2-(*N*-morpholino)ethanesulfonic acid (MES), one of the Good's buffer, was an effective spacer for phosphorylated MK2 and PKA substrate and could provide clear separation between each of the MK2 and PKA substrates and their phosphorylated products (4 bands) when used in conjunction with ampholytes (0.001%, pI 5-7) in 5 mM Tris-HCl buffer (pH 7) (**Figure 4.11**).

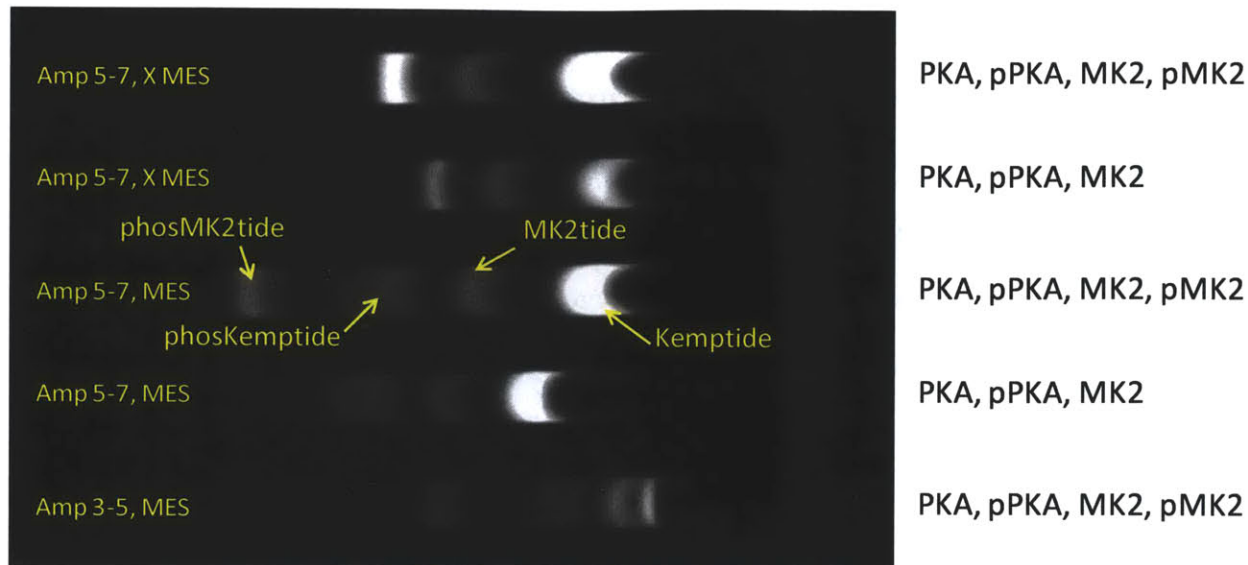


Figure 4.11: Experimental results showing separation of two kinase substrates (MK2tide for MK2, Kemptide for PKA) and their products by adding ampholytes with different pI ranges to the buffer. Ampholyte (0.001%, pI 5-7) in conjunction with 10 μ M MES was effective at separating the phosphorylated and unphosphorylated kinase substrates.

There are some inadequacies of using ampholytes as a spacer. As we have just observed, in some instances the ampholyte compounds could not provide spacer function for our analyte of interest, and we have to source for other form of spacer molecules. The exact mixture of ampholyte is proprietary, so we do not know *a priori* if a compound of a desired mobility is present. Finally, ampholytes are premixed and optimized to ensure that they cover a uniform range of pI value. When used as spacers in the concentration-enhanced mobility shift assays, we lose the freedom to arbitrarily tune the electric field profile by varying the concentration of each individual compound.

Since we are interested in separating peptide substrates and their post-translationally modified products, a natural candidate for spacer molecules is synthetic peptides. Custom synthetic peptides can be obtained at low cost and high purity, but one of the most attractive features for our application is that their mobilities can be tailored by adding different charged and different molecular weight amino acids during peptide synthesis. Thus, spacer molecules of any mobilities can be designed and synthesized. The

mobilities of the peptide substrates and spacers can be approximated with the Offord Model^{47, 48} $\mu = Q / M^{2/3}$. To test this approach, we synthesized 12 different peptides with different mass and charge to be used as spacer molecules in the concentration-enhanced mobility shift assay. We adopted a simple approach to design these spacer peptides: to increase mass we added extra neutral glycine (G) molecules to the carboxylic acid terminal of the peptides, to increase charge we added extra negatively charged glutamic acid (E) molecule separated by one glycine molecule to the amine end of the peptide. The predicted mobilities of the synthetic spacer peptides are placed alongside the predicted mobilities of the kinase peptide substrates in **Figure 4.12**. Peptides with mobilities in between kinase substrates or phosphorylated products that we wish to resolve can be chosen as spacers.

Figure 4.13 shows that by rationally choosing the appropriate peptide spacers, we can simultaneously concentrate and baseline resolve substrates and products corresponding to three kinases PKA (substrate: 5-FAM-EELGRTGRRNSI), AKT (substrate: 5-FAM-GRPRTSSFAEG-NH₂) and MK2 (substrate: FITC-EEKKLNRTLVA). This general capability would allow us to simultaneously monitor several kinase activities from the same sample and study their functional relationship to yield insights on the inner-workings of cell regulatory pathways.

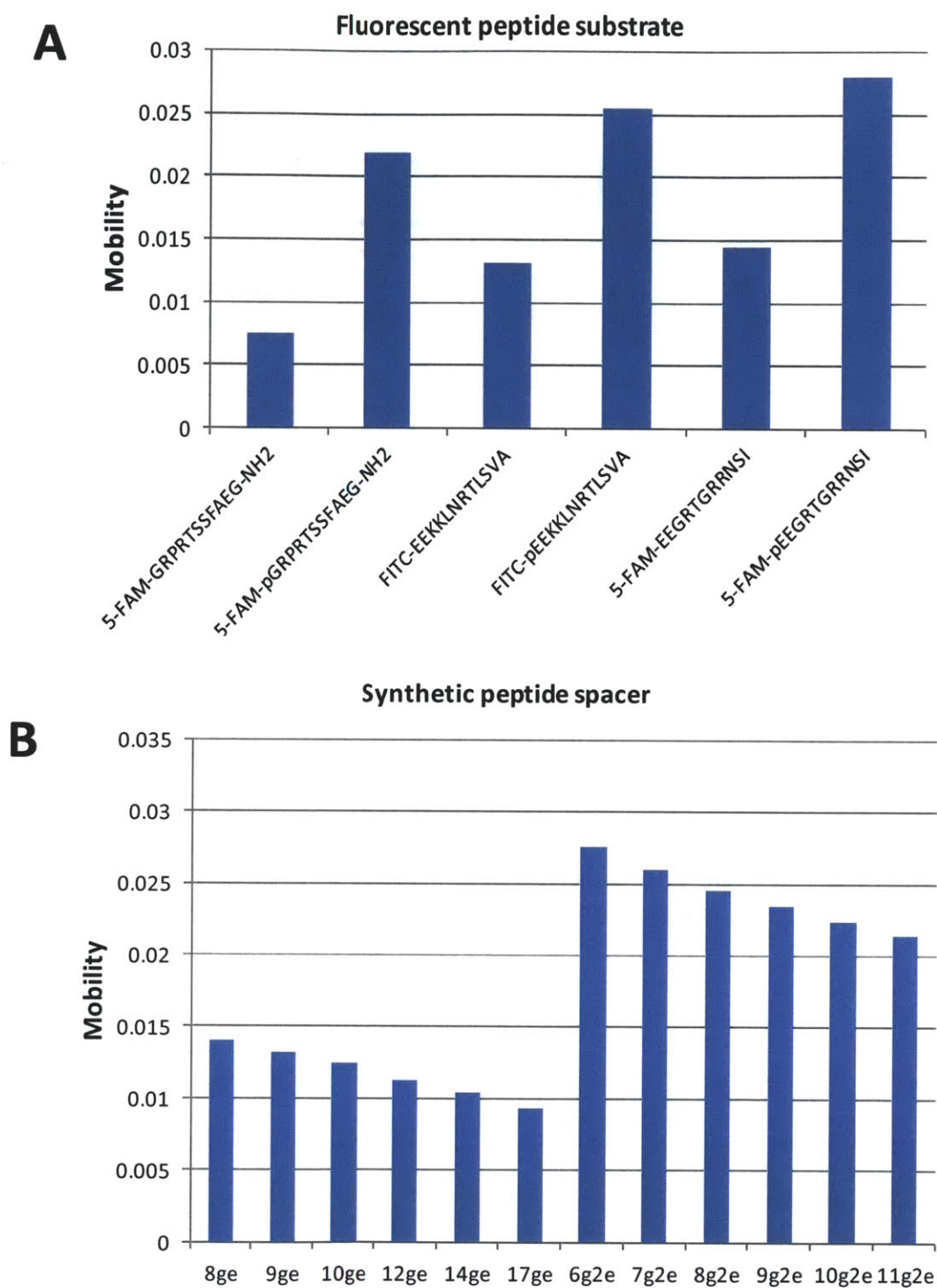


Figure 4.12: Predicted mobilities of the fluorophore-tagged peptide substrates and synthetic peptide spacers according to the Offord Model $\mu = Q / M^{2/3}$. To resolve a pair of analytes of interest, a synthetic peptide with an intermediate mobility can be chosen as a spacer.

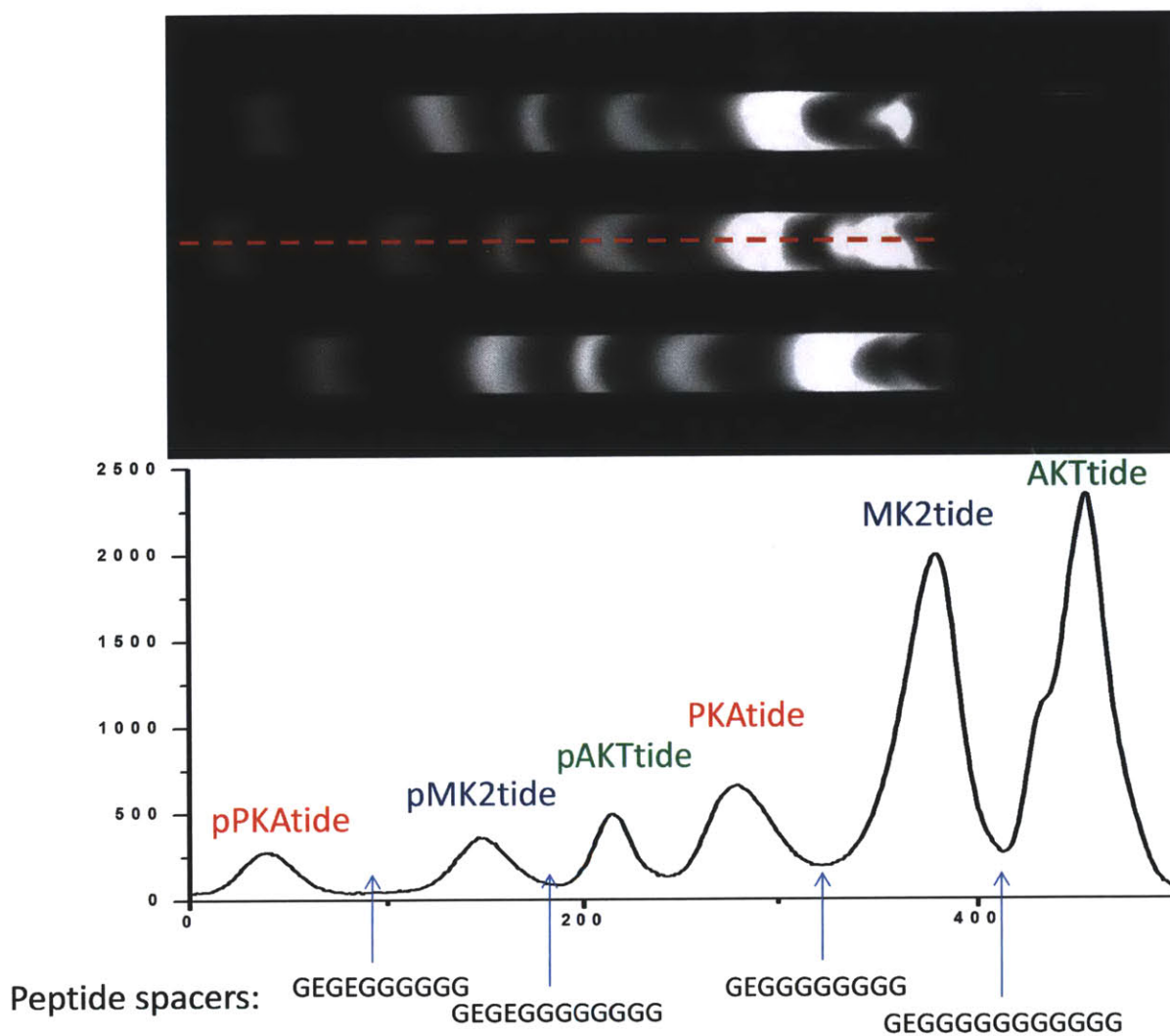


Figure 4.13: Simultaneous concentration and baseline separation of substrates and products corresponding to three kinases PKA (substrate: 5-FAM-EEGRTGRRNSI), AKT (substrate: 5-FAM-GRPRTSSFAEG-NH₂) and MK2 (substrate: FITC-EEKKLNRTLVA) using rationally designed synthetic peptide spacers.

4.6 Single adherent cell culture

In this section, we describe methods that we developed to culture and isolate single cells, as well as techniques to perform cell lysis, incubation of kinase substrate with lysate and finally transfer of reaction products to a separate chip where we perform the concentration-enhanced kinase activity assay. Most cells derived from solid tissues are adherent, and therefore we sought to develop techniques to assay for kinase activity in adherent cells. While cell handling and various operations such as lysis have been demonstrated on suspension cells⁴⁹⁻⁵², they are considerably more challenging for adherent cells. Also, since we are developing tools that would ultimately be used by biologists in their investigations, we aim to develop our assays to be compatible with current methods of cell culture, keeping to standard materials such as polystyrene, glass, silicone and avoiding complicated fluidic handling systems such as growing cells in enclosed microfluidic channels.

To comply with standard tissue culture techniques, we decided to grow cells in an open system where cell culture media and gases can diffuse freely instead of closed microfluidic channels where media needs to be perfused constantly to supply nutrients and remove waste. Conventional single adherent cell isolation is performed by serial dilution in multiwell plates. However the large volumes of this well plates (~100 μ L) means that once lysed, the intracellular contents of a single cell is extremely diluted and it would be far below the detection limit of any assay available. Growing single cells in smaller wells would reduce the dilution factors to make single cell kinase activity assay possible. One attractive option is the commercially available CultureWell (Grace Biolabs) setup, where μ L volume cell culture chambers are defined by non-cytotoxic silicone well gaskets on coverglass. However, as commercially available CultureWell system consists of only 16 wells, too few for our application, we decided to fabricate our own silicone gasket based cell culture chamber arrays that best suit our purpose.

To fabricate the silicone gasket wells, we first start with a stack of two thin PDMS sheets (250 μ m, Silicone Specialty Products). PDMS is a non-cytotoxic silicone material that has been used successfully in many cell cultures. To make the hole arrays (7 \times 7, 2.8 mm pitch), we initially manually punched through the PDMS sheets with a 500 μ m OD biopsy punch (Harris). This array was designed to

fit within the boundaries of a 22 mm×22 mm coverglass slip. Later, we successfully automated the hole-punching process by mounting the biopsy punch on a CNC drilling machine (Sherline) and using open-source software (Modrilla) to control the exact coordinates where the holes will be drilled. The automated hole punching process took less than 3 minutes to punch 49 holes.

To prepare the microwells for cell culture, the silicone sheet with punched holes was treated with oxygen plasma (Harrick) for one minute and bonded permanently onto a piece of acid washed coverglass slip (22 mm×22 mm). The oxygen plasma treatment sterilized the PDMS gasket and increased its wettability to facilitate cell seeding in the later step. The devices were immediately immersed in 1× Phosphate Buffered Saline (PBS) after bonding and placed in a vacuum dessicator for 10 minutes to remove any trapped bubbles. Devices were kept in 1× PBS until ready to use.

To seed single cells in the microwells, the devices were first immersed in 1mL of complete cell culture media in a 35 mm tissue culture polystyrene plate. Freshly trypsinized HepG2 single cell suspension was diluted to 1250 cells / mL in 1 mL complete culture media and added to the tissue culture plate. The cell suspension was mixed by gently pipetting up and down and allowed to settle overnight at 37 °C in 5% CO₂. Cells settled randomly into the microwells following a Poisson distribution. At the above cell seeding density, on average 30% of the 49 wells contained single cells.

4.7 Single cell lysis and kinase reaction

There are several methods reported in the literature on performing single cell lysis⁵³, these include optical lysis using a laser pulse^{15, 34, 35, 54-56}, electrical lysis^{57, 58}, chemical lysis^{59, 60} and ultrasonic lysis⁶¹. We choose to implement an ultrasonic lysis method since it does not require expensive and complicated setting, does not require integrated electrodes, and result in minimal chemical denaturation of the kinase molecules. Ultrasonication is a proven technique for cell lysis and has been shown to be able to lyse cells in microfluidic devices in less than 10 s⁶¹. It also has the advantage of being a parallel process where cells in an array of microwells can be simultaneously lysed. The mechanism of ultrasonic cell lysis is thought to be due to extreme shear forces and pressure transients generated during microbubble cavitation. The

ability to lyse cells in a very short period of time makes this an attractive method for use in signal transduction studies where fast lysis is required to minimize changes in the kinase activities during the process.

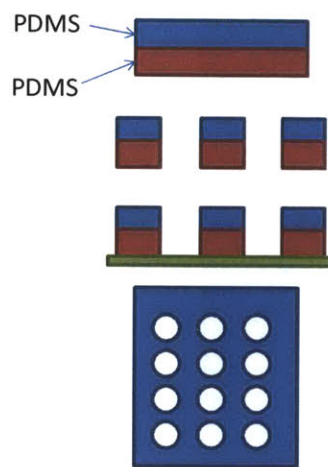
We developed a technique to ultrasonically lyse single cells confined in nL size microwells, so that the released intracellular kinases can catalyze phosphorylation of peptide substrates that we pre-added to the wells just before lysis. Since the enzymes and substrates are confined in nL sized chambers which prevent further dilution, there are at effective concentrations which allows kinase reaction to occur with reasonable kinetics. This approach is parallel to many recent works that make use of microfluidic confinement to increase effective concentrations of target biomolecules and enable ultrasensitive detection⁶²⁻⁶⁴. One unique advantage of this approach compared to many existing single cell kinase activity assay is that various inhibitors (for off-target kinase, protease, phosphatase) can be added in the reaction buffer to increase specificity, reduce cross-talk, maintain stability and preserve phosphorylation states in the kinase assay.

To perform cell lysis in reaction buffer, the cells (treated or control) in microwells were first washed once with ice-cold PBS and followed by ice-cold Tris-Buffered Saline (TBS). The microwells were then overflowed with kinase reaction buffer (Buffer C with 2 μ M fluorescent substrate, 1 mM ATP, 0.01% Triton X-100, 10 μ g/mL protease and phosphatase inhibitors, and inhibitors of off-target kinases) containing the substrates. Next, the wells were sealed with a piece of Kapton tape and the excess substrate was squeezed out. The sealed device was then immediately placed in a ultrasonic water bath and sonicated at full power for 30 s to lyse the cells within the microwells. Cell lysis was confirmed by imaging under the microscope. The kinase reaction was then allowed to proceed in the sealed microwells for 90 minutes in a 37 °C incubator.

Next, we developed a method to transfer the reaction mixture from the nL reaction chamber into the biomolecular concentration device. Since fluid handling in the nL scale is challenging, we adopted the strategy of diluting the nL reaction mix into a larger volume (μ L) to facilitate transfer. This dilution step also effectively stops the kinase reaction, resulting in an endpoint assay. This strategy of confinement

followed by dilution has the advantage that kinase reaction can occur with an appreciable rate during the confinement incubation period, while the later dilution step stops the reaction and facilitate fluid handling. The preconcentration capability of our device would provide the additional sensitivity needed to detect signal from this diluted mixture. To perform the dilution step, another piece of PDMS (1 mm thick) with 2 mm diameter holes (2 mm biopsy punch) was aligned and reversibly bonded on top of the Kapton tape side of the device to form dilution chambers. 5 μ L of the dilution buffer (Buffer B) was pipetted into each dilution chamber. This device is then placed in a dry 35 mm polystyrene dish for imaging under an inverted microscope. While looking under the microscope, we pierced through the Kapton tape above using a hypodermic needle (27G1/2, BD). While the reaction product could diffuse into the dilution buffer, the process could be slow. We enhanced the mixing of the reaction product and the reaction buffer by floating the device above an ultrasonic bath operating at low power for 30 s. The mixture in each dilution chamber was pipetted into a 96 well PCR plate and further topped up to 12 μ L with dilution buffer before being stored at -80 °C. **Figure 4.14** shows the complete process flow for the cell culture, lysis, reaction and fluidic transfer operation.

Figure 4.15 demonstrates successful cell lysis using the ultrasonic method. The left panel show adherent HepG2 cells growing in the microwells. The cells were pre-labeled with a cytoplasmic live-cell dye (Cell Tracker Orange, Invitrogen) before cell seeding to facilitate cell tracking. Upon sealing with Kapton tape and 30 s ultrasonication, the cells are lysed, releasing their intracellular contents including the cytoplasmic dye (right panel). Wells with initial larger number of cells are more fluorescent after ultrasonication due to release of larger amounts of cell tracker orange dye.

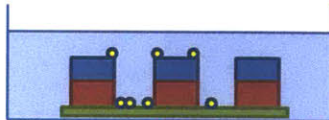


1. Start with 2 layer 250um thick PDMS device, reversibly bonded

2. Automatic hole punching with biopsy punch mounted on a CNC machine (500um diameter)

3. Plasma treat and bond PDMS to coverglass slide

Top view of device (actual: 7X7 array)



4. Seed trypsinized HepG2 cells into nanowells in culture media. Top up tissue culture dish with media. Grow cells in incubator overnight



5. Wash twice with 1X TBS, peel off top PDMS, overflow chamber with kinase buffer + substrate



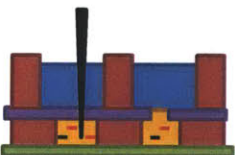
6. Seal chamber with Kapton tape. Press out excess liquid



7. Sonicate 30s to lyse cells. Incubate at 37C for 90 min to let reaction proceed



8. Align large PDMS chambers on top of small chambers manually. Fill with dilution buffer (5uL)



9. Pierce Kapton tape with hypodermic needle to release content of small chamber into dilution buffer. Mix. Collect contents from big chamber to be loaded into device

Figure 4.14: Complete process flow for the cell culture, lysis, reaction and fluidic transfer operations.

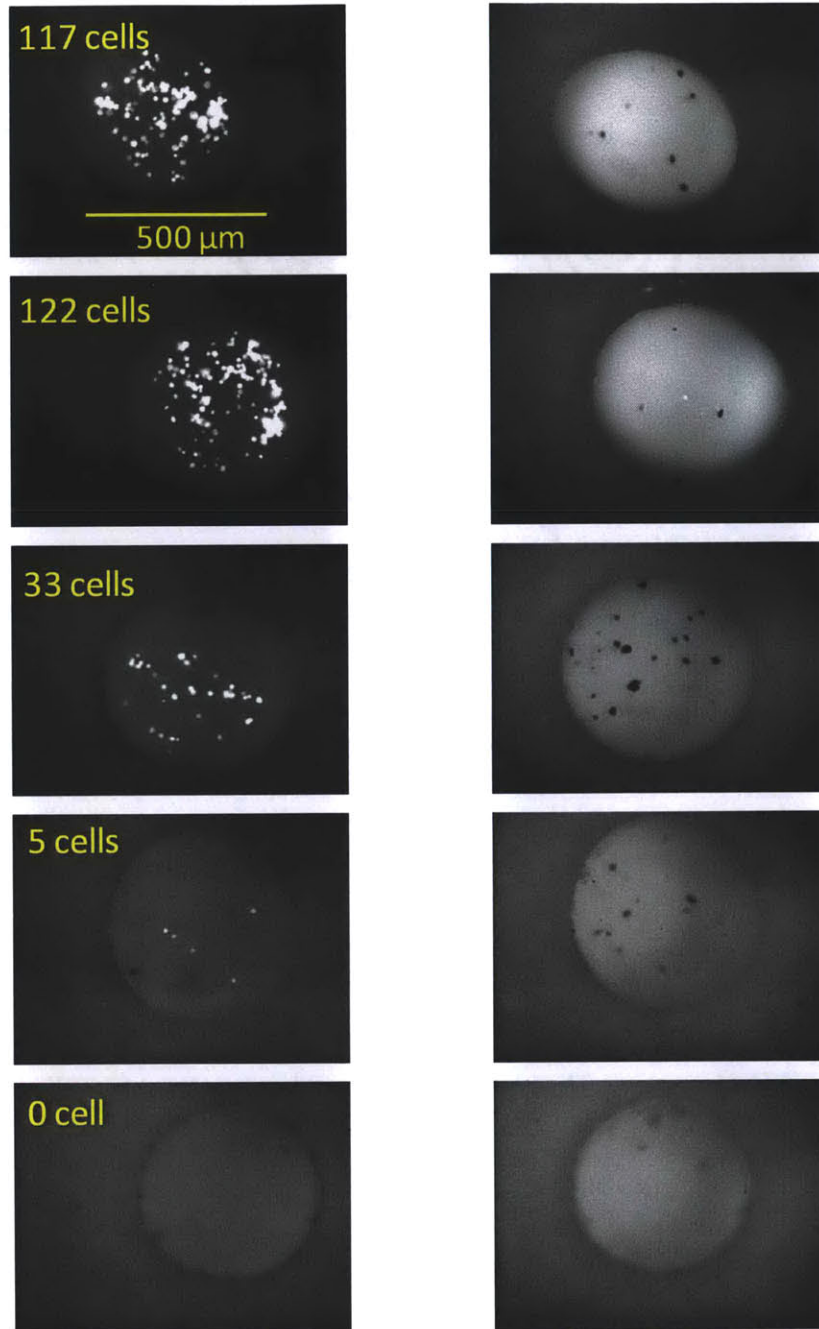


Figure 4.15: Left panel shows HepG2 adherent cells (labeled with Cell Tracker Orange dye) growing in 500 μm diameter microwells. Right panel shows images of microwells after 30s ultrasonic lysis. Intracellular contents including the cytoplasmic live cell dye were released and confined in the microwells

4.8 Concentration-enhanced single cell kinase activity assay

To demonstrate the concentration-enhanced single cell kinase activity assay, we performed cell seeding at low densities to obtain microwells that contain single HepG2 cells. After allowing cells to attach and spread in a 37 °C incubator overnight, the cells were lysed, incubated with kinase substrate and the reaction product was collected as described in the previous section. Each time, 5 different samples each containing 10 µL of the diluted reaction product was loaded into the biomolecular concentrator device to perform the concentration enhanced mobility shift assay.

Figure 4.16 shows the results of single cell kinase activity assay using AKT as a substrate (4 µM PKC inhibitor, 4 µM calmidazolium, 0.4 µM PKI-tide and 5 µM GF109203X added to inhibit off-target kinase activity). The top panel shows the fluorescence image of the cells just before lysis while the bottom panel shows the corresponding concentration-enhanced AKT activity assay. In the samples corresponding to wells with no cells (negative controls), we saw only one band corresponding to the unphosphorylated AKT substrate. On the other hand, in samples corresponding to wells containing one cell, we saw two fluorescent bands corresponding to the phosphorylated and unphosphorylated AKT substrate. This result shows conclusively that our assay can detect AKT kinase activities from single cells.

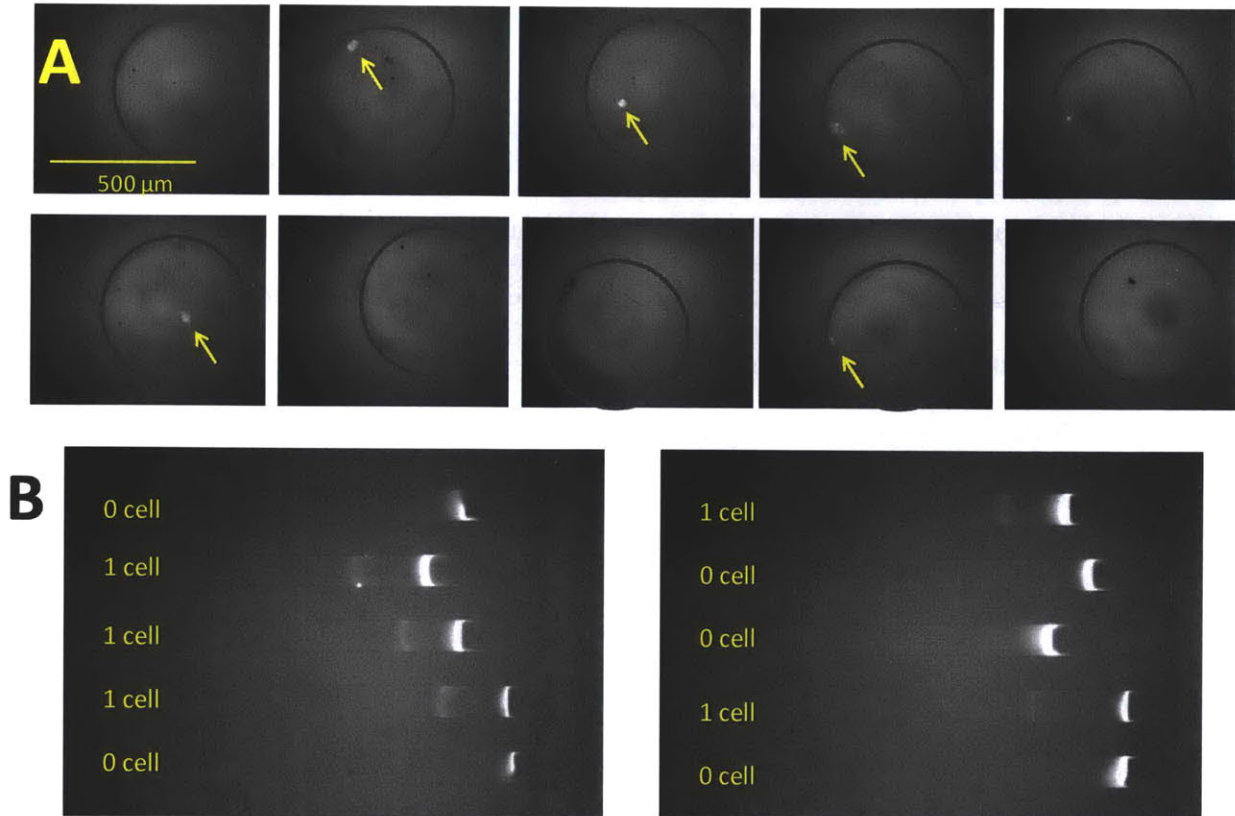


Figure 4.16: a) Fluorescence image of single HepG2 cells growing in microwells before lysis, b) the corresponding concentration-enhanced AKT activity assay. In the samples corresponding to wells with no cells (negative controls), we see only one band corresponding to the unphosphorylated AKT substrate. On the other hand, in samples corresponding to wells containing one cell, we see two fluorescent bands corresponding to the phosphorylated and unphosphorylated AKT substrate.

One additional capability of our device is that it is straightforward and possible to look at total kinase activity from multiple cells that growing in the same well. This might be interesting to compare kinase activities when two cells are growing next to or in contact with each other versus two cells that are growing far apart in the well. Since our biomolecular concentrator can currently assay for five samples simultaneously (this is not the upper limit – recently we have demonstrated multiplexing of up to 128 channels⁶⁵), we can obtain reasonable assay throughput to perform some statistical analysis. **Figure 4.17** shows the results of single, double and triple cells kinase activity assay using MK2tide as a substrate to measure MK2 activity. As expected, there is a clear trend indicating that total kinase activity increases with the total number of cells in the well. The variance in the total kinase activity also increases with the number of cells, as expected for sum of random variables from independent identical distributions. We observed that there are some outlier points in the activity distribution. Upon reference with the cell image taken before cell lysis, we found that these high kinase activities were due to abnormally large cells. This highlights the ability to correlate single cell phenotype with cellular kinase activity in our method.

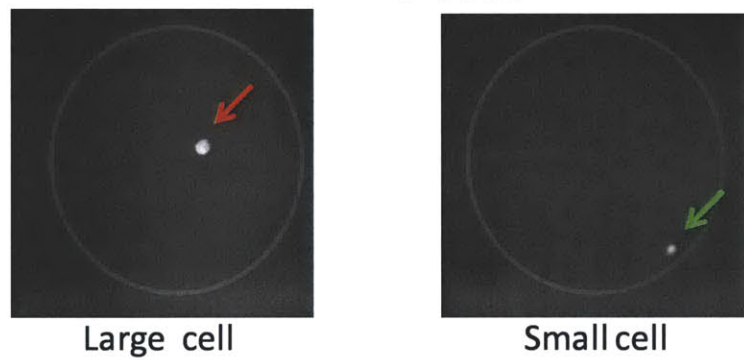
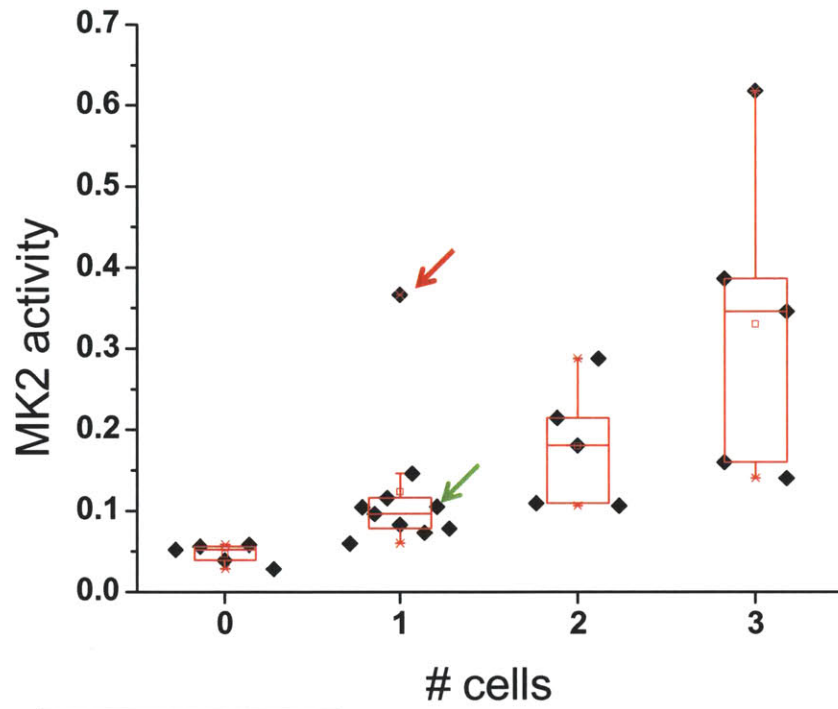


Figure 4.17: Scatter plot shows the total kinase activities in microwells containing zero, one, two and three cells. Total kinase activity increases with the number of cells. Outlier data points correspond to large cells.

We could observe the relationship between single cell phenotype (e.g. cell size) and single cell kinase activity by plotting the kinase activity vs phenotype measure on a scatter plot (**Figure 4.18**). Using total cellular fluorescence (due to live cell labeling) as a proxy for cell size, we found that the total kinase activity follows a linear trend with respect to cell size. This is not surprising as kinases are intracellular enzymes, and the concentration (instead of absolute amount) of active kinase in a cell is the regulated parameter that determines cell fate. From this scatter plot, we can also decouple the effects of cell size and obtain the single cell heterogeneity in kinase activity per unit cell volume, which would arguably be a more relevant factor in single cell signal transduction studies.

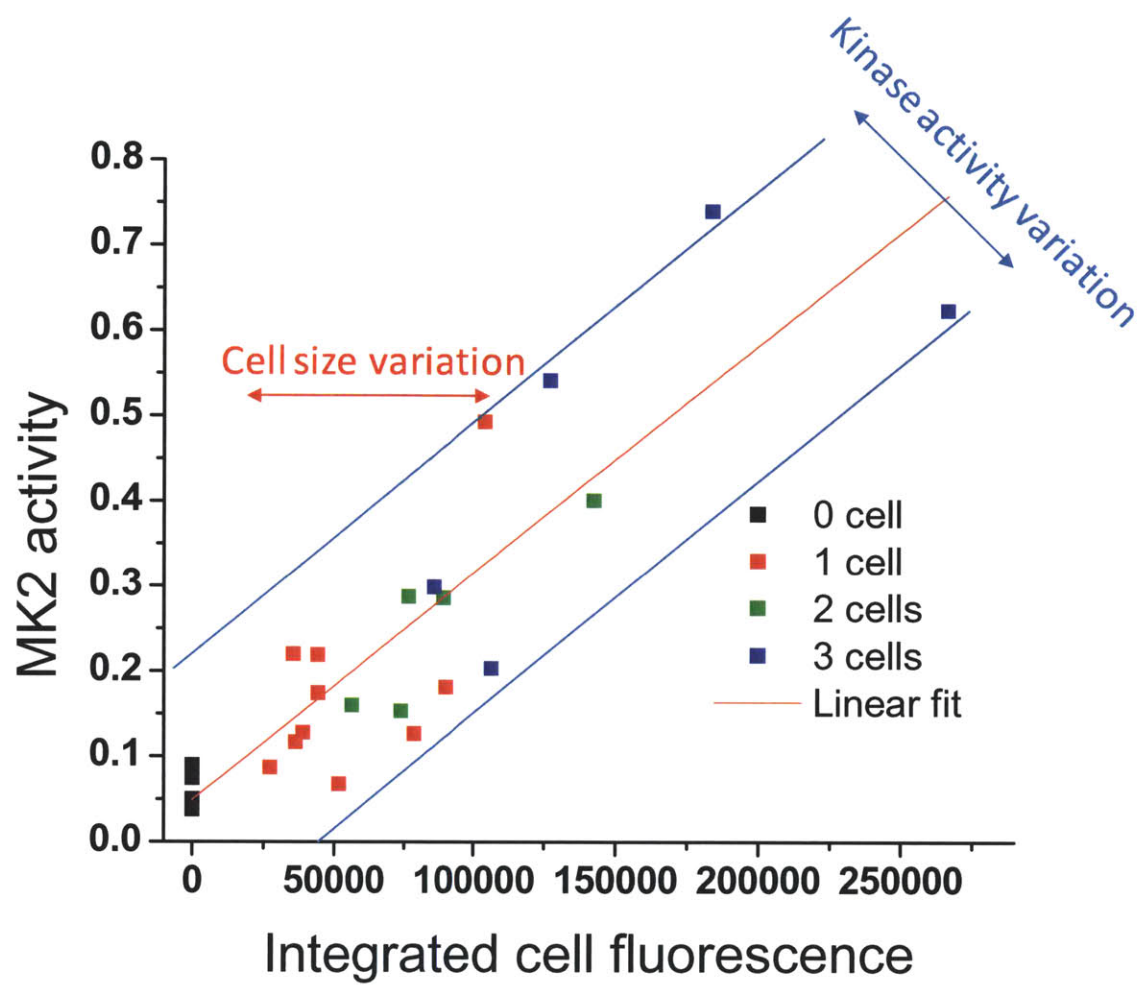


Figure 4.18: Linear relationship between kinase activity and total cell volume (using cell fluorescence as a proxy).

In **Figure 4.19**, we plotted the single cell MK2 activity vs cell number after normalizing by the average cell volume. We saw that this transformation removed the outlier points. We performed a Student's 2-tailed t-test and showed that the samples with different number of cells have significantly different normalized kinase activities. Thus, we demonstrated that our assay have both single cell sensitivity and single cell resolution.

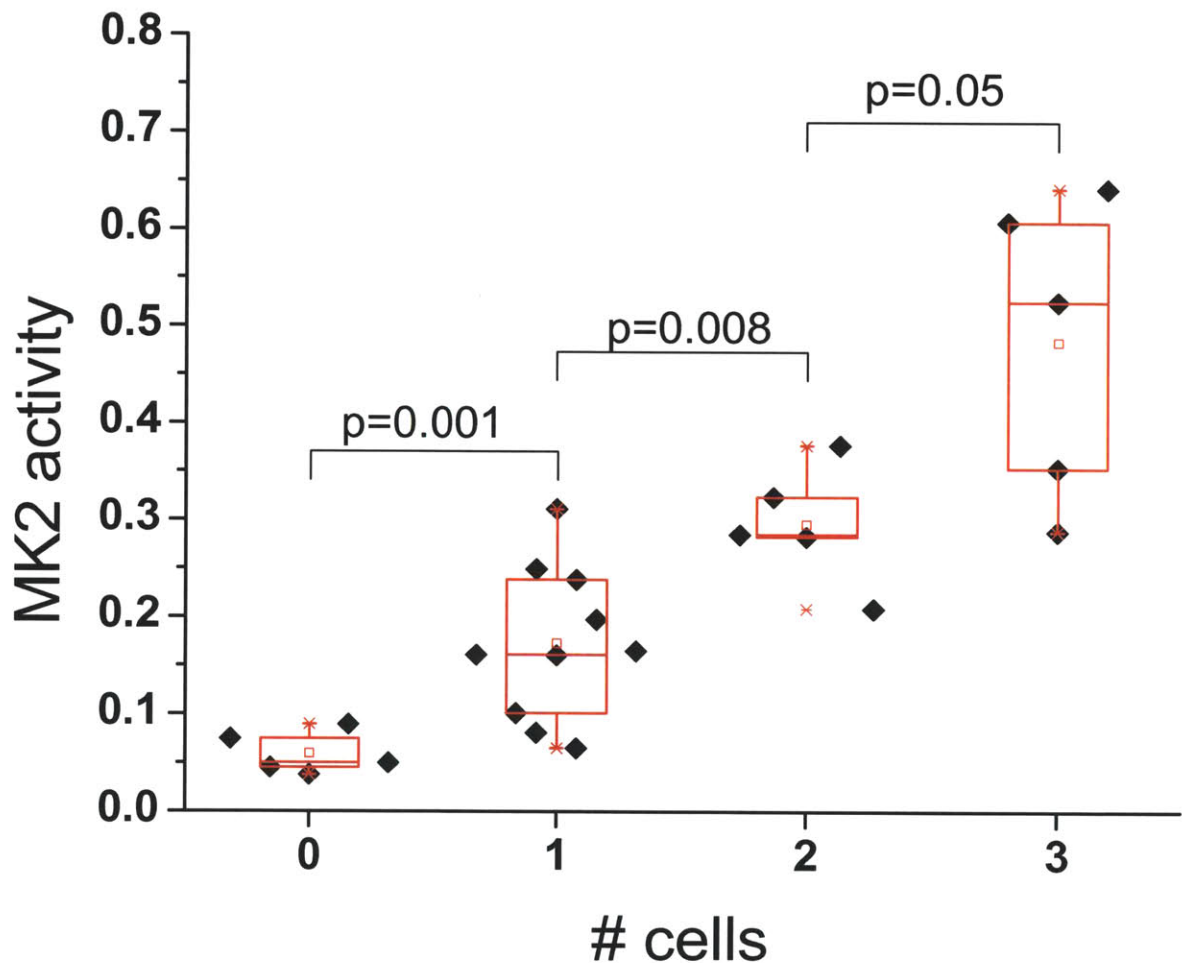


Figure 4.19: MK2 activity vs cell number after normalizing by the average cell volume. Different numbers of cells have significantly different normalized kinase activities by Student's 2-tailed t-test. This shows the concentration-enhanced kinase activity assay has both single-cell sensitivity and resolution.

4.9 Concentration-enhanced single cell multiple kinase activity assay

Finally, we performed experiments to assay for multiple kinase activities in single cells. The experimental protocol was the same with the exception of addition of multiple substrates in the reaction buffer. Spacer molecules (0.001% Ampholyte pI 5-7, 10 μ M MES) were added in the dilution buffer to enable simultaneous concentration and separation of multiple substrates. In **Figure 4.20**, we demonstrated that we can simultaneously measure MK2 and PKA activities in single cells. Multiple kinase activity measurement from single cells is currently very challenging to perform using existing techniques, yet it could provide vital clues about the functional relationships between different pathways in the signal transduction network. We believe that our platform can bridge this technological gap.

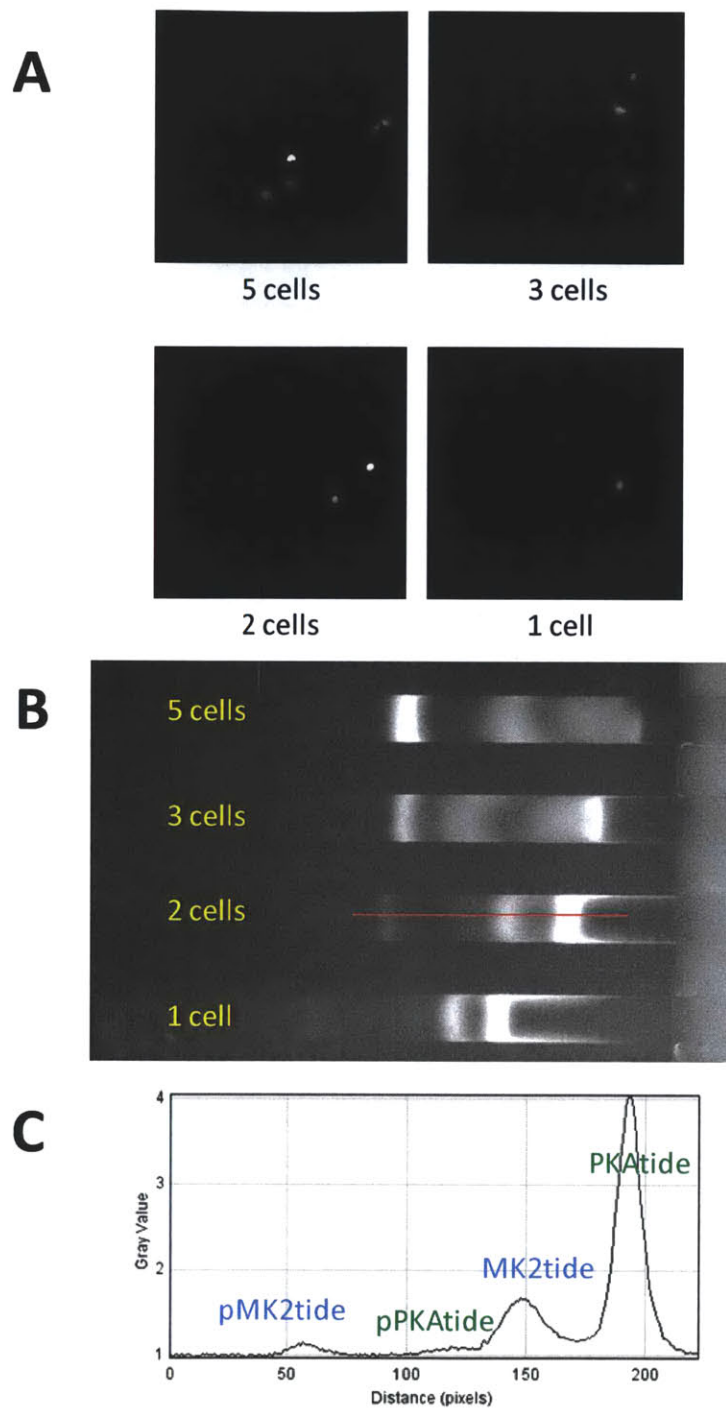


Figure 4.20: Concentration-enhanced multiple kinase activity assay (for MK2 and PKA). a) Images of cells in microwells before lysis, b) Experimental results showing concentration-enhanced multi-kinase activity assay, c) Electropherogram showing baseline separation of the two fluorescent substrate and product pairs.

4.10 Summary

In this chapter, we outlined the use of concentration-enhanced mobility shift assay platform to measure cellular kinase activity with high sensitivity. We also developed a new capability to separate multiple species in the concentration-enhanced mobility shift assay platform by using ampholytes or rational design of peptide substrate and spacers. This capability enables users to perform multi-kinase profiling using different substrates.

To enable single cell kinase assay, we have developed technology to first grow, isolate and observe single adherent cells, followed by parallel cell lysis and enzyme reaction in confined nL chambers, and lastly methods to recover reaction products and transfer to a separate chip for analysis. By combining these methods, we demonstrated kinase activity assay with single cell sensitivity and resolution. We also demonstrated multiple-kinase activity assay with single cell sensitivity.

Although we have only demonstrated this platform with three kinases, it is straightforward to apply this technique to assay for various other kinases on different cell types. This platform is an enabling technology which allows for quantitative measurement of multiple cellular kinase activities at single cell level. We believe that it could be a generic and powerful tool for diagnostics, drug development and systems biology research.

4.11 References

- (1) Bardet, V.; Tamburini, J.; Ifrah, N.; Dreyfus, F.; Mayeux, P.; Bouscary, D.; Lacombe, C. *Haematologica* **2006**, *91*, 757.
- (2) Lee, J. H.; Cosgrove, B. D.; Lauffenburger, D. A.; Han, J. *Journal of the American Chemical Society* **2009**, *131*, 10340-10341.
- (3) Berenbaum, M. C. *Cancer Chemotherapy Reports. Part 1* **1972**, *56*, 563.
- (4) Spencer, S. L.; Gaudet, S.; Albeck, J. G.; Burke, J. M.; Sorger, P. K. *Nature* **2009**, *459*, 428.
- (5) Lahav, G.; Rosenfeld, N.; Sigal, A.; Geva-Zatorsky, N.; Levine, A. J.; Elowitz, M. B.; Alon, U. *Nature Genetics* **2004**, *36*, 147-150.
- (6) Nair, V. D.; Yuen, T.; Olanow, C. W.; Sealfon, S. C. *Journal of Biological Chemistry* **2004**, *279*, 27494.
- (7) Nelson, D. E.; Ihekweba, A. E. C.; Elliott, M.; Johnson, J. R.; Gibney, C. A.; Foreman, B. E.; Nelson, G.; See, V.; Horton, C. A.; Spiller, D. G. *Science* **2004**, *306*, 704.
- (8) Hanahan, D. *Cell* **2000**, *100*, 57-70.
- (9) Hill, M. M.; Hemmings, B. A. *Methods in Enzymology* **2002**, *345*, 448-463.
- (10) Perry Hall, J.; Davis, R. J. *Methods in Enzymology* **2002**, *345*, 413-425.
- (11) Whitmarsh, A. J.; Davis, R. J. *Methods in Enzymology* **2001**, *332*, 319-336.
- (12) Noble, M. E. M.; Endicott, J. A.; Johnson, L. N. *Science* **2004**, *303*, 1800.
- (13) Witt, J. J.; Roskoski, R. *Analytical Biochemistry* **1975**, *66*, 253-258.
- (14) Hastie, C. J.; McLauchlan, H. J.; Cohen, P. *Nature Protocols* **2006**, *1*, 968-971.
- (15) Meredith, G. D.; Sims, C. E.; Souhayer, J. S.; Allbritton, N. L. *Nature Biotechnology* **2000**, *18*, 309-312.
- (16) Pommereau, A.; Pap, E.; Kannt, A. *Journal of Biomolecular Screening* **2004**, *9*, 409.
- (17) Park, Y. W.; Cummings, R. T.; Wu, L.; Zheng, S.; Cameron, P. M.; Woods, A.; Zaller, D. M.; Marcy, A. I.; Hermes, J. D. *Analytical Biochemistry* **1999**, *269*, 94-104.
- (18) Wu, J. J. *Methods in Molecular Biology* **2002**, *190*, 65-86.
- (19) Shults, M. D.; Janes, K. A.; Lauffenburger, D. A.; Imperiali, B. *Nature Methods* **2005**, *2*, 277-284.
- (20) Seethala, R.; Menzel, R. *Analytical Biochemistry* **1997**, *253*, 210-218.
- (21) Ng, T.; Squire, A.; Hansra, G.; Bornancin, F.; Prevostel, C.; Hanby, A.; Harris, W.; Barnes, D.; Schmidt, S.; Mellor, H. *Science* **1999**, *283*, 2085.
- (22) Higashi, H.; Sato, K.; Ohtake, A.; Omori, A.; Yoshida, S.; Kudo, Y. *FEBS Letters* **1997**, *414*, 55-60.
- (23) Kawai, Y.; Sato, M.; Umezawa, Y. *Analytical Chemistry* **2004**, *76*, 6144-6149.
- (24) Schleifenbaum, A.; Stier, G.; Gasch, A.; Sattler, M.; Schultz, C. *Journal of the American Chemical Society* **2004**, *126*, 11786-11787.
- (25) Sasaki, K.; Sato, M.; Umezawa, Y. *Journal of Biological Chemistry* **2003**, *278*, 30945.
- (26) Violin, J. D.; Zhang, J.; Tsien, R. Y.; Newton, A. C. *The Journal of Cell Biology* **2003**, *161*, 899.
- (27) Kunkel, M. T.; Ni, Q.; Tsien, R. Y.; Zhang, J.; Newton, A. C. *Journal of Biological Chemistry* **2005**, *280*, 5581.
- (28) Sato, M.; Ozawa, T.; Inukai, K.; Asano, T.; Umezawa, Y. *Nature Biotechnology* **2002**, *20*, 287-294.
- (29) Ting, A. Y.; Kain, K. H.; Klemke, R. L.; Tsien, R. Y. *Proceedings of the National Academy of Sciences* **2001**, *98*, 15003.
- (30) Zhang, J.; Ma, Y.; Taylor, S. S.; Tsien, R. Y. *Proceedings of the National Academy of Sciences* **2001**, *98*, 14997.
- (31) Kurokawa, K.; Mochizuki, N.; Ohba, Y.; Mizuno, H.; Miyawaki, A.; Matsuda, M. *Journal of Biological Chemistry* **2001**, *276*, 31305.
- (32) Nagai, Y.; Miyazaki, M.; Aoki, R.; Zama, T.; Inouye, S.; Hirose, K.; Iino, M.; Hagiwara, M. *Nature Biotechnology* **2000**, *18*, 313-316.

- (33) Yeh, R. H.; Yan, X.; Cammer, M.; Bresnick, A. R.; Lawrence, D. S. *Journal of Biological Chemistry* **2002**, *277*, 11527.
- (34) Li, H.; Sims, C. E.; Kaluzova, M.; Stanbridge, E. J.; Allbritton, N. L. *Biochemistry* **2004**, *43*, 1599-1608.
- (35) Li, H.; Wu, H. Y.; Wang, Y.; Sims, C. E.; Allbritton, N. L. *Journal of Chromatography B: Biomedical Sciences and Applications* **2001**, *757*, 79-88.
- (36) Zarrine-Afsar, A.; Sergey, N. *Analytical Chemistry* **2003**, *75*, 3720-3724.
- (37) Cross, D. A. E.; Alessi, D. R.; Cohen, P.; Andjelkovich, M.; Hemmings, B. A. *Nature* **1995**, *378*, 785-789.
- (38) Kemp, B. E.; Graves, D. J.; Benjamini, E.; Krebs, E. G. *The Journal of Biological Chemistry* **1977**, *252*, 4888.
- (39) Manke, I. A.; Nguyen, A.; Lim, D.; Stewart, M. Q.; Elia, A. E. H.; Yaffe, M. B. *Molecular Cell* **2005**, *17*, 37-48.
- (40) Munson, M. S.; Meacham, J. M.; Ross, D.; Locascio, L. E. *Electrophoresis* **2008**, *29*, 3456-3465.
- (41) Cheow, L. F.; Han, J. *Analytical Chemistry* **2011**, *83*, 7086-7093.
- (42) Kim, S. J.; Li, L. D.; Han, J. *Langmuir* **2009**, *25*, 7759-7765.
- (43) Wang, Y. C.; Stevens, A. L.; Han, J. *Analytical Chemistry* **2005**, *77*, 4293-4299.
- (44) Quist, J.; Janssen, K. G. H.; Vulto, P.; Hankemeier, T.; van der Linden, H. J. *Analytical Chemistry* **2011**, *83*, 7910-7915.
- (45) Bercovici, M.; Kaigala, G. V.; Backhouse, C. J.; Santiago, J. G. *Analytical Chemistry* **2010**, *82*, 1858-1866.
- (46) Bercovici, M.; Kaigala, G. V.; Santiago, J. G. *Analytical Chemistry* **2010**, *82*, 2134-2138.
- (47) Jalali-Heravi, M.; Shen, Y.; Hassanisadi, M.; Khaledi, M. G. *Electrophoresis* **2005**, *26*, 1874-1885.
- (48) Janini, G. M.; Metral, C. J.; Issaq, H. J.; Muschik, G. M. *Journal of Chromatography A* **1999**, *848*, 417-433.
- (49) Schilling, E. A.; Kamholz, A. E.; Yager, P. *Analytical Chemistry* **2002**, *74*, 1798-1804.
- (50) Waters, L. C.; Jacobson, S. C.; Kroutchinina, N.; Khandurina, J.; Foote, R. S.; Ramsey, J. M. *Analytical Chemistry* **1998**, *70*, 158-162.
- (51) Gao, J.; Yin, X. F.; Fang, Z. L. *Lab Chip* **2003**, *4*, 47-52.
- (52) Lu, H.; Schmidt, M. A.; Jensen, K. F. *Lab Chip* **2004**, *5*, 23-29.
- (53) Brown, R. B.; Audet, J. *Journal of The Royal Society Interface* **2008**, *5*, S131-S138.
- (54) Brown, R. B.; Audet, J. *Cytometry Part A* **2007**, *71*, 882-888.
- (55) Rau, K. R.; Guerra Iii, A.; Vogel, A.; Venugopalan, V. *Applied Physics Letters* **2004**, *84*, 2940.
- (56) Rau, K. R.; Quinto-Su, P. A.; Hellman, A. N.; Venugopalan, V. *Biophysical Journal* **2006**, *91*, 317-329.
- (57) Han, F.; Wang, Y.; Sims, C. E.; Bachman, M.; Chang, R.; Li, G. P.; Allbritton, N. L. *Analytical Chemistry* **2003**, *75*, 3688-3696.
- (58) Nashimoto, Y.; Takahashi, Y.; Yamakawa, T.; Torisawa, Y.; Yasukawa, T.; Ito-Sasaki, T.; Yokoo, M.; Abe, H.; Shiku, H.; Kambara, H. *Analytical Chemistry* **2007**, *79*, 6823-6830.
- (59) Marc, P. J.; Sims, C. E.; Allbritton, N. L. *Analytical Chemistry* **2007**, *79*, 9054-9059.
- (60) Sasuga, Y.; Iwasawa, T.; Terada, K.; Oe, Y.; Sorimachi, H.; Ohara, O.; Harada, Y. *Analytical Chemistry* **2008**, *80*, 9141-9149.
- (61) Wu, C.; Lillehoj, P. B.; Sabet, L.; Wang, P.; Ho, C. M. *Biotechnology Journal* **2011**, *6*, 150-155.
- (62) Ottesen, E. A.; Hong, J. W.; Quake, S. R.; Leadbetter, J. R. *Science* **2006**, *314*, 1464.
- (63) Rissin, D. M.; Walt, D. R. *Nano Letters* **2006**, *6*, 520-523.
- (64) Li, L.; Du, W.; Ismagilov, R. *Journal of the American Chemical Society* **2009**, *132*, 106-111.
- (65) Ko, S. H.; Kim, S. J.; Cheow, L. F.; Li, L. D.; Kang, K. H.; Han, J. *Lab Chip* **2011**, *11*, 1351-1358.

Chapter 5

Conclusion

5.1 Thesis contribution

With recent advances in basic science, we understand a lot more about disease pathogenesis than we did several decades ago. Most of the diseases can now be fully treated or kept under control if diagnosed at an early stage, leading to a drastic improvement in quality of life. However, the healthcare infrastructures for disease diagnosis and surveillance have lagged behind medical progress. Most countries in the world have centralized medical centers and laboratories in cities, but access to adequate healthcare is limited at remote areas. This problem is most serious in resource poor regions, which includes many developing countries. Millions of people are dying each year from diseases that are treatable due to lack of early diagnosis. With increasing global connectivity, some of these endemic diseases can even be global health threat. In recent years, there has been resurgence of many diseases such as malaria and various flu viruses. As part of the Global Health Initiative, health workers are tasked to rapidly diagnose diseases and administer proper treatment at point-of-care in remote and resource-poor settings. To do so, it is critical to develop portable and sensitive diagnostic technologies.

Despite advances in laboratory based biomolecule detection systems that has enabled unprecedented sensitivity, these technologies are not readily adapted to point-of-care diagnostics systems due to many practical limitations. As a result, current point-of-care diagnostics products in the market are still fundamentally based on technologies developed decades ago. Recent developments in micro total analysis systems (μ TAS) have shown promises to address these problems. Microfluidic platforms have been developed to integrate multiple functionalities in a single chip, leading to many successful portable lab-on-chip systems that can perform multistep bioanalysis. Nevertheless, many of these microchip-based assays are still lacking in sensitivity due to inferior portable detection instruments and the inherent low optical path lengths of microfluidic devices. As ease of use is an important criterion, many widely used

platforms in laboratories such as the heterogeneous assay formats might be unsuitable for these portable diagnostic devices due to the complicated procedures. Finally, there are reagent compatibility issues such as the limited stability of antibodies upon storage.

To address these problems, this thesis has focused on using micro/nanofluidic technologies to alleviate several critical bottlenecks of biosensing in lab-on-chip devices. First, we developed a microfluidic platform to amplify signal for homogeneous mobility shift assay. Using this platform, we could boost the sensitivity of an aptamer based mobility shift binding assay for biomarker detection. We demonstrated that this technique can be used for sensitive detection of multiple biomarkers (IgE and HIV-1 RT) and in real sample condition (10% serum). This work addresses the sensitivity shortcomings of using aptamers as alternative capture agents in point-of-care applications. Furthermore, this method has an advantage over many other assays since it is rapid, uses low voltage and can be multiplexed.

Next, we have developed a herringbone nanofilter array device for continuous flow size-selective concentration of biomolecules. Among other things, this platform can be used to perform homogeneous immunoassays for rapid quantification of biomarkers. A cardiac biomarker, CRP, was detected using this device at clinically relevant concentrations. While the use of nanostructures to separate molecules has been previously reported, the novel biomolecule concentration capability demonstrated here would improve the sensitivity of such assays, particularly when low optical path length in typical lab-on-chip devices reduces detection sensitivity.

Lastly, these homogeneous signal amplification platforms are useful tools for scientific studies. As an example of application, we are able to measure cellular kinase activities with very high sensitivity using the electrokinetic concentration-enhanced mobility shift assay. We have also developed technology to isolate, grow and lyse single cells, and use our platform to measure kinase activities from single cells. By rational design of peptide substrates and spacers, we developed a new capability to separate multiple analytes in the concentration-enhanced mobility shift platform. This enables users to obtain simultaneous measurements of multiple cellular kinase activities that could reveal important information about their

functional relationships. To the best of our knowledge, this is one of the very few measurement technologies that enables the direct detection of many kinase activities from a single cell.

5.2 Directions for future research

The field of micro/nanofluidics is relatively young, as many basic principles that govern their operation are still being worked out. On the other hand, these devices tremendous design flexibility, and new applications are discovered from time to time. The novel phenomena presented in this thesis could lead to exciting possibilities of new applications and better scientific understanding of fluid behaviors in the microscale.

In the course of completing this thesis, we came across several interesting ideas that we have yet to explore fully in view of the scope of the thesis. We briefly outline some of these ideas below as topics for future research.

5.2.1 Concentration-enhanced mobility shift assay

The concentration-enhanced mobility shift assay principle is truly a platform technology. It can be readily adapted for various applications, as we have done so for the aptamer-based biomarker assay in Chapter 2 and multiplexed kinase activity assay in Chapter 4. From an application point of view, it can be easily modified to improve the sensitivity of various homogeneous binding assays (e.g. immunoassays, protein-protein interaction, and protein-DNA interaction) and enzymatic assays (e.g. protease activity assay and other post-translational modification assays) which involve mobility shifts.

Another potential application of this platform is for high sensitivity affinity analysis of binding assays. Recently, it has been demonstrated that Nonequilibrium Capillary Electrophoresis of Equilibrium Mixtures (NCEEM) can be used to obtain equilibrium binding constant and complex decay rate constant of protein-DNA interactions, by measuring the characteristic peaks and exponential decay curves of the electropherogram¹. In the concentration-enhanced mobility shift assay, we believe that additional kinetics information about biomolecular binding reaction can be obtained by considering the electropherogram profile and concentration rates of the analytes. Furthermore, due to the continuous injection and

accumulation of analyte which improves the signal, low affinity binding interaction can be measured. This could be useful in applications such as characterization of binding affinity between transcription factors and DNA promoter sites, and screening for aptamers with distinct binding affinity parameters.

In this thesis, we have shown sensitive detection using the mobility shift assay format, where the relative abundance of analytes with different mobilities is measured by two distinct bands in the electropherogram. An alternative detection modality using this platform can be suggested based on the isotachophoretic properties of the electrokinetic concentration process. We have shown that addition of intermediate mobility spacers would increase the separation distance between the two distinct bands, and the separation distance is proportional to the amount of spacer added. Based on this observation, we can envision a scheme where we can detect a nonfluorescent analyte based on the amount of separation that it induces between two fluorescent markers which have higher and lower mobilities respectively compared to the analyte of interest. Similar schemes have been previously reported in isotachopheresis systems²⁻⁴, but the continuous injection scheme in our platform could potentially allow higher detection sensitivity upon long period of electrokinetic concentration. This detection modality would enable sensitive measurements of chemical analytes and small biomolecules such as metabolites where no effective affinity binding agents are available.

5.2.2 Size-based concentration of biomolecules using herringbone nanofilter array

We have demonstrated the use of herringbone nanofilter array for analytical measurements such as protein-DNA interactions, protein-protein interactions and homogeneous immunoassays. As this is a platform technology, it can be adapted to improve the detection sensitivity of other size-based fractionation assays. Due to its fabrication compatibility, it could serve as a useful sample preconcentration module for microfabricated nanostructure based separation methods.

Another research direction that could be pursued is the use of this size-based concentration concept for sample preparation. Although the throughput of the current device is too low for this purpose, there are well established methods to increase throughput such as using high aspect ratio nanochannels⁵ and self-assembled colloidal particle packing techniques⁶⁻⁸. The major challenge of biomarker detection in

complex biofluids is the sheer complexity of the samples. Most of the plasma proteins are introduced by low-level tissue leakages and are generally present at very low concentrations (\ll pg/ml), while others, such as albumin, are present in very large amounts (\gg mg/ml). For biomarker detection in blood serum, it is well documented that the high-abundance serum proteins (mostly albumin and immunoglobulin) present significant limitation to the detection specificity and sensitivity. The specificity and sensitivity of biosensing and detection is critically dependent on the effectiveness of sample pre-fractionation and pre-separation processes. By continuous size-based fractionation and concentration of sample, we can remove the high-abundance molecular background and enhance the sensitivity of downstream detection modules. The nanofilter array based separation component will be able to function without gelatinous materials or complex and expensive surface chemistry, thus allowing for an easy integration within the common point of care diagnostic platform and convenient implementation in resource-limited settings.

5.2.3 Multiplexed single cell biological activity assay

Finally, on the scientific front, our platform could be used as an important tool to detect various cellular biological activities with very high sensitivity. We have demonstrated the ability to measure intracellular kinase activities from single cells. Other single cells activity assays, such as secretion of protease from single cell into the media and measurements of metabolites from single cells, could also be potentially realized in this platform.

With this sensitive tool providing single cell measurements that were previously very difficult to obtain, we can start to explore some fundamental biological questions. This technique can be combined with other single-cell analysis techniques such as RT-PCR to correlate between gene expression and protein activity. We can study how individual cells in different states (cell cycle, morphology etc.) respond to external stimuli such as cytokines. Imaging based phenotypical assays such as measurement of the migration capability of individual cells, when coupled with the single cell kinase activity profile assay, would enable us to better understand the complex cellular decision processing. We believe that this platform could be a generic and powerful tool for diagnostics, drug development and systems biology research.

5.3 References

- (1) Berezovski, M.; Sergey, N. *Journal of the American Chemical Society* **2002**, *124*, 13674-13675.
- (2) Khurana, T. K.; Santiago, J. G. *Analytical Chemistry* **2008**, *80*, 279-286.
- (3) Bercovici, M.; Kaigala, G. V.; Backhouse, C. J.; Santiago, J. G. *Analytical Chemistry* **2010**, *82*, 1858-1866.
- (4) Bercovici, M.; Kaigala, G. V.; Santiago, J. G. *Analytical Chemistry* **2010**, *82*, 2134-2138.
- (5) Mao, P.; Han, J. *Lab Chip* **2008**, *9*, 586-591.
- (6) Liu, L.; Li, P.; Asher, S. A. *Nature* **1999**, *397*, 141-144.
- (7) Nykypanchuk, D.; Strey, H. H.; Hoagland, D. A. *Science* **2002**, *297*, 987.
- (8) Zeng, Y.; Harrison, D. J. *Analytical Chemistry* **2007**, *79*, 2289-2295.